# Towards understanding organ-derived metabolic signatures in blood

**Dissertation**

zur Erlangung des akademischen Grades des Doktors der Naturwissenschaften
(Dr. rer. nat.)

eingereicht im

**Fachbereich Biologie, Chemie, und Pharmazie**
der
**Freien Universität Berlin**

Vorgelegt von

Peter Henning Julius Lloyd Kuich

aus Hamburg, Deutschland

März 2014


Diese Arbeit wurde unter Anleitung von anfangs Dr. Jan Siemens, und dann Dr. Stefan Kempa am Max-Delbrück-Center für Molekulare Medizin zwischen Juni 2010 und März 2014 angefertigt.

1. Gutachter: Dr. Stefan Kempa

2. Gutachterin: Prof. Dr. Simone Spuler

Datum der Disputation: 28.07.2014

## Danksagung

I will be forever thankful to Dan Foltz, who allowed me to learn more in two years than I would have thought possible and supported me irrespective of his own best interest in a time of need.

I would like to thank Jan Siemens for the support at the inception and early stages of the torpor project, and the MDC Fellowship Committee for financial support during the pursuit of this dissertation. Special thanks to Fabian Paul and Kun Song, who helped with the mouse dissections at all times of the night, and Kun Song specifically for being of great help whenever, wherever, and always with a kind smile. Thanks also to Jana Rossius for the many little things without which nothing would be possible at all, and the rest of the Siemens lab that shared their working hours with me.

I am indebted and grateful to Stefan Kempa who supported me in far more than just science and for providing all the opportunity, inspiration, and atmosphere one could ask for. I am grateful to the Kempa lab in its entirety for the warm welcome at the beginning and the wonderful atmosphere ever since. I now remember why I like to work and most often forget that I am working. I am indebted to Julia Diesbach for many things, but most importantly for help with the sample preparation of the torpor tissues at the very beginning. I am thankful to Matthias Pietzke for a great many insights into the specifics of GC-MS and support throughout this thesis, and also Christin Zasada for being of assistance in theory and praxis whenever she was asked. I would like to thank also Tobias Opialla, not only for the Campus Run collaboration, but for freely lending ideas, thoughts, time and energy, for music, always thinking again and never believing a thing I say. I am also thankful to Nils Hoffmann for so openly sharing his work, helping whenever I asked at all times of the day, and collaborating as it should be done. I would like to also thank Simone Spuler for advice and discussions on the thesis topic.

I would like to thank my family for never ending support in all things. Especially my mother and father for always enabling, always helping, always supporting, and always with my best interest at heart. You make every step much easier.

Sylvia, I thank you for setting everything into perspective and sharing your life with me. It is the greatest gift of all, and the only one I'd ever ask of you.

Please remember that the answer to life, the universe, and everything is 42.

*Errare humanum est, sed in errare perseverare diabolicum* - Seneca

# Table of Contents

# i. Summary

In the global effort of translating systems biology research into clinical applicability, metabolomics harbors great potential for blood-based medical diagnostics. Gas chromatography-mass spectrometry (GC-MS) is a popular platform for metabolomics and aims at the identification and quantification of metabolites in biological samples of interest.

This dissertation describes efforts that span a wide spectrum of systems biology and concludes with the first promising steps of its translation into the clinically relevant context of systems medicine. It was aimed at understanding how the physiological states of organ metabolism are reflected in the blood metabolome through the dynamic monitoring of a hypometabolic state in mice and an exercise regime in a human volunteer. These biological investigations were made possible by method and extensive software development.

A novel software package named SILVIA that provides functions for faster and more complete processing of GC-MS data is presented. It allowed for the in-depth analysis of a metabolically dynamic process in liver, muscle, white adipose tissue, cerebrospinal fluid, and blood serum. Daily torpor, the process under investigation, is a hypometabolic state similar to hibernation and is employed by small rodents to conserve energy during times of low food availability. It is characterized by precipitous drops in metabolic rate, core body temperature, heart rate, blood pressure, and breathing rate.

The discovery of mechanisms that control the entry into, maintenance of, and arousal from hypometabolic states are of importance to many medical issues of our time, including, but not being limited to, ischemia and reperfusion injury as well as other trauma injuries, autoimmune diseases, and cancer.

In addition to novel findings of hepatic gluconeogenesis and changes in amino acid metabolism during torpor, as well as a contribution of glycolysis to torpor arousal, the data were able to confirm a metabolic suppression during torpor entry in both liver and muscle. Importantly, by monitoring both organs and blood serum metabolomes simultaneously, it was possible to attain a rudimentary first glance at how organ physiology is reflected in blood, and translate mechanistic insight gained in mice to the human blood metabolome. A combination of a fast, simple, and minimally invasive

blood sampling method with GC-MS technology was developed and employed in a proof-of-principle study of a human volunteer undergoing an exercise regime. With the additional establishment of a method for robust absolute quantification by use of internal isotopologue standards, blood metabolomics in human patients to categorize disease phenotypes and provide diagnostic insights in a clinical setting might soon be within reach.

# ii. Zusammenfassung

Als Teil globaler Bemühungen, systembiologische Forschung in den klinischen Anwendungsbereich zu übersetzen, birgt die Metabolomforschung großes Potential für die blutbasierte medizinische Diagnostik. Von zentraler Bedeutung ist hierbei die Gas Chromatographie-Massen Spektrometrie (GC-MS), mit deren Hilfe Metabolite identifiziert und quantifiziert werden können.

Diese Dissertation beschreibt umfassende Bemühungen auf verschiedenen Ebenen der systembiologischen Forschung und liefert Ansätze für deren Übersetzung in den Kontext der systemmedizinischen Verwendung. Ziel dieser Arbeit war es, durch die dynamische Nachverfolgung experimentell veränderter physiologischer Zustände (Torpor in Mäusen, sportliche Belastung in Menschen), die Zusammenhänge zwischen metabolischen Abläufen in den Organen und der Zusammensetzung des Blutmetaboloms zu verstehen. Ermöglicht wurden diese Studien durch methodische und informatische Neuentwicklungen.

Um eine schnellere und vollkommene Prozessierung von GC-MS Daten zu gewährleisten, wurde die Software SILVIA speziell entwickelt. Durch sie war erstmals die detaillierte Analyse eines metabolisch dynamischen Prozesses in der Leber, Muskulatur, dem Fettgewebe, Cerebrospinalfluid, und Blutserum möglich. Der an Mäusen untersuchte, als Torpor bekannte Prozess ähnelt dem Winterschlaf. Dieser hypometabolische Zustand ermöglicht es kleinen Säugetieren, Energie in Zeiten geringer Futtervorkommen einzusparen. Er ist durch extremes Abnehmen der metabolischen Rate, Körpertemperatur, Herzfrequenz, Atmungsfrequenz, und des Blutdrucks charakterisiert.

Mechanismen die dem Eintritt, der Aufrechterhaltung, und des Verlassens des Torpors zugrunde liegen, könnten bedeutsam sein für die medizinische Behandlung einer Vielzahl menschlicher Leiden wie Ischämie, Reperfusions- und Traumaschäden, und Autoimmun- und Krebserkrankungen.

Neben der Entdeckung aktiver hepatischer Glukoneogenese und Veränderungen der Aminosäurehomöostase im tiefen Torpor, sowie aktiver Glykolyse während des Erwachens, konnten die Daten eine bereits beschriebene Hemmung des Leber- und Muskelstoffwechsels im Torporeintritt bestätigen. Durch zeitgleiches Erfassen von Organ- und Blutmetabolomen war es möglich, sowohl ein erstes rudimentäres

Verständnis für die Reflektion physiologischer Zustände der Organe im Blut zu erlangen, als auch in der Mausstudie gewonnenes mechanistisches Verständnis auf den Menschen zu übertragen.

Dank der Verknüpfung der uns verfügbaren GC-MS Technologie mit einer schnellen, simplen und minimalinvasiven Methode der Blutentnahme am Menschen wurde an einem Volontär eine Machbarkeitsstudie durchgeführt, in der die physiologische Reaktion auf eine sportliche Belastung im Blutmetabolom erfasst wurde.

Mit der Etablierung einer weiteren Methode, die eine robuste absolute Quantifizierung durch Verwendung messungsinterner isotopologischer Standards erlaubt, ist der Traum von klinisch anwendbarer metabolomischer Blutdiagnostik nun in greifbarer Nähe.

# 1. Introduction

Systems biology aims at the quantitative characterization of the constituents of life and promises great opportunity for a deeper understanding of biology, but its realization does not only require advances in technology and methodology. The change from qualitative assessments and interpretations of biological systems to the confrontation with massive quantitative datasets, a single experiment often containing vastly more information than is possible to consider in its entirety without computational aid, requires sophisticated bioinformatic and mathematical support. This is true not only for data analysis but also for the processing of raw machine data, the correct treatment of which forms the basis of and is therefore crucial for identification, quantification, and subsequent biological interpretation. The use of omics technologies in systems biology has thereby transformed life science research itself, as its quantitative nature and strong ties with complex technology necessitates changes in both perspectives and skill sets.

The "omics" technologies, namely genomics, transcriptomics, proteomics, and metabolomics, aim at the complete identification and quantitative characterization of the molecular constituents of their respective domain (Likić et al. 2010). From determining genome sequences and the mapping of epigenetic landscapes across the genome, to measurements of abundances of the various RNA species, sequencing technology has provided insight into the true scale of regulatory processes that control the flow of information from DNA sequence to protein translation. Proteomics, in combination with other technologies, has allowed for measurements of protein abundance, dynamics, and interactions, and has further delved into investigations of their regulation through posttranslational modifications (PTMs) (Yaoyang Zhang et al. 2013). Metabolomics, including lipidomics, has begun to determine the constituents of metabolism and their abundance, and with recent improvements is now able to elucidate the dynamic changes and mechanisms that provide the energy for and biochemical building blocks of life (Kosmides et al. 2013; Milne et al. 2013).

Metabolomics occupies a rather unique niche in the world of omics: While genomics, transcriptomics, and proteomics document genotype or a momentary snapshot of the expression thereof, they provide no measure of phenotypic consequence. Even

proteomics investigating PTMs to assess the state of activity of proteins does not measure the phenotype caused by the differing states of activity.

Proteomics and transcriptomics are therefore used in combination with assays measuring a function of interest and disturbing the RNA/proteins hypothesized to be causally involved. In contrast, metabolomics measures metabolite abundances and therefore the phenotype of the metabolic state of the cell, similar to assessing the migratory behavior of a cell by observing its movement under a microscope. Transciptomics and proteomics, in this context, would instead provide information about the abundance of mRNA and the corresponding proteins required for movement.

Metabolomics measures the consequence of the composition and activity of the cellular machinery involved in metabolism, whereas proteomics and transcriptomics provide a measure of the composition and theoretical potential of the machinery. While the interpretation of transcriptomic, proteomic, and metabolomic data could in theory correlate well, the plethora of regulatory mechanisms within and in between the biological layers of DNA, RNA, proteins, and metabolites makes this unlikely. In fact, stark differences between coding RNA and corresponding protein abundances have been proven (Schwanhäusser et al. 2011).

In the future, the combination of all omics technologies may provide the greatest understanding of biological systems, when all their components can be quantitatively assessed simultaneously to obtain a near complete representation. In the meantime, metabolomics might contain the greatest diagnostic potential (Kosmides et al. 2013). It is able to measure the manifested metabolic phenotype of homeostatic and pathological states, and its interpretation is greatly simplified by established knowledge of metabolic networks and reactions. Partial or systemic metabolic states can be inferred from pathway intermediate abundances and relationships between metabolites that are important branching points between pathways, so that despite the inability to assign observations to the altered behavior of specific enzymes, major re-routing of carbon flow and significant bottlenecks are often easily identified.

Blood is currently one of the most important sources of information for medical diagnostics. It is one route of communication between organs and might therefore

represent their intercommunication and the overall physiological state of the body. Metabolite accumulation and/or depletion might signal changes in activity of specific metabolic pathways, indicate specific requirements during times of metabolic challenge, or represent organ dysfunction during measurements of the steady state.

There are a multitude of panels measuring a selection of metabolites, hormones, or proteinaceous species in blood to attain information on bodily functions (Song et al. 2014). Its complete metabolic characterization in the form of blood metabolomic analysis would represent a dramatic improvement in systems medicine for two main reasons: The greater number of metabolites measured, known and unknown, as well as their relationships to one another contain vastly more information than obtained from much smaller panels. This increased information content will greatly facilitate the classification of patients as normal or pathological as well as the elucidation of mechanisms underlying poorly understood diseases, metabolic and otherwise, in humans. Both classification and mechanistic investigations will be most successful when complemented by studies in animal models that concurrently monitor organ and blood metabolomes to understand how the physiology of organs is reflected in the blood.

It is the goal of this dissertation to present recent efforts in improving both technical aspects of and biological understanding through metabolomic analysis of blood for both mechanistic studies and, in the near future, medical diagnostics. It is split into three major components, each consisting of an introduction, results section, and discussion, which together span a wide spectrum of the interdisciplinary nature of systems biology. Their interrelation is considered throughout and summarily discussed in the final section of this thesis.

At first, I will introduce and present Maui-SILVIA, a software package that provides critically improved and faster data processing capabilities. Secondly, I will present a comprehensive metabolomic investigation of torpor. Torpor is a hypometabolic state similar to hibernation which, in addition to being of great medical interest in itself, serves as a first attempt to decipher the interrelationships between the organ and blood metabolomes. Furthermore, I will describe a proof-of-principle study in a human volunteer that addressed technical issues of sample acquisition and measurement, and

drawing on insights gained in the torpor study, warranted a first interpretation of organ behavior from the blood metabolome in humans. Finally, mechanistic insights from mice were translated into the context of the human blood metabolome, and an experiment establishing a method for near optimal normalization and quantification of human patient blood samples to improve technical robustness and reproducibility is shortly described. Altogether, this dissertation addresses and provides possible solutions for some of the most crucial issues that need be resolved before metabolomics can be translated into the realm of diagnostic systems medicine.

# 2. Maui-SILVIA

## 2.1 Introduction

Metabolomics is an umbrella term for the use of several different technologies to achieve an identical goal: the identification and quantification of metabolites in a given sample. Three common technological platforms are nuclear magnetic resonance (NMR), liquid chromatography-mass spectrometry (LC-MS), and gas chromatography-mass spectrometry (GC-MS), each of which have their respective merits and disadvantages (Dunn et al. 2011). The large variety of chemical characteristics of metabolites in biological samples is such that a complete metabolomic coverage, including lipids (a field of research on its own that has been termed lipidomics (Blanksby & Mitchell 2010)), requires a combination of technological platforms (Zhang et al. 2012).

GC-MS provides the means to measure a large variety of polar and apolar metabolites. The system employed in the Kempa laboratory has been optimized for the characterization of the central carbon metabolism (CCM) and is able to track many of the intermediates of glycolysis, the tricarboxylic acid (TCA) cycle, the urea cycle, amino acid metabolism, nucleotide metabolism, ketone bodies, glycerol and its derivatives, and is able to resolve even the highly similar sugars and their derivatives. Furthermore fatty acid species and their derivatives can also be characterized. All data described hereafter were obtained from a LECO GC time-of-flight (TOF) mass spectrometer. For information on sample preparation and more details on methodology, please refer to the Materials and Methods of the torpor and Campus Run sections.

Proteomic research has witnessed the development of many commercial and non-commercial types of analysis software. Two commonly used in the academic research setting at this time are MaxQuant and the open source software OpenMS, both of which are actively maintained by a core of developers (Sturm et al. 2008; Cox & Mann 2008).

In contrast, metabolomics is a much less advanced field of research when it comes to bioinformatic analysis of raw data generated by mass spectrometers, with many different labs having developed their own solutions and only some being actively maintained (Smith et al. 2006; Katajamaa et al. 2006; Lisec et al. 2006; Lommen &

Kools 2012; Xia et al. 2009). The gold standard of data processing in the Kempa Lab has therefore been the use of the commercial LECO ChromaTOF software in combination with MetMax (Kempa et al. 2009). Despite several shortcomings of ChromaTOF that will be highlighted in the relevant results sections, it has proved most useful because it allows for the manual visual inspection and correction of each processing step, so that despite the inconvenience, frequently occurring errors, and immense demands on time, experienced users are able to vouch for the validity of all measurements. Nonetheless, several factors, among other important considerations, made a novel software solution absolutely essential:

1) The increasing experiment complexity led to a greater number of samples to be processed, the inconvenience and time consuming inefficiencies of ChromaTOF prohibiting in-depth analysis.
2) While identified compounds could be tracked across experiments, ChromaTOF provided no solution to record and maintain information on unknown peaks, rendering the majority of information contained in biological samples inaccessible.
3) Several newly developed methods in the Kempa Lab went far beyond the intended uses of ChromaTOF, making their implementation ever more inconvenient and time consuming to the point of impracticality.

I therefore decided to search for a software framework that allowed for its modular extension so as to incorporate new software analysis functionality specifically optimized for developed methodology. Maltcms User Interface (Maui, http://maltcms.sourceforge.net/maui/, March 2014) is a Java software based on the Netbeans Rich-Client Platform written by Nils Hoffmann from the University of Bielefeld (Hoffmann 2014). It is a user interface for the processing and exploration of GC-MS, LC-MS, and two-dimensional GC-MS data, and based on his published algorithms that were collectively named Maltcms (Hoffmann et al. 2014; Hoffmann et al. 2012). After exploring the available GC-MS data analysis tools mentioned before, none of which were satisfactorily documented, maintained, or conveniently extendable, I decided to use Maui as the basis on which to build a custom software solution through novel implementation of the following functions:

1) Automated retention index (RI) calculation.
2) Quality control, normalization, and sample alignment.
3) Improved compound identification by combining an identification mixture developed previously in the Kempa lab, improved library search algorithms, and a novel interface to enable subsequent rapid manual supervision and correction.
4) A more robust quantification strategy.
5) Automation of an absolute quantification strategy developed previously in the Kempa lab.
6) The recording of unknown peaks resulting in a dynamically extendable "unknown library".
7) Manual correction of peaks incorrectly defined by the error-prone ChromaTOF software.
8) The ability to handle stable isotope standards for normalization and absolute quantification.
9) An automation of the calculation of $^{13}C$ label incorporation of pulsed stable isotope resolved metabolomics (pSIRM) experiments (methodological paper by Matthias Pietzke and Christin Zasada currently under review at Cancer and Metabolism) (Liu et al. 2012).

The collection of modules that accomplish these tasks was named SILVIA, and stands for:
**S**elective compound normalization,
**I**ntegration of unknowns,
**L**abel incorporation,
**V**isual alignment aided
**I**dentification, and
**A**bsolute quantification,
and will be discussed in the following sections.

Functions inherent to Maui (programmed by Nils Hoffmann and co-workers) will from now on be referred to as "Maui", whereas my contributions will be referred to as "SILVIA". The results section will walk through a SILVIA GC-MS project and describe the function and use of the most important novel modules contained in SILVIA. The software has removed the main data processing bottleneck to allow for

the full annotation of biological samples (including unknown peaks) and implements key algorithms that allow the methodology developed to make metabolomics robust and reproducible to come to fruition. Its simplicity and user-friendliness allows previously complicated and involved tasks to be carried out by non-expert personnel, altogether moving GC-MS metabolomics from an involved research task towards a time-efficient and broadly accessible technology, an essential step on the road to becoming a diagnostic platform.

## 2.2 Materials and Methods

### 2.2.1 SILVIA Programming

SILVIA was programmed as a collection of NetBeans modules, and like Maui, is based on NetBeans Rich-Client Platform Development, a Java framework that supplies reliable, tested, and flexible application architecture (https://netbeans.org/features/platform/, March 2014).

### 2.2.2 Data Pre-Processing

Samples were measured on a LECO GC-TOF (see methodological details in the Materials and Methods of the torpor section). The LECO ChromaTOF software, Version 4.50.8.0, served to acquire the raw data and was used for initial processing, consisting of resampling (sample reduction rate = 4, Mass bins of 70-600, export into peg format), baseline subtraction of individual mass bins and peak detection (baseline offset = 1, data points for smoothing = 13, peak width = 4, signal to noise ratio = 50). The raw data and associated peaklists were then exported in netcdf and csv formats, respectively. Raw and peak data served as input for Maui-SILVIA, the use of which will be described in extensive detail in the results section. Briefly, retention indices were calculated, cinnamic acid (an internal standard, see below) annotated and used for normalization of variations in sample preparation, identification and quantification mixes were annotated and used for identification and absolute quantification, respectively. An in-house "Ident" database, the Buch Metabolome Database (BMD, unpublished), and the Golm Metabolome Database (GMD) were used for the identification of metabolites (Kopka et al. 2005). Compound quantification is based on the five most abundant masses of the library mass spectrum of each individual

metabolite (see Results). The final data matrix was exported as a csv file and further processing conducted using R (see R-References).

### 2.2.3 Cosine Similarity Measure

The similarity between two mass spectra is calculated by cosine similarity that is penalized by the difference in RI between library and sample metabolite. The cosine similarity function of the ucar.ma2.MAVector Java class was employed and adheres to the common cosine similarity equation:

$$similarity = \frac{\sum_{i=1}^{n} A_i \times B_i}{\sqrt{\sum_{i=1}^{n} (A_i)^2} \times \sqrt{\sum_{i=1}^{n} (B_i)^2}}$$

where A and B are the two mass spectrum vectors being compared and *n* the number of masses in each mass spectrum. Since the intensities of masses are never negative but start at 0 (not detected), the cosine similarity between two mass spectra will range from 0 to 1. Multiplication of the cosine similarity by 1000 provides a more convenient number format, so that a perfect match of two vectors would produce a similarity score of 1000. Since peaks are matched not only based on mass spectrum similarity but also their RI, the reverse search employs a simple penalty scheme to avoid false positive matches based on mass spectrum similarity of metabolites whose RIs do not match the library metabolite. In these cases, the RI is the defining feature that differentiates between true and false positive identifications (see Identification Reference and Reverse Library Search). The similarity score multiplied by 1000 is penalized as follows when searching from the Ident reference into samples:

| **RI Difference** (RI units) | **< 1.5** | **> 1.5 < 3** | **> 3 < 4** | **> 4 < 5** | **> 5** |
|---|---|---|---|---|---|
| **Score Penalty** (%) | **0** | **3** | **5** | **7** | **15** |

While there are mathematically more elegant penalty strategies (such as the use of sigmoid functions to determine penalty magnitude as RI differences increase), this simple strategy has proved sufficient. The minimal score for a positive identification was set to 800.

## 2.3 Results

### 2.3.1 GC-MS Data Structure

The two characteristics that uniquely identify metabolites using a GC-MS system are the time they take to traverse the GC column (retention time, RT) as well as the mass spectrum resulting from the fragments they produce after electron impact ionization (Skoog et al. 2007).

The elution of metabolites off a GC column is identical in behavior to other chromatography systems, in that each metabolite, as long as it does not co-elute with another, produces a single peak. One of the key features of a GC-MS data processing software is therefore the identification, or "calling", of peaks throughout the chromatogram, each peak corresponding to a chemical species (Figure 2.1).

The spectra are composed of a range of masses the MS detector can detect and count, the counts of individual masses commonly referred to as intensities. The relative intensities of distinct masses correspond to fragments created after electron impact ionization and together comprise the mass spectrum of a given metabolite (Figure 2.1). In contrast to measurements of, for example ultraviolet light (UV) absorption employed on other chromatography systems, the peaks in a GC-MS chromatogram are not a result of a single signal but represent the sum of intensities of a range of masses, called the total ion count (TIC), over time. Each MS sampling time point therefore contains intensity values for all masses it is able to detect at that time. The second crucial function of a GC-MS data processing software is therefore the assignment of a mass spectrum to each peak called in the chromatogram. The combination of its RT and mass spectrum provides a fingerprint that, assuming infinite GC resolution, allows for the unique identification of any given chemical species.

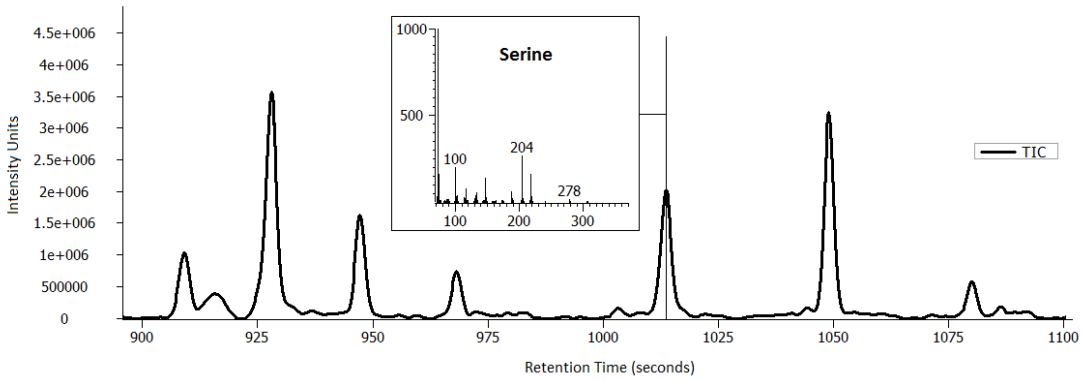


**Figure 2.1 – The chromatogram of a GC-MS sample.** The chromatogram displays column retention time on the x-axis and arbitrary intensity units on the y-axis. Plotted is the total ion count (TIC), meaning the sum of intensities of all masses detected at each sampling time point. The peak corresponding to the amino acid serine is indicated by a vertical line and its mass spectrum, composed of the relative intensities for individual mass bins (unit resolution in our case), displayed.

ChromaTOF records the raw data acquired by the GC-MS system, which contains all mass spectra obtained at all sampling time points, altogether comprising the complete information obtained from the sample. Additionally, it contains reasonable basic processing and peak calling algorithms that were used for all data described in this dissertation. SILVIA takes both raw data and corresponding files containing all peaks called by ChromaTOF (peaklists) as input, and is thus able to build on the available functions of ChromaTOF while maintaining the ability to draw on the true raw data where necessary.

### 2.3.2 Project Initialization

A typical SILVIA project consists of a wash sample (containing only processed solvents and the alcane mix), four identification (Ident) mix samples (A, B, C, and D), eight quantification (Quant) mix samples (dilutions 1:200, 1:100, 1:50, 1:20, 1:10, 1:5, 1:2, 1:1), and the biological samples in technical and biological replicates. In the case of the torpor dataset described in this thesis, each tissue was treated as a separate project. Each tissue project included one set of Ident and Quant mixes, as well as several washes in between samples, and each of the seven biological states consisted of three biological replicates measured in technical duplicate. This resulted in roughly one hundred samples measured per tissue for a total of five hundred samples.

All data was acquired and pre-processed in LECO's ChromaTOF software with satisfactory quality. First, the data was "resampled" by averaging four spectra into one, a four-fold data reduction and concurrent four-fold reduction in time resolution that does not significantly reduce analytical power. Next, baselines for each mass bin were calculated and subtracted, after which peak detection was carried out. Resampled, baseline-corrected data were exported in netcdf format, and identified peaks in csv format.

Maui creates projects in the form of db4o databases, a Java and .NET native open source object database by Versant (www.db4o.com, March 2014), with references to the large netcdf raw files as its basis and allowing for the import of the corresponding peaklists in csv format. It also provides methods to import metabolite databases for peak identification into the project database, which SILVIA converts into a structure identical to the peaklists of samples to allow for the visualization of the metabolite databases along with the samples (described below). With all data imported and metabolite databases converted in the project database, the user is ready to calculate the peak retention indices.

### 2.3.3 Retention Index Calculation

The combination of gas chromatography and mass spectrometry allows for the identification of metabolites based on the two properties being measured: the time it takes for a metabolite to travel through the column (RT), and the masses produced when it is fragmented (by electron impact ionization in this case). Since some metabolites have identical components and only differ in their spatial arrangement (hexoses, for instance), they produce identical or nearly identical mass spectra, so that the only way to reliably differentiate them is to detect the sometimes subtle differences in RT. It is therefore critical to align two samples to one another in such a way that technical variability can be reduced mathematically. This is accomplished by the addition of standard substances to every sample, a so-called alcane mix, consisting of a number of alcanes that do not occur in biological systems and are robustly measured by a GC-MS system. By normalizing the RTs of sample peaks to the RTs of the peaks corresponding to the alcane standards, one can calculate a retention index (RI) that is more comparable

between different samples, as all column differences affect absolute RTs of alcanes and sample compounds alike, while their relative time differences remain constant.

To automate the calculation of the retention index for all samples in a given project, SILVIA searches a wash sample (containing only processed solvents and the alcane mix) routinely measured before, in between, and at the end of sample batches, for the alcane peaks. Given the RT of the alcanes in the wash, it creates a search window within which it looks through all other samples to identify alcanes by spectral matching using cosine similarity measure without any penalties. It then displays its suggestions in the novel visualization interface described below to allow for manual inspection and, if necessary, correction. After manual confirmation of the correct identification of all alcanes in all samples by the user, SILVIA calculates retention indices for all peaks in the peaklists of all samples based on the principles of gas chromatography retention indeces first described by Kovats (Kovats 1958).

### 2.3.4 Quality Control and Normalization

To control for pipetting inaccuracies and MS injection volume differences between samples in a batch of measurements, another internal standard in the form of cinnamic acid (CA) is added to the samples at the very beginning of biochemical processing. CA is a stable plant metabolite that elutes off the GC column at a time when few other metabolites of interest elute. Since it is added to all samples at the same concentration, differences in CA amounts measured between samples reflect sample preparation and injection differences. CA can then be used to normalize the samples to one another by calculating and adjusting all other metabolite intensities by the ratios of CA levels between the samples. SILVIA automatically calculates and adds this normalization factor to the peaks' characteristics, and after setting the quantification masses (see below), calculates and exports both the raw and CA-normalized intensities for each peak. By furthermore providing a plot of CA intensities of all samples in a project, SILVIA allows the user to easily spot more severe technical errors and with a simple selection interface exclude erroneous samples from further processing and analysis, providing a convenient quality control report at the very beginning of data processing.

### 2.3.5 Identification Reference and Reverse Library Search

Since metabolites are identified by the combination of RT (or RI) and their mass spectra, the more reproducible these two variables are and the more closely they match the library data, the higher the confidence in the identification. Mass spectra quality is largely dependent on metabolite abundance, which is beyond improvement once samples have been measured. However, the RI information content can be optimized.

Even though the normalization from RT to RI described previously improves identification robustness, some metabolites with near-identical or identical composition and therefore very similar mass spectra are also so similar in RI that a confident identification cannot be guaranteed. This technical difficulty can be overcome by obtaining an empirical representation of column performance for each individual sample batch on the particular day of measurement using the Ident mix.

It is composed of a large number of metabolites routinely detected in biological samples and split into four separate mixtures that contain different combinations of metabolites that are difficult to differentiate.

An example will serve best to explain the reasoning: Let us consider two sugars that have identical spectra and elute at almost the same time, for example glucose and galactose. Ident mixes A and C would contain galactose, and mixes B and D glucose. By aligning the Ident mixes to one another using the RI information calculated before, one can unambiguously determine the exact RI of glucose and galactose on a particular column on a particular day, even if they differ only marginally, by looking at the peaks of Ident mixes A, B, C, and D. Should a sample of interest in the measurement batch contain a peak at the retention index of the two peaks in A and C, it can be confidently identified as galactose. Would the sample peak RI match those of Ident mix B and D, it would be identified as glucose (Figure 2.2).

By first identifying all metabolites in the Ident mixes unambiguously because of the inherent binary code of the mixtures, we can create a measurement batch-specific metabolite library called the Ident “reference”, which allows us to differentiate metabolites that we would not be able to using the metabolite library alone.

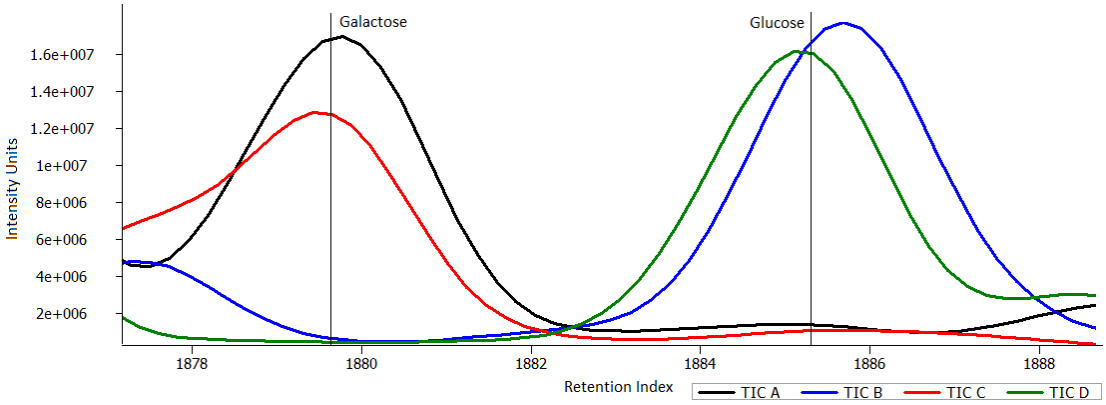


**Figure 2.2 – An example of the binary nature of the Ident mix to allow for unambiguous identification of highly similar metabolites.** The TIC of Ident mix A (black), B (blue), C (red), and D (green) display the peaks of galactose and glucose. Although their RI is very similar and within possible technical variation, obtaining a batch-specific RI for each compound by use of the Ident mix leads to unambiguous identification of these two highly similar sugars in biological samples.

Another advantage of determining batch-specific RIs even for more easily identifiable metabolites is that the library search needs to consider smaller time windows in which to search for a metabolite. If the algorithm tries to look for alanine, for example, and the RI of the library and sample is known by experience to differ up to 5 RI units, the algorithm would have to look at all peaks within at least a 10 RI unit window (library RI +/- 5 units) and compare them to the library peak of interest. If the Ident reference restricts RI differences to within a single unit, algorithm execution time and misidentifications, which have to be manually corrected subsequently, are decreased.

Some weaknesses in the library search conducted by ChromaTOF have been eliminated in SILVIA as well. While ChromaTOF starts with each peak in a sample and searches its library to find a possible match, leading to many different peaks being identified as the same metabolite (especially those similar in spectrum) and ignoring the RI information entirely, SILVIA uses what I have termed a reverse search (RS). SILVIA starts in a metabolite library (or the Ident reference) and uses the RI information to create a RI unit window in all of the samples being analyzed. It then only compares the library spectra with those of peaks within the RI window and gives them a score based on cosine similarity between library and sample spectra that is weighted by a penalty for RI unit differences. A score threshold prevents low confidence assignments, and the user is left with at most one peak identification per metabolite in the library per sample,

massively reducing the amount of time spent manually correcting senseless redundancies.

### 2.3.6 Visualization of GC-MS Data: The Annotation Interface

ChromaTOF visualizes GC-MS data with line plots representing chromatograms. Individual lines represent different samples, mass bins, or both; peaks are indicated by numbered vertical lines and their mass spectra shown in a separate window with various combinatorial options (such as showing a library spectrum, a peak spectrum, and the difference between the two) (Figure 2.3). While this is useful for few samples or few masses, the chromatograms become unintelligible when working with larger datasets (Figure 2.4). Furthermore, every step required to validate the library search or correct mistakes seems unintuitive and takes several clicks, which is tolerable for a low number of metabolites in a few samples, but becomes impractical when working with a dataset as large as the torpor study or, as desired for diagnostics, measurements from hundreds of patients. In addition, ChromaTOF is prone to freezing up and loosing painfully validated identifications, which happens more frequently the larger the datasets.

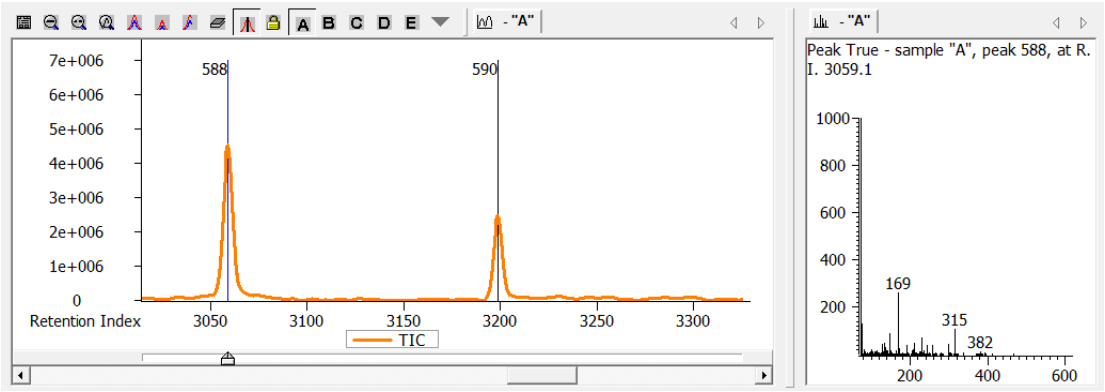


**Figure 2.3 – The ChromaTOF interface for visual examination of GC-MS data.** The left panel shows the chromatogram of a sample with two peaks as indicated by the vertical lines. The mass spectrum of the currently selected peak (blue line) is displayed in the right panel.

The novel approach to GC-MS data visualization implemented in SILVIA facilitates the identification and correction of peaks to allow for the manual supervision of a hundred or more samples simultaneously. It consists of two windows, one displaying

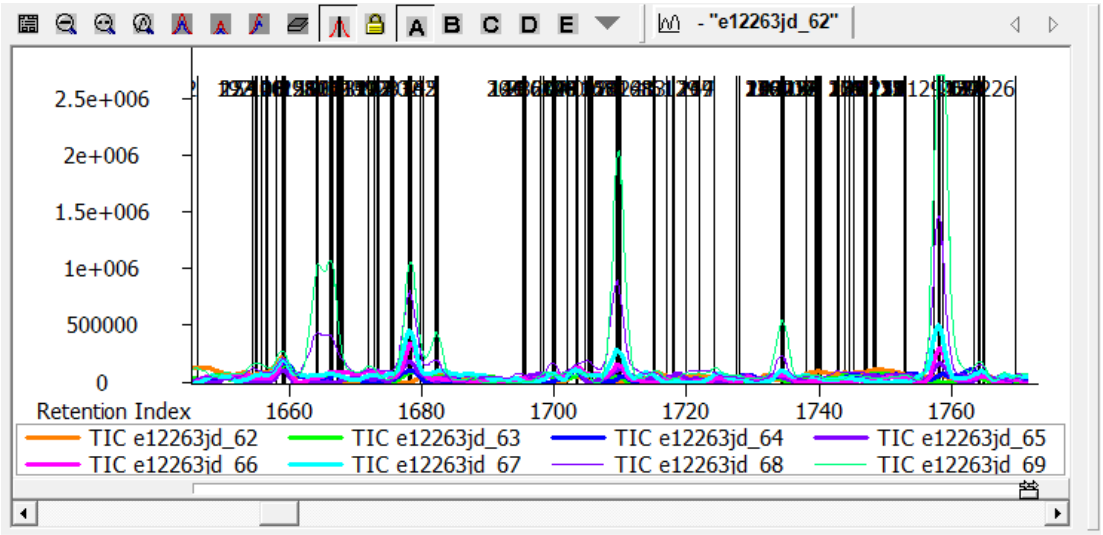


**Figure 2.4 - The ChromaTOF interface for visual examination of GC-MS data.** An example of the unintelligibility of a small section of the chromatogram in the ChromaTOF interface when visualizing eight samples and the peaks detected therein simultaneously.

the RI information (RIview) and the other the full mass spectra of selected peaks (MSview) (Figures 2.5 and 2.6). The RIview lists all samples currently being annotated on the y-axis, with the currently selected metabolite library (or Ident reference) always in the first row, and the RI on the x-axis. Each peak called by the ChromaTOF software is represented by a thin vertical box that displays only binary information (a peak being present or not present), meaning that all peaks, no matter what kind of spectrum or what intensity, have the same width and height. The interactive RIview visualization is based on the extensive customization of the IntervalBarRenderer and CategoryPlot classes of the open source Java package JFreeChart (http://www.jfree.org/jfreechart/, March 2014). It leads to a fast and clear representation of the peak data and looks not unlike a western blot turned by ninety degrees. As can be immediately and intuitively grasped, peaks that lie directly underneath one another have a near-identical RI and therefore very likely correspond to the same metabolite. Peak groups and regions of high and low peak density are intuitively recognized.

The information lacking in the RIview is displayed in the MSview that contains four rows of graphs that are also generated using customized JFreeChart classes. The top middle panel always displays the mass spectrum of the library peak currently selected. The middle panels of the three rows below display the mass spectra of the three peaks

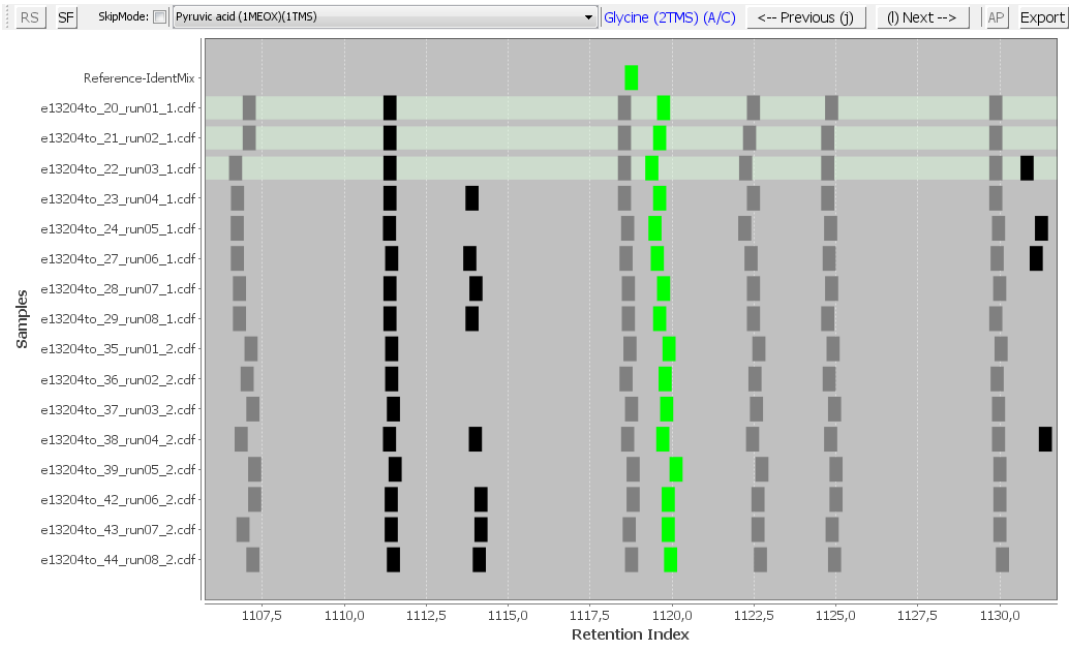


**Figure 2.5 – The RIview.** Sample names are listed on the y-axis and the RI on the x-axis. The first row is occupied by a metabolite library or the Ident reference. Each peak detected in a sample is represented by a bar, its color indicative of different processing steps. This intuitive visual representation renders peak groups easily discernible and aids the visual investigation of GC-MS data.

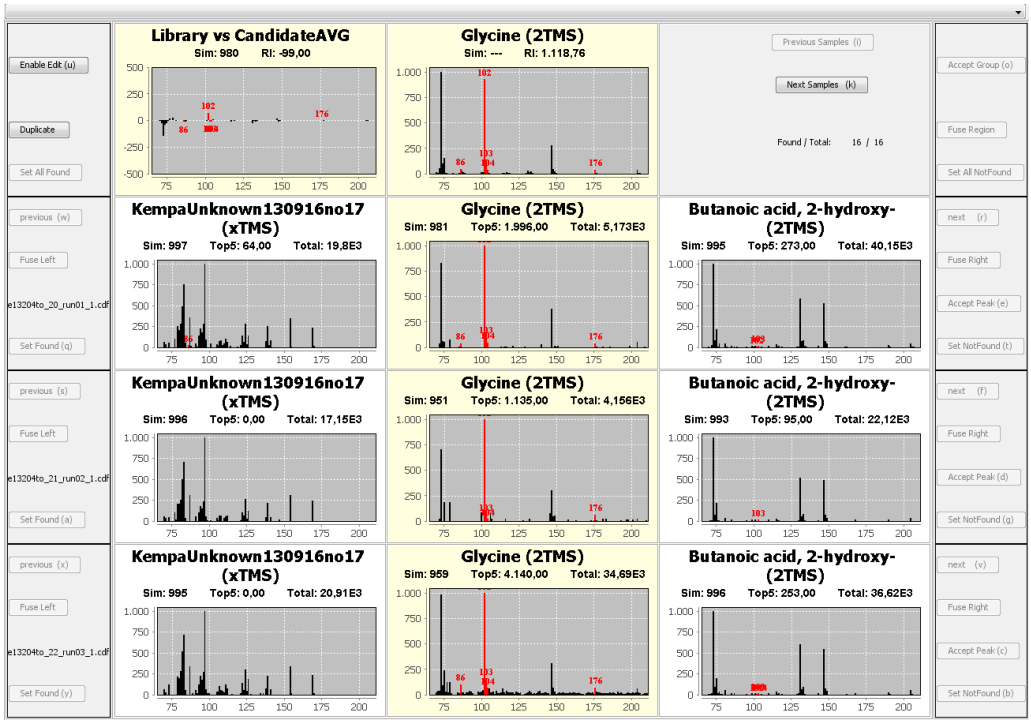


**Figure 2.6 - The MSview.** The top middle panel displays the mass spectrum of the currently selected library metabolite. The three rows underneath display the mass spectrum of peaks that have been putatively identified as the library metabolite, as well as the mass spectra of the peaks to the immediate left and right. The top left panel shows the difference between the library entry and the average spectrum of identified peaks. Masses used for quantification (Top5) are indicated in red, all others in the mass spectrum in black. A similarity score indicates the confidence in the putative identification. The intensities of the Top5 and other masses (Total) give an indication of peak size.

selected in the three samples highlighted in the RIview, as well as their neighboring peaks to the immediate left and right. The top left panel displays the difference spectrum of the library peak subtracted from the average of the mass spectra of the identified peaks. Each spectrum caption contains the total intensity of the peak in black and the cumulative intensity of the Top5 masses of the library spectrum in red, which will later be used to quantify the abundance of the metabolite (see "Quantification Masses"). The workflow with the new interface is as follows:

1) The user selects a library from which to search into the samples and performs a RS. Two examples would be the search from an Ident library into the Ident mixes or from the Ident reference into biological samples as shown in the figure (Figure 2.7). The RS looks for every metabolite in the database in all the samples in a defined RI window (as described above). If it finds one peak to be a likely match, it colors that peak red in the RIview, and putatively assigns it the metabolite name. After the RS is complete, all putative identifications are red, while all other peaks remain black.

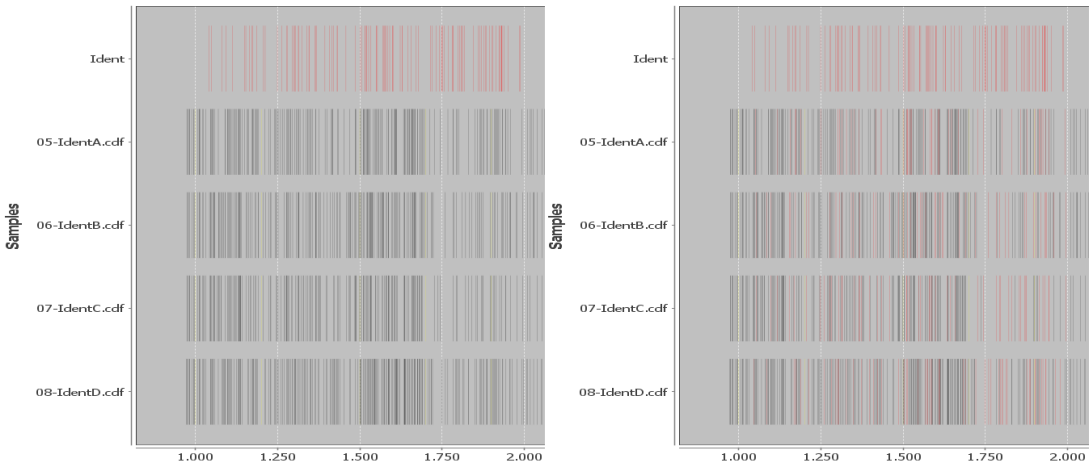


**Figure 2.7 – Overview of the Ident mixes before and after the reverse search (RS).** On the left are Ident mixes before the completion of the RS. On the right, peaks putatively identified as library matches are colored red.

2) As even the optimized RS will make mistakes, the next phase uses the interface for manual revision and correction of putative identifications. The interface can be controlled by either using the mouse to click on the buttons in the RIview or MSview windows or keys and keyboard shortcuts that are more convenient and time efficient. While the specific key bindings are not important, the system is designed so that the left hand controls the MSview and the right hand the RIview. When using "next" or

"previous" in the RIview, metabolites ordered by RI in the metabolite library are selected. The RIview jumps to the RI of a given library metabolite and displays the peaks that were found in the RI window in the samples that were searched. To differentiate peaks actively being displayed in the MSview, all peaks putatively identified as the currently selected library metabolite are colored blue, while other peaks identified as other metabolites from the library are still red, and all others black (Figure 2.8). The user can then use the "Previous samples" and "Next samples" buttons in the MSview to navigate the y-axis, and traverse the peaks of individual samples with the "previous" and "next" buttons in the different rows. When moving in the horizontal direction, the originally suggested peak remains blue, while the actively selected peak turns orange in the RIview, with the spectrum in the middle of each row in the MSview always displaying the actively selected peak (blue, or orange after horizontal movement) (Figure 2.8). To change an assignment, each row in the MSview has an "Accept peak" button, which moves the assignment for the current library compound in the current sample to the orange peak, turning it blue. Once all peaks have been confirmed, and if necessary, changed, the peak group can be accepted by the "Accept group" button in the MSview, which locks them from further modification and marks them as available for export and quantification. Once a peak group is accepted, its peaks are displayed as green when the peak group library compound is selected, and gray when another library compound is selected (Figure 2.9).

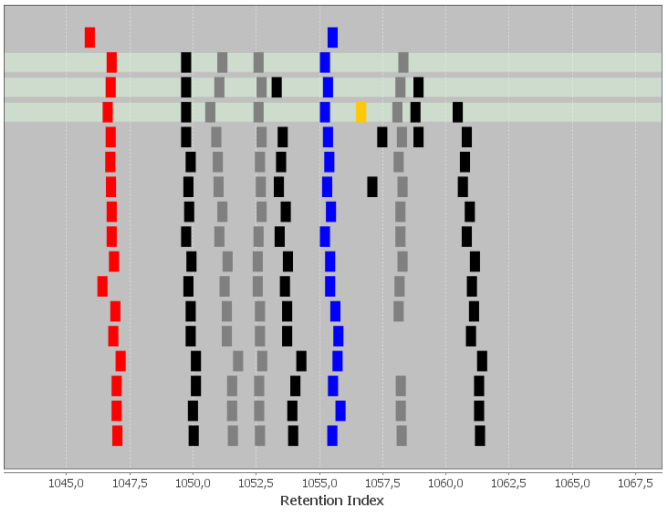


**Figure 2.8 – Different peak colors indicate different stages of processing**. Red peaks are putative library matches identified by the RS. Blue peaks are putative library matches of the currently selected library metabolite, which are simultaneously displayed in the MSview. Horizontal movements within a sample color the currently selected peak orange, while the original suggestion remains blue. Gray peaks have been manually validated as true identifications of a different library metabolite.

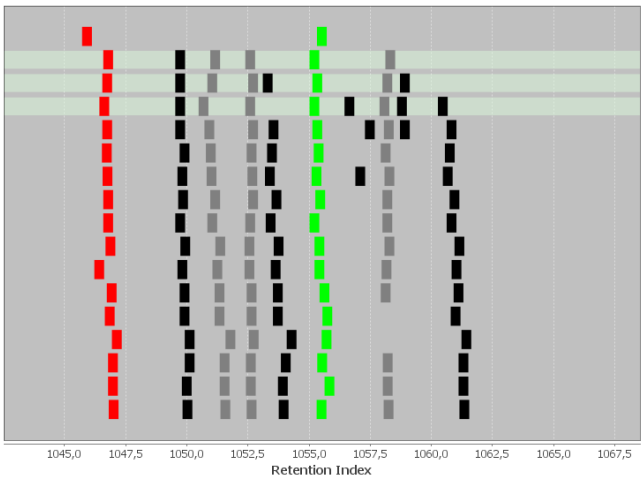


**Figure 2.9 – Green and gray indicate the completion of the manual validation of peak identifications**. Peak groups that have been validated and accepted as true identifications of a library metabolite are colored gray, or if currently selected, green.

Other options of the SILVIA annotation interface include the "Set NotFound" option, which is used when a metabolite is not present in a sample but was erroneously found by the RS, a "Set Found" option, when a peak was not detected by the RS but is present upon manual inspection, "Fuse Left" and "Fuse Right", which allow for the fusion of peaks, an action necessary when ChromaTOF erroneously called a single peak as two separate peaks, and "Duplicate", which allows for the duplication of peaks when ChromaTOF erroneously called two peaks as a single peak or when two metabolites co-eluted. They can be duplicated without affecting their quantification if the two metabolites do not share any quantification masses (see below), which is most often the case.

### 2.3.7 Unknown Peaks/Metabolites

While there are several metabolite libraries with spectral and RI information measured by GC-MS systems freely available online, the only stringent way of positively identifying a peak as a certain metabolite is to have measured the metabolite on the GC-MS setup in use. To validate or create a library, one should buy a collection of metabolites of interest and measure them singly to be certain of their RI and mass spectrum.

The Kempa lab Ident library contains many biologically relevant metabolites and can be extended by using the Golm Metabolome Database (GMD) created at the Max-Planck-Institute in Golm, Germany, which uses a setup very similar to our own (Kopka

et al. 2005). However, the vast majority of peaks detected in a biological sample cannot be confidently identified, either because a similar spectrum does not exist in an available library or because spectrum and RI do not match any library entry well enough.

In general, of about three to five hundred peaks detected in a biological sample, only about ninety can be identified. Considering only these "known" metabolites in downstream analysis leads to an information loss of up to 80%, so that there is great interest in being able to keep track of and quantify unknown peaks. If their spectra and RIs can be recorded, they can be searched for in other unrelated samples, and once identified in the future by manual validation, can be reconsidered in samples where they were tracked as "unknown".

Since there are different levels of confidence in metabolite libraries (highest in the Ident reference, next highest in the library of metabolites that have been measured on our setup (BMD, Buch Metabolome Database), next highest the GMD), SILVIA employs a layered approach to metabolite identification. First, the user annotates samples with the Ident reference, where peak groups of high confidence are "locked" (as described above). Once the entire Ident reference has been searched for, the user repeats the same for the BMD, and then the GMD, where all metabolites identified in the previous, higher confidence library can no longer be searched or edited. The Ident reference therefore searches all peaks, the BMD only those that were not annotated as an Ident metabolite, and the GMD searches only those that are neither Ident nor BMD. After annotating the three libraries, the remaining peaks are considered "unknown".

To create the first unknown library, SILVIA considers all not already annotated peaks and attempts to find peak groups, meaning a collection of peaks in different samples that have nearly identical spectra and RIs. The stringency of these two parameters is high (similarity score of 950 or above), because a library of low quality spectra is not useful. It therefore collects all peak groups that have at least three members with a high spectral similarity based on the cosine similarity measure (another quality control step, because a library spectrum should be an average of several "real" spectra) and thereby creates a putative unknown library. This putative library is then loaded into the SILVIA annotation interface where the user can now manually correct the putative library

entries. Once all peaks of sufficient quality have been annotated in all of the samples, SILVIA calculates an average spectrum for every "locked" peak group, assigns an unknown identification number, and allows for its export into the database msp file format. SILVIA then renames the recorded unknowns appropriately in the project and quantifies them using the Top5 strategy as described below.

After the creation of the initial unknown library, every user can discover new unknowns in new projects. To do so, one first annotates the Ident reference, the BMD, the GMD, and then the most current unknown database. All remaining peaks have never been recorded before, and by following the steps described above, one can then annotate and collect new unknowns into the project and export them in the library format. New unknowns are then simply added to the most current unknown library. Over time as more and more samples of different kinds are measured, a point should be reached where no "new unknowns" are discovered.

To improve the understanding of biology using metabolomics, a key step will be the creation of a near-perfect library, in which all peaks measurable on a given setup are known. The ultimate goal, therefore, is to move all unknown and GMD metabolites into the BMD (meaning that they have been identified and measured on our setup in a purified form), and to include metabolites that are difficult to distinguish into our Ident mixes to achieve unambiguous near-perfect and near-complete coverage of the metabolome of interest. Tracking and quantifying as of yet unknown peaks is a first and very significant step towards achieving that goal, as it lends tremendous additional power to computational investigations of datasets by vastly increasing the number of features that can be used to compare different samples.

### 2.3.8 Quantification Masses

The quantity of a metabolite is reflected by the number of times its fragments are detected in the mass detector of the MS. These mass counts are expressed in units of intensity and together comprise the mass spectrum of the metabolite. On the one extreme, it is possible to quantify metabolite abundance by choosing the intensity value

of a single specific mass out of all masses that result from its ionization. On the other extreme, one could sum all intensity values of all masses of the metabolite.

The masses used to quantify a metabolite need to be specific to the metabolite of interest, as co-eluting compounds that have a mass in common would otherwise lead to an overestimation of its abundance. Additionally, masses at the detection threshold do not robustly represent the abundance of their metabolite as their detection is likely non-linear and prone to stochastic variation. Furthermore, the variation of detection of a single mass is likely to be higher on average than the detection variation of the average of multiple masses. One therefore looks for a compromise in the quantification strategy. The selection of multiple quantification masses decreases technical detection variation and makes the quantification more resistant to near-detection threshold issues and non-specific masses. Nonetheless, one should refrain from including masses that are often measured near the detection threshold as well as those that are not specific for the metabolite of interest, as the inaccuracies of quantification increase with their contribution to the quantification strategy.

ChromaTOF allows the user to manually set a single or multiple quantification masses. However, when having to validate them for five hundred peaks by manual input, it becomes impractical. SILVIA therefore automatically selects the five most abundant (Top5) masses of the library spectrum for each metabolite individually, known or unknown, for quantification. It is also possible to specify a group of masses for each metabolite individually if it is known that masses other than the Top5 are more robust and/or specific. SILVIA calculates the area under the curve of the intensities of each of the Top5 masses for every peak. It recovers the intensities out of the raw files and sums them into a cumulative area representing the metabolite abundance. This “raw area” is saved in the project database for each peak and subsequently multiplied by the CA normalization factor calculated previously to produce the “area”. Both “raw area” and “area” are measured in intensity units and can be exported for downstream analysis.

The Top5 approach has several advantages over the previously employed single-mass quantification strategy in ChromaTOF. Mainly, the quantification is more robust due to the greater number of masses considered. Furthermore, users need not spend any time manually verifying and correcting quantification masses. Datasets generated using

SILVIA are more comparable since every user uses the same quantification masses for every peak and when more optimal masses for individual compounds are determined in the future, the improvement can be integrated centrally to make it available to all other users as soon as possible.

### 2.3.9 Absolute Quantification - Quant Mix

With the relative quantification strategy described in Quantification Masses, one is able to compare the same metabolite measured in different samples. The ultimate goal, however, is to determine their absolute concentrations in the biological samples to be able to consider stoichiometric ratios and have a way to compare measurements not only within a single experimental batch, but also across experiments, time, and machines.

One possible solution is the use of the Quant mix created by Matthias Pietzke and Stefan Kempa. It is a mixture of metabolites in a dilution series of known absolute amounts. The Quant mix is measured at the beginning of an experimental batch and serves as a reference for biological samples measured closely thereafter, thereby allowing for the conversion of their intensity values to absolute concentrations by application of metabolite-specific linear regression equations from the dilution curve of the Quant mix. The procedure, reproducibility, and other technical details of the Quant mix can be viewed in Matthias Pietzke's dissertation at the Free University of Berlin, 2014.

SILVIA allows for the speedy annotation of the Quant mix samples, the determination of the intensities of the contained metabolites as described in Quantification Masses, fits a linear regression to the dilution curve intensities to produce the linear regression equation and provides the absolute quantities of the metabolites in the biological samples of interest in a convenient csv export format.

### 2.3.10 Data Export

After calculating the RIs, normalizing to cinnamic acid values, annotating and creating the Ident reference, annotating the Quant mix and biological samples using the SILVIA annotation interface, and setting quantification masses for all metabolites, SILVIA allows for the convenient export of both relatively and absolutely quantified compounds in csv format. The resulting export is a data matrix with one dimension representing all biological samples of the project, the second dimension listing the identified metabolites, and the content of the matrix being either their relative or absolute abundances in every sample. Further data analysis is then carried out in R.

### 2.3.11 SINQ – Stable Isotope Normalization and Quantification

Due to the mass difference in the carbon isotopes $^{12}C$ and $^{13}C$, mass spectra of isotopologues are distinct (for example, glucose with six $^{12}C$ atoms vs. glucose with six $^{13}C$ atoms), while the metabolites have essentially identical RIs. The additional neutron in $^{13}C$ leads to a +1 mass shift of a fragment that contains one $^{13}C$ atom, a +2 mass shift of a fragment that contains two $^{13}C$ atoms, and so on (Figure 2.10).

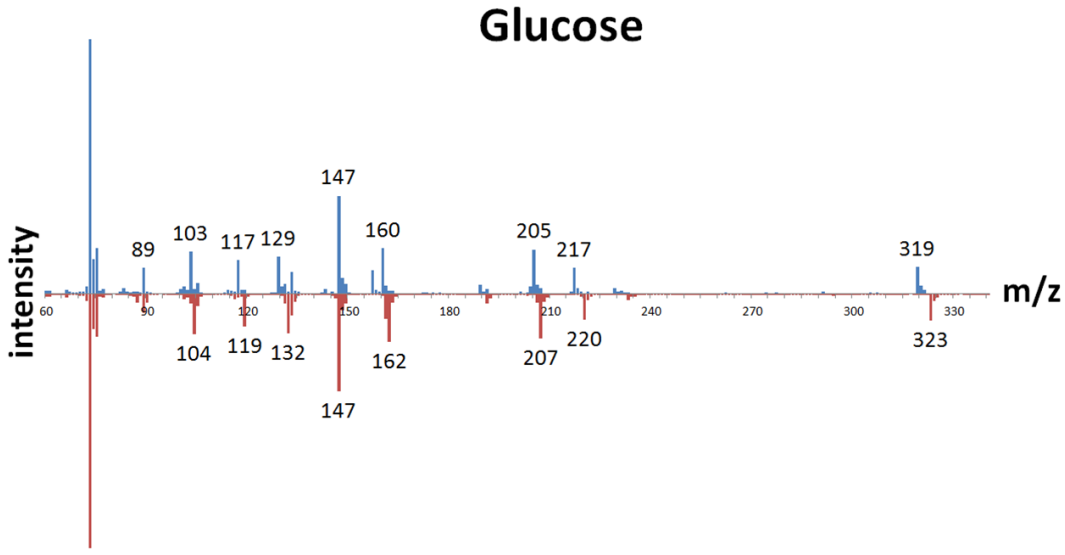


**Figure 2.10 – Mass spectrum differences between $^{12}C$ and $^{13}C$-containing glucose.** Mass shifts of individual fragments (blue = $^{12}C$, red = $^{13}C$) correspond to the number of carbon atoms they contain. Ratios of intensities of mass pairs (for example, 319 ($^{12}C$) and 323 ($^{13}C$)) are used in SINQ to absolutely quantify metabolite abundance. Please note that the fragment of mass 147 represents the derivatization agent and is therefore not shifted. This figure was kindly provided by Matthias Pietzke and only slightly modified.

When adding a $^{13}C$-containing metabolite standard of known concentration to a sample, the ratio of the $^{12}C$ (sample compound) to $^{13}C$ (labeled standard) allows for the calculation of the absolute concentration of the sample compound (Meija & Mester 2008). This strategy is known as isotope dilution and has major advantages both over the CA normalization and the absolute quantification using the Quant mix:

1) Each compound is automatically and individually normalized to its $^{13}C$ standard, which is identical in all samples, requiring no global CA normalization.
2) The quantification is relative to a metabolite measured in the same sample, at the same time, and is not subject to potential technical variation-induced errors of comparing across measurements and time.

This strategy of normalization and quantification was employed on the human serum dataset acquired in collaboration with the group of Prof. Dr. Tobias Pischon described later in this dissertation. SILVIA contains a list of empirically validated $^{12}C$ and $^{13}C$ mass pairs for each SINQ standard. The absolute concentration of the sample metabolite is then calculated by multiplication of the ratio of intensities of the $^{12}C$ and $^{13}C$ mass pair with the known quantity of the $^{13}C$ standard (Figure 2.11). SILVIA automates this calculation of the absolute concentration and the data export for SINQ metabolites in the format described above.

Of particular note to datasets containing $^{13}C$ labeled compounds are the “Fuse left” and “Fuse right” options in the annotation interface only briefly mentioned before. Because $^{13}C$ compounds are slightly heavier than their $^{12}C$ counterparts, their migration through the column is not exactly identical, and the ChromaTOF software has a tendency to split the two metabolites into two separate peaks (called peak deconvolution), which prevents the user from calculating meaningful ratios because the mass pairs used to calculate the ratio are not contained in a single peak and mass spectrum. SILVIA allows a quick resolution of these cases by allowing the user to fuse adjacent peaks into a single one, correcting the well-meant feature of separating non-identical metabolite species.

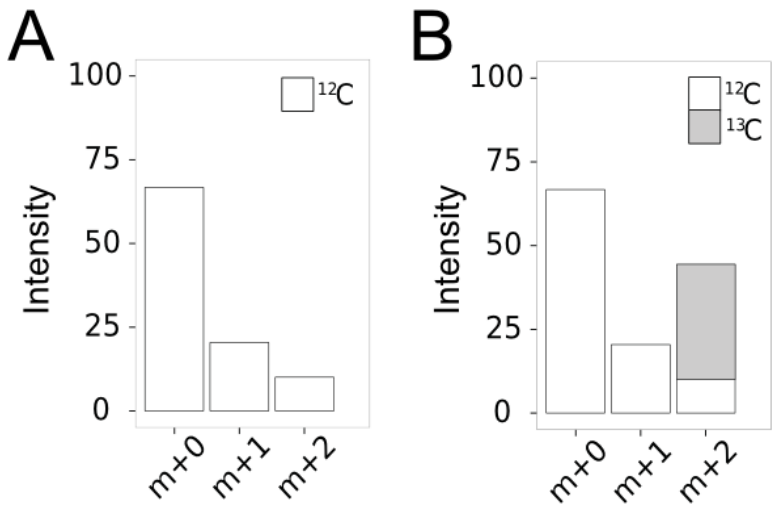


**Figure 2.11 – Calculation of the absolute quantity of a sample metabolite using SINQ.** A) An example of the isotope "flute" of a fragment of a metabolite is shown. The m+0 mass corresponds to the fragment containing only $^{12}C$ atoms. The m+1 and m+2 intensities correspond to the fraction of fragments containing naturally occurring $^{13}C$. B) An example of a fragment spectrum in the presence of a $^{13}C$ SINQ standard. In this example, the empirically determined "mass pairs" are m+0 and m+2, on which the quantification will be based. To calculate the absolute concentration of the sample metabolite, the sum of the intensity of its m+0, m+1, and m+2 fragment is divided by the intensity of the m+2 fragment corresponding to the $^{13}C$ SINQ standard. The percentage of naturally occurring m+2 intensity relative to the m+0 fragment from the sample metabolite is determined from the fragment flute in either Quant or Ident mix samples (which do not contain the SINQ standards) and is then subtracted. The absolute quantity is then calculated by multiplication of the obtained ratio by the absolute amount of $^{13}C$ SINQ standard added to the sample. This figure is a modification of a figure kindly shared by Matthias Pietzke and Christin Zasada.

## 2.4 Discussion

The data processing and visualization modules contained in SILVIA address the issues of handling large data volumes, identifying new and tracking unknown peaks, as well as providing the computational tools to efficiently use several methodological developments. Whereas previously a smaller fraction of all available information from experiments was recovered and more time than was necessary to measure the samples on the GC-MS was required to do so, SILVIA has sped up the data processing so that the processing of the torpor screen described below, whose measurement required three weeks, was in its entirety completed within four days, for the first time considering every single peak, known or unknown (Figure 3.4). SILVIA has realized the full

potential of the Ident and Quant mixes, and incorporates algorithms to handle both pSIRM (not described) and SINQ experimental setups, the data required for which had to previously be manually extracted and processed. It provides for the first time the means for in-depth analysis of a dataset as large and complex as the torpor screen, and in combination with the incorporation of the SINQ methodology, has readied our technological platform to advance beyond basic research into the realms of diagnostic medicine that is characterized by both large data volume and the need for high reproducibility, robustness, and comparability over a large time span.

The development of SILVIA, however, has not yet reached its full potential. It is now equipped with modules optimized for manual inspection and correction, with little emphasis having been placed so far on true automatization. It is my goal in the near future to use machine learning and artificial intelligence approaches to improve peak calling and identification of metabolites so as to further decrease the amount of time required for data processing.

For example, the RS currently implemented uses a cosine similarity measure and RI-dependent penalties to compare library and sample metabolites and finally provides a score of confidence of the identification. This approach is identical for all metabolites, although different metabolites show differences in RI variation and mass spectrum quality. To consider the metabolite specific GC-MS behavior and thereby create a metabolite-specific RS, I plan to train logistic regression and/or neural net classifiers for every library metabolite with validated training data from a variety of biological samples. This requires a large manually verified labeled dataset (peaks that correspond to the metabolite in question and those in the surrounding that could be false positive matches). With the development of SILVIA and its use in the Kempa lab, hundreds of biological samples from cell culture and animal experiments have been processed in the last months, providing sufficient training data to create metabolite-specific artificial intelligence classifiers in the near future.

The SILVIA modules now in existence will be used for extensive troubleshooting of these classifiers and will allow the user to manually validate and correct inaccuracies. The final goal is to reach a state in which a blood metabolome, and eventually any metabolome, can be confidently processed without human supervision in its entirety.

This will not only decrease processing time but also make the technology more available to non-specialists. It is possible that GC-MS and other omics systems will be used on a daily basis in hospitals around the world to aid in diagnostics, and it is my goal to contribute significantly to this future by creating automized data-processing systems. Apart from the clinic, the less time researchers will have to spend on technical details and data processing, the more time will be available for biological interpretation of acquired data, the step where medically relevant knowledge is created. Removing the bottlenecks of data processing should shift the proportion of time researchers spend on their projects towards the extraction of biological mechanisms from metabolomic datasets, thereby increasing the rate of knowledge acquisition.

# 3. Metabolic Changes During Daily Torpor in Mice

## 3.1 Introduction

### 3.1.1 Daily Torpor – A Hypometabolic State

Daily torpor is a physiological hypometabolic state similar to hibernation that serves to conserve energy by drastically lowering the core body temperature (CBT), the maintenance of which is especially costly for small animals with a high surface to volume ratio. Whereas hibernation is employed to bridge the cold and food scarce winter and can last for months, intermitted by only short periods of rewarming, daily torpor is observed in many small mammals and birds and occurs during the daily resting phase, usually lasting between a few and ten hours. In hypometabolic states, the metabolic rate (MR), CBT, heart rate (HR), breathing rate (BR), and blood pressure (BP) drop precipitously (Geiser 2004; Swoap 2008; Morhardt 1970). Example values for daily torpor can be viewed in Table 1.

| **Species** | **CBT** normal [°C] | **CBT** Torpor [°C] | **MR** normal [ml O2/(gh)] | **MR** Torpor [ml O2/(gh)] | **HR** normal [bpm] | **HR** Torpor [bpm] | **BP** normal [mmHg] | **BP** Torpor [mmHg] |
|---|---|---|---|---|---|---|---|---|
| *Mus musculus* | 37.4 | 19 | 1.47 | 0.3 | 612 | 158 | 118.6 | 62.3 |

**Table 1.** Example values of core body temperature (CBT), metabolic rate (MR), heart rate (HR), and systolic blood pressure (BP) in the laboratory mouse *Mus musculus* (Hudson & Scott 1979; Swoap & Gutilla 2009).

The torpor cycle consists of an entry phase during which the CBT slowly and MR quickly decrease, a maintenance phase during which the CBT and MR stabilize at their minimal value, and an arousal phase during which the animal returns to euthermia, which is accompanied by a stark increase of the metabolic rate before CBT rises (Swoap 2008).

The physiological changes observed in daily torpor are greatly exacerbated in hibernation, where CBTs of below 0°C have been reported for the arctic ground squirrel (*Urocitellus parryii*), periods of apnea can last for more than an hour, and metabolic rates can drop to well below 5% of awake animals (Geiser 2004; Barnes 1989). While

hibernation is arguably the most extreme of hypometabolic states, and some might argue therefore the most interesting, it is a diverse phenotype. Most ground squirrels that have been studied maintain their deep torpor CBT at or below 5°C, whereas bears are known to hibernate at a CBT of above 30°C (Tøien et al. 2011). Their relative savings differ as well, and the reasons for the differences in magnitude of CBT are under debate. Nonetheless, it is a reasonable assumption in the field of hypometabolic research that the essential underlying physiological mechanisms, although the magnitude of their expression might differ between species, are likely very similar between the different forms of hibernation and daily torpor. The entry into, maintenance of, and exit from hypometabolic states represent a controlled alteration of nearly all measureable functions of mundane physiology, and the understanding of many of them would be relevant to some of the most pressing medical issues of the modern world. Known neurological and molecular mechanisms will be introduced next, before describing but a subset of observations that justify the interest in hypometabolism of medically-oriented research.

### 3.1.2 Neurological Regulation of Hypometabolic States

Crude ablation studies in the brain have provided evidence for the involvement of three regions of the hypothalamus in hibernation and torpor, corresponding to three defining characteristics of hypometabolic states:

1) Suprachiasmatic nucleus (SCN) - Timing of occurrence
2) Preoptic area/anterior hypothalamus (POA/AH ) - CBT regulation
3) Arcuate nucleus (ARC) - Energy homeostasis

The SCN in the hypothalamus contains the "master clock" of the body, in which the transcription and translation of so-called clock genes function in negative feedback loops as a timer. While all other tissues, for example the liver, have their own clocks, the SCN synchronizes the body through autonomic and humoral signaling, and is itself set by the light-dark cycle, called the "Zeitgeber" (Radziuk 2013). While the SCN is involved intricately in the circadian rhythm of the sleep-wake cycle among other physiological mechanisms, it has also been shown to play a crucial role in the regulation of hibernation. When radiofrequency-induced lesions were applied stereotaxically to ablate the SCN in golden-mantled ground squirrels (*Spermophilus lateralis*), the

number of torpor bouts during hibernation increased by 159%, the total time spent in hibernation by 58%, and periodic arousals from torpor were 47% longer. Some squirrels stayed in hibernation for almost two years, clearly showing the importance of the SCN in the temporal control of hibernation (Ruby et al. 1996). However, denervation of serotonin fibers innervating the SCN seemed to have no effect whatsoever on daily torpor in Djungarian hamsters (*Phodopus sungorus*) (Ouarour et al. 1995). Whether the SCN therefore only plays a role in seasonal hypometabolic states and is unimportant for daily torpor induced by food restriction is as of yet unresolved. Nonetheless, torpor occurs only during an animal's inactive phase, making its involvement, even if more subtle, likely (Geiser 2004).

The POA/AH is critically involved in euthermic CBT regulation and is said to contain both temperature-sensitive neurons, responsible for sensing local brain temperature, as well as neurons that integrate brain temperature information with the temperature sensed in peripheral tissues and the skin to coordinate cold- or heat defense mechanisms such as sweating, shivering, vasoconstriction or vasodilation, and behavioral adaptations (Morrison & Nakamura 2011). Electrolytic POA/AH lesions were shown to be lethal after eleven to twelve days in hibernation in thirteen-lined ground squirrels (*Citellus tridecemlineatus*), presumably due to an inability to arouse from low CBTs (Satinoff 1967). Despite the caveat that crude ablations in the brain are difficult to interpret due to the high probability of damaging neuronal extensions originating in other brain regions, considering the known role of the POA in euthermia maintenance, it is very likely that the POA neurons play a crucial role in the CBT regulation during torpor as well.

Repeated postnatal monosodium glutamate (MSG) treatment produces neuronal degeneration primarily in the ARC, which integrates peripheral leptin, insulin, and other metabolic signals to regulate food intake, energy expenditure, and more generally, energy homeostasis (Könner et al. 2009). Upon MSG ablation of the ARC in Siberian hamsters (*Phodopus sungorus*), a reduced incidence of photoperiod-dependent torpor was observed, a difference that persisted even after body weight normalization through food restriction (Pelz et al. 2008). ARC ablation also prevents mice from entering daily torpor upon food restriction (Gluck et al. 2006).

### 3.1.3 Molecular Mechanisms of Daily Torpor

Recently, molecular mechanisms underlying the torpor phenotype have been elucidated, the strongest evidence provided by use of genetically modified mice in combination with pharmacological studies.

Leptin is a protein hormone that is secreted by white adipose tissue (WAT) in direct proportion to WAT abundance and has been shown to be involved in energy expenditure and food intake regulation (Friedman & Halaas 1998; Zhang et al. 1994; Flier 1998). It signals to several sites in the body, among them neurons in the ARC (Könner et al. 2009). Its involvement in torpor was first demonstrated by the observation that *ob*/*ob* mice, which contain a mutation in the leptin gene, spontaneously enter torpor despite their vast fat stores and without prior food restriction (Webb et al. 1982). Furthermore, continuous application of leptin prevents or blunts torpor responses in Siberian hamsters, establishing low leptin levels as a required permissive signal for torpor entry (Freeman et al. 2004). Other metabolic phenotypes, like that of the Farnesoid X nuclear receptor knock-out mouse, have been linked to torpor susceptibility by altering leptin levels (28). Similarly, dopamine β-hydroxylase knock-out mice cannot synthesize norepinephrine (NE) and epinephrine (Epi), two of the major neurotransmitters of the sympathetic nervous system (SNS) that controls a variety of homeostatic functions in counterbalance with the parasympathetic nervous system. The knock-out mice were unable to enter torpor, and their phenotype traced to a peripheral NE requirement for torpor induction signaling through the β3-adrenergic receptor whose activation initiates lipolysis in WAT and the inhibition of leptin release (Swoap et al. 2006; Swoap & Weinshenker 2008). Without the permissive signal of low circulating leptin indicating energy shortage, mice appear unable to enter torpor.

The downstream effects of low leptin levels are entirely unclear in the context of hypometabolic states. A first step towards enlightenment has been taken by a recent study of the G protein-coupled orphan receptor GPR50, which is expressed in the dorsomedial nucleus (DMN) of the hypothalamus and in tanycytes, which line the third ventricle in direct contact with the cerebrospinal fluid (CSF). GPR50 knockout mice require less food restriction to enter torpor. While GPR50 expression is induced by leptin, leptin administration was unable to blunt the strong torpor response. GPR50 is therefore likely downstream of leptin signaling in the DMN (Bechtold et al. 2012).

Leptin, however, is not the sole metabolic signal regulating torpor entry. A-ZIP/F-1 mice, which through a genetic ablation have essentially no WAT and like *ob/ob* mice, low leptin levels, much more readily enter torpor than wildtype controls. However, this phenotype was not rescued by leptin administration, indicating that while low leptin levels are required for torpor induction, they are not sufficient. The animals rely on more than just low leptin levels to detect energy deficiencies and to make the decision to enter torpor, which is further supported by the simple fact that *ob/ob* mice are not in torpor at all times (Gavrilova et al. 1999).

Following the evidence of elevated ghrelin levels during torpor (a hormone involved in food-intake regulation and satiety), Gluck and others found that peripherally administered ghrelin significantly deepened torpor bouts in mice (Gluck et al. 2006). Upon ARC ablation by MSG, where many ghrelin receptor-containing neurons reside, mice failed to enter torpor at all and ghrelin administration had no inductive effect. The two major pathways regulating food intake and energy homeostasis in the ARC are the neuropeptide Y (NPY), representing orexogenic signaling, and the anorexigenic α-melanocyte stimulating hormone (α-MSH) pathways. Both $A_y$ mice, defective in the α-MSH pathway, and *npy -/-* mice showed a blunted torpor response. Ghrelin had its torpor deepening effect only in the $A_y$ knock-out mice, indicating that the torpor exaggerating effect of ghrelin is signaled through the NPY population in the ARC. Ghrelin is the second metabolic hormone besides leptin significantly involved in torpor, both signaling at least in part through ARC neuronal pathways.

To my knowledge, all reported phenotypes of altered torpor are of metabolic origin. Uncovering the metabolic changes that occur before and during torpor to discover the crucial signals enabling its induction, progression, and termination, are therefore elemental for its understanding.

### 3.1.4 Metabolic Changes in Daily Torpor

Since metabolic rate anticipates the fall of CBT, much research has been aimed at the identification of mechanisms of metabolic suppression that are independent of low body temperature effects during torpor entry.

Several studies have found respiratory adjustments in both hibernators and torporic animals that retain carbon dioxide and thereby cause the acidification of their blood and tissues to varying degrees of severity (P. E. Bickler 1984; P. Bickler 1984; Nestler 1990b; Nestler 1991; Nestler 1990c; Nestler 1990a). This acidosis is thought to cause metabolic suppression to differing degrees in different tissues, but mechanistic explanations are often variable, likely resulting from the use of many different model organisms. Observations most comparable to daily torpor in mice will be considered in detail in the discussion of this section. As a side note, brain acidosis is hypothesized to reduce the temperature set-point in the hypothalamus, providing a potential explanation for the controlled decline in body temperature during hibernation and torpor entry (Matsumura et al. 1987; Schaefer & Wünnenberg 1976; Wright & Boulant 1985).

Another avenue of investigation is the characterization of enzyme activity of tissue isolates of hibernating and control animals. In this way, mitochondrial activity has been characterized in tissues isolated from torporic and non-torporic animals. Different studies generally span the entire interpretive range of unchanged, decreased, or increased enzyme or mitochondrial activities. Again, the disagreements might stem from different model organisms and sampling time points, but likely also from different biochemical preparations of enzymes and mitochondria. The general disagreement was summarized in a comprehensive review (Staples & Brown 2008). Observations made in model organisms most relevant to daily torpor in mice will be considered in detail in the discussion.

Even if the evidence for particular enzyme activities or overall mitochondrial activity were in agreement, the interpretation of the commonly used assays is arbitrary. Enzyme productivity is not only determined by its state of activity in a purified context, but influenced by localization, substrate abundance, and other *in vivo* factors. Similar to the low correlation between mRNA and corresponding protein abundance, *in vitro* enzyme abundance or activity does not necessarily correlate with *in vivo* reaction rates (Schwanhäusser et al. 2011). Rather, the assays measure a part of the cellular potential to carry out reactions, rather than the actual phenotype, as a fully activated enzyme without substrate is biologically inactive.

Metabolomic analysis, in contrast, provides information about the actual abundance of metabolites and might allow the determination of pathway activity by inference. Only a few investigations have attempted metabolomic analysis of hypometabolic states by studying the hibernation phenotype, analyzing the metabolic composition of the liver using NMR and LC-MS, and blood serum using LC-MS or a combination of LC-MS and GC-MS (Nelson et al. 2009; Nelson et al. 2010; Serkova et al. 2007; Epperson et al. 2011).

Serkova and others used NMR on liver samples taken from thirteen-lined ground squirrels that were either summer active, in the late torpor phase when CBT was lowest, or in the entry phase of one of the hibernation torpor bouts (Serkova et al. 2007). They identified forty-three metabolites, thirty-six of which differed in at least one of the three phases. They found glucose, lactate, alanine, and succinate decreased, and the ketone body β-hydroxybutyrate to be increased in the two torpor phases when compared with summer active controls. Additionally, betaine and glutamine appeared highest in the late torpor phase, whereas the lipid classes phosphocholine and phosphatidylcholine were decreased. They concluded that an accumulation of ammonia is buffered by a production of glutamine, carbohydrate metabolism is substituted by lipolysis and ketone consumption, and that phospholipids may serve as a source for betaine to increase osmotic protection.

In a second study using LC-MS on liver tissue collected in entry, deep, exit, and interbout arousal states, as well as a summer control, fourteen metabolites were identified (Nelson et al. 2009). Four of these metabolites were carnitine esters that were all decreased in entry and deep torpor, similar to tryptophan, phenylalanine, and tyrosine. Inosine, a purine metabolism intermediate, and uridine were also decreased in deep torpor, but during the interbout arousal recovered to levels similar to the summer controls. Flavin nucleotides were decreased during entry and deep torpor, but elevated during exit and the interbout arousal when compared to the summer animals, indicating a general correlation with metabolic rate. While cholesterol sulfate (in the NMR study, cholesterol was significantly increased), sphingosine, and a lipid were decreased in the deep, exit, and interbout arousal phases, the fatty acid hexadecanedioic acid was the only measured metabolite accumulating during the deep torpor phase, consistent with fatty acid, lipid, and triacylglycerol accumulation described in the previous NMR study.

Although the two studies gave general indications about liver metabolism in hibernation, it is difficult to draw detailed conclusions from only fourteen metabolites in one study, or forty-three measured in only two torpor phases in the other.

The same group of investigators also performed an LC-MS study on blood serum in the same squirrel species in the deep and interbout arousal phases, and active spring squirrels, finding significant changes in around one hundred putative metabolites, of which they validated twenty-five (Nelson et al. 2010). They found carnitine esters to be decreased during torpor, as previously observed in the liver, just like tyrosine and methionine, all of which recovered to near spring active levels in the interbout arousal. However, pantothenate was increased four-fold in the deep phase compared to the other stages. All fatty acids measured showed a trend of accumulation during the deep phase, with interbout arousal levels elevated compared to the spring control.

The most comprehensive metabolomics study was performed on blood serum using both GC-MS and LC-MS technologies and measured in cooperation with a company specializing in metabolomic analysis (Epperson et al. 2011). Thirteen-lined ground squirrels were sampled in seven stages, identifying a total of two-hundred-thirty-one compounds. The study defined a biomarker signature for hibernation torpor bouts and provided evidence that interbout arousals might be required in hibernation to reestablish homeostatic levels of several metabolites that either accumulate or are depleted during deep torpor, but whose levels return to pre-torpor abundance before entering the next torpor bout. The most significant observation was an accumulation of modified amino acids in the late phase that were rebalanced in the interbout arousal. Similarly, a large group of metabolites showed the opposite pattern, including glycine, methionine, and threonine. Several metabolites increased specifically in the exit phase, among them fatty acids, glycerol, and succinate.

The authors focused their discussion on modified amino acids, antioxidants, and different free fatty acid species. However, none of the four metabolomic studies was able to provide mechanistic insight from metabolite abundances or has investigated the essential parts of energy metabolism in detail: glycolysis, the TCA cycle, the urea cycle, and crucial pathway intermediates thereof that might provide information about the activity and direction of metabolic pathways. It is also of note that none of the studies

have investigated more than a single tissue at the same time, and only one study contained all relevant time points to be, in principle, able to deduce mechanisms of the progression of metabolic changes through torpor. The meaningful mechanistic interpretation of this last study was complicated by the fact that blood is not a single active tissue, but the connection between many.

I therefore decided to investigate the metabolome of mice in blood serum, CSF, liver, muscle, and WAT in all six phases encompassing the entire torpor phenotype using a GC-MS setup that has been optimized to address central carbon metabolic pathways. The study was designed with two purposes in mind:

1) To provide a metabolic atlas of critical tissues and body fluids throughout torpor so as to elucidate the mechanisms underlying metabolic changes driving the entry into, progression of, and exit from daily torpor in mice.
2) To obtain a metabolomic dataset of both organs and blood simultaneously sampled throughout a process in which strong metabolic changes occur in order to gain first insights into the reflection of organ metabolic states and their interactivity in the blood metabolome.

While the second purpose reflects the overall theme of this dissertation, researching hypometabolic states is not a mere academic exercise, as it may well be of aid in alleviating a variety of medical complications.

### 3.1.5 Clinical Implications of Hypometabolic Research

As BR and HR decrease during the entry phase of torpor, less oxygen is distributed throughout the body, carbon dioxide concentrations increase, and the blood and tissues acidify to varying degrees as a consequence (P. E. Bickler 1984; Nestler 1990a; Nestler 1990b). Due to the lower circulation rate, nutrient availability decreases and cellular waste products are removed more slowly. All of these changes are reversed quickly during the return to euthermia, in which high breathing rates and a fast return to metabolic activity occur before the return to euthermic circulation, without ill effect on the animal (Carey et al. 2003). This cycle observed in natural hypometabolic states is analogous to the ischemia-reperfusion injury cycle that occurs in humans. In this pathology, blood supply to part of an organ is first restricted or blocked for a time

(called ischemia) and then reinstated (called reperfusion). Ischemic damage is due to nutrient/oxygen deprivation and waste/reactive oxygen species accumulation, while reperfusion injury results, from among other mechanisms, an overreaction of the immune system to the blood-deprived tissue (Datta et al. 2013; Sanderson et al. 2013; Schofield et al. 2013). The number one and two causes of death in middle- to high-income countries, ischemic heart disease and stroke/cerebrovascular disease, are caused by ischemia and reperfusion injury (WHO, http://who.int/mediacentre/factsheets/fs310/en/, March 2014).

Importantly, studies have shown an increased resistance to ischemic-reperfusion injury damage of animals undergoing hypometabolic states (Drew et al. 2001). These beneficial effects have been attributed to increased resistance to nutrient and oxygen deprivation, as well as the lack of an overreaction of the immune system during the waking phase of the torpor cycle (Bouma et al. 2012). Induced hypometabolism may therefore not only benefit ischemia and reperfusion injury patients, but could be applicable for many other kinds of physical trauma in which tissue injury results in similar circulatory problems, including, but not being limited to, surgical procedures that are performed on millions of patients worldwide every year (Aslami & Juffermans 2010).

Furthermore, a group of autoimmune diseases have in common the underlying phenotype of an immune system that is overactive, either causing unwarranted inflammation or erroneously recognizing its own body as foreign. Examples of mistakenly initiated immune responses are the progressive destruction of the myelin sheath in multiple sclerosis, the chronic inflammation of cartilage in joints in rheumatoid arthritis, or the continuous damaging of the digestive tract in Crohn's disease, among many others (Bandzar et al. n.d.; Broux et al. 2013; Pablos & Cañete 2013). Debilitating dermatological diseases like psoriasis or atopic dermatitis are also attributed to deregulated immune responses and afflict 1-4% of the general population (Saito 2005; Parisi et al. 2013). Gaining an understanding of how the immune system in the arousal from torpor is repressed to prevent reperfusion injury might allow for a more physiologic suppression of an overactive and misguided immune system in several autoimmune diseases in humans.

In addition, tumor-preventative effects, decreased susceptibility to induced and spontaneous lung tumors, and suppressed mitotic activity have been attributed to daily torpor in mice (Koizumi et al. 1992; Koizumi et al. 1993; Koizumi et al. 1996). While the molecular mechanisms are yet to be elucidated and their interpretation complicated by the simultaneous occurrence of energy restriction and torpor, it is possible that the metabolic change to fat metabolism during food restriction leading up to torpor plays a significant role. In fact, the prescription of a ketogenic diet, which minimizes carbohydrate intake and increases the consumption fat, leads to an accumulation of ketone bodies in the blood and is said to "starve" tumors, most of which are notoriously glucose-dependent (Hamanaka & Chandel 2012; Klement 2013; Simone et al. 2013; Woolf & Scheck 2014). Ketone bodies have been attributed cytoprotective effects as well as significant signaling functions and therefore might contribute to an increased resistance to cancer observed in torporic mice (Newman & Verdin 2014; Maalouf et al. 2009). Whatever the mechanistic details, torpor might provide new insights into mechanisms of tumor suppression.

Due to the wide theoretical applicability of beneficial effects observed in hypometabolic states, a major effort in hypometabolism research has been directed at the identification of signals that mediate torpor entry. It is the hope that in the future, humans will be able to enter hypometabolic states at will to protect themselves from ischemic injury and reperfusion damage, suppress their immune system when necessary, extend their lifespan, and facilitate spaceflight to distant planets (Bouma et al. 2012).

So far, most investigations have been focused on the mechanisms of torpor entry only, which are often reduced in complexity to mechanisms of metabolic suppression only, with less emphasis on mechanisms of arousal, which appears to be assumed to simply "happen" once the metabolic suppression is alleviated.

The first evidence of the existence of torpor-inducing molecules came from a report claiming that blood from a hibernating animal was able to induce hibernation in another, leading to the concept of a hibernation induction trigger, or HIT. The results, however, were not reproducible and contested heavily (Dawe & Spurrier 1969; Dawe et al. 1970; Wang et al. 1988; Bouma et al. 2012).

More recently, hydrogen sulfide ($H_2S$), which is known to be able to inhibit mitochondrial respiration by competing with oxygen in binding to cytochrome c oxidase, was used to cause a reversible inhibition of metabolism. $H_2S$ treatment of mice was tried in various concentrations and led to a metabolic rate decrease of 90% and a concurrent CBT decrease to about 2 °C above ambient temperature, reminiscent of that observed in daily torpor (Blackstone et al. 2005). While the results are reproducible in mice, reports in larger animals are less consistent and represent an area of active research (Haouzi et al. 2008; Li et al. 2008; Simon et al. 2008). While $H_2S$ holds promise for metabolic suppression, it is quite obviously artificial and has little to do with natural hypometabolic states other than the manifestation of their ultimate symptoms.

A group in Texas identified adenosine-monophosphate (AMP) in blood as a marker for torpor. Injection of AMP decreases CBT and induces transcription of makers associated with the circadian rhythm and torpor phenotype. Since the involvement of the circadian clock in the SCN is known to be crucial in hibernation, AMP was proposed as a compound of importance in inducing torpor physiologically (Zhang et al. 2006). In direct response, a paper with the title of "AMP does not induce torpor" was published a year later, using a series of experiments to show that adenosine-diphosphate (ADP), adenosine-triphosphate (ATP), and adenosine were as effective in lowering the CBT of mice as AMP. Furthermore, the rate of CBT decrease in response to any of the adenine nucleotides was twice that observed in natural torpor, while the heart rate dropped to below natural torpor levels within a minute instead of over a period of about thirty-five minutes. Finally, the AMP response was observed even in animals that cannot enter torpor because of an ARC ablation, and could be blunted by pharmacologically blocking adenosine receptors, further questioning the specificity of AMP in the natural torpor phenotype (Swoap et al. 2007). In a follow-up paper, the same authors further investigated the role of adenosine receptors, and were able to show that adenosine signaling is required for torpor expression, a central adenosine signaling block provoking premature torpor exit (Iliff & Swoap 2012). Similarly, adenosine stimulation in the brain was found to play a significant role in hibernation in arctic ground squirrels (Olson et al. 2013). While AMP is elevated during daily torpor and adenosine signaling

of importance, it appears that neither is involved in the triggering of the induction of torpor under physiological conditions.

Of considerable current interest is the naturally occurring thyroid hormone derivative 3-iodothyronamine, also referred to as T1AM. It was initially identified as an agonist of the G protein-coupled trace amine receptor TAR1, whose administration induced strong CBT and heart rate decreases (Scanlan et al. 2004; Panas et al. 2010). It has recently been used to provoke sustained mild torpor for up to two days by administering multiple doses in laboratory mice with resulting CBTs between 28 and 33 °C, which are target temperatures for human patients in trauma surgery (Ju et al. 2011). Its role in the natural progression of torpor, however, is unstudied.

In conclusion, while some factors are known to inhibit metabolism and decrease CBT, an endogenous ligand inducing natural hypometabolism like daily torpor has not yet been identified. By metabolomic analysis of different tissues, blood serum, and the CSF, I hoped to obtain candidate molecules that peaked before and/or during the entry or exit phases of torpor, thereby potentially signaling the induction or reversal of a hypometabolic state. Future studies could then attempt to induce daily torpor by supplication of such a factor in mice and other organisms on the road to metabolic rate control in humans.

### 3.1.6 Daily Torpor as a Model System

The hypometabolic states of daily torpor and hibernation are closely related and may therefore have the same or very similar underlying molecular mechanisms. I selected daily torpor as my model system for three principal reasons: First, hibernation studies commonly trap wild animals, not only restricting the line of research to particular areas of the world, but also requiring considerable time to be spent in the field, very likely necessitating expert knowledge as to the handling of wild animals. Secondly, even inbred mice display large biological variation that need not be increased by sampling from unstudied, potentially very variable and ever-changing wild populations to unnecessarily complicate analysis. Thirdly, mice are a widely used model system, allowing for the use of all the genetic tools and already created knock-out mice to study the molecular mechanisms of torpor, allowing for the validation of hypotheses arisen from metabolomics datasets and other mechanistic studies.

## 3.2 Materials and Methods

### 3.2.1 Animals and Experimental Design

All mice were females of the C57/Bl6-j mouse strain provided by Charles River. Mice were ordered at the age of seven weeks, kept in quarantine for four weeks, and then acclimated for three weeks to the 30 °C housing temperature in a customized Tissue Culture incubator (KB720, Binder GmbH, Germany) to allow for adequate air ventilation. The mice were provided with food and water *ad libitum* (Ssniff, Germany, Art. No. V1124-300) and maintained on a twelve hour light/dark cycle (light from 06:00 to 18:00 hours). At the start of each experiment, mice were transferred to custom cages built by the MDC workshop, the ceilings of which consist of a thin metal grid that can easily be removed by a sliding mechanism, allowing the infrared camera to monitor the surface temperature of up to twelve mice simultaneously (Figure Setup). To initiate torpor, food restriction was carried out at 18:00 hours. Twenty-four hours later the ambient temperature was dropped to 17 °C. Mouse surface temperatures were monitored online using the InfraTec Irbis3 software, and mice removed at desired sampling time points throughout the torpor process. All mouse housing, care, and experiments were registered with and approved by the appropriate federal authorities (State of Berlin; TVV042911; G0051/11).

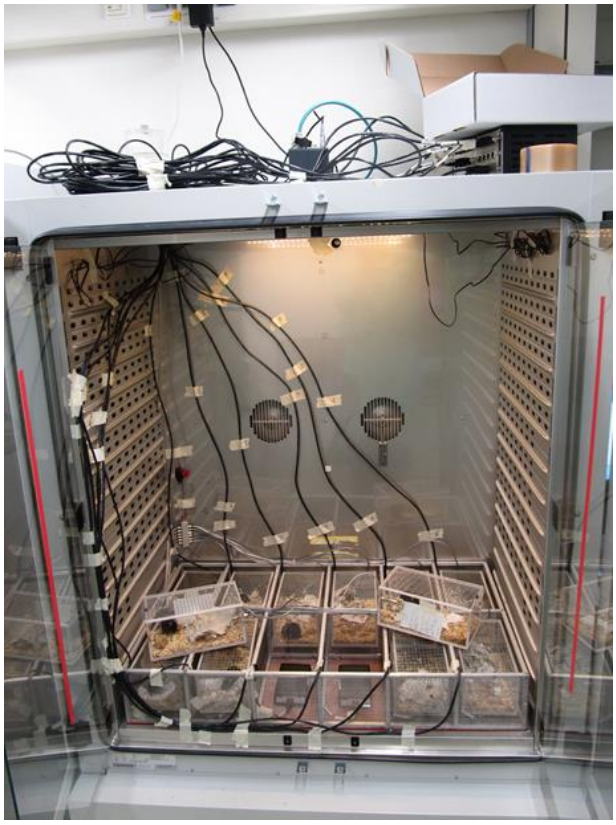

**Figure Setup – The experimental setup for the study of daily torpor in mice**.
A Binder tissue culture incubator was modified to allow for air exchange (not visible), light/dark cycling, equipped with an infrared camera (top middle) and a grid-system of custom mouse cages that allowed for monitoring of mouse body surface temperatures. Also visible, but not employed in this study, is a telemetry system to record core body temperature.
(eigene Abbildung, Henning Kuich, 2011)

### 3.2.2 Infrared Surface Body Temperature Monitoring

The infrared camera VarioCAM® hr was obtained from InfraTec (Dresden, Germany). It was mounted in the modified Binder Tissue Culture Chamber. Mouse surface temperatures were monitored online to determine torpor stages using the InfraTec Irbis3 software supplied with the camera.

### 3.2.3 Sample Collection

Mice were collected at seven distinct time points, consisting of a control "baseline" phase, a "pre" torpor phase, the "entry", "deep", and "exit" torpor phases, and after having completed a bout of torpor and recovered euthermic body temperatures ("post"). In the baseline phase, mice were at 30 °C ambient temperature and had food and water available *ad libitium*. The pre phase was sampled 2-3 hours prior to the expected time of torpor entry. Entry was defined as a surface temperature that was declining and below 23 °C. The deep phase was defined as surface temperatures below 20 °C for over 2.5 hours. The exit phase was defined as a rising surface temperature, just having reached 23 °C. The post phase was collected 1 to 1.5 hours after surface temperatures recovered to pre phase levels and animals were observed to be physically active. All mice were anaesthetized in a box containing isofluorane until unresponsive to a tail

pinch. First, CSF was extracted after having removed an area of fur in the neck by inserting a small butterfly needle between the spinal canal and the base of the mouse skull. Immediately after CSF collection, the mouse was killed by cervical dislocation. Blood was taken from the neck wound after decapitation, and immediately spun at 7,000 rcf at 4 °C in a tabletop centrifuge for 90 seconds to obtain blood serum. Organs were dissected after opening the body cavity, the WAT being of the epididymal kind, the muscle being sampled from the quadriceps femoris. The average time of tissue collection after isofluorane anaesthetization was approximately ninety seconds.

### 3.2.4 Metabolite Extraction

Liver, muscle, and WAT were pulverized using the BioPulverizer (Biospec Products, Cat. No. 59012N) in a frozen state. Of the resulting tissue powder, 50 mg were suspended in 1 mL ice cold MCW (5:2:1, methanol, chloroform, water, respectively), likewise 5 µL blood and 1.5 µL CSF were suspended in 200 µl MCW, and shaken at 4 °C for one hour. Next, half the volume of MCW of Milli-Q-filtered water (EMD Millipore, USA) was added, and samples were shaken for another 30 minutes at 4 °C. They were then centrifuged at 20,000 rcf in a tabletop centrifuge to separate the polar from the lipid phase at 4 °C. Polar and lipid phases were collected separately and dried in a Speed Vac (Martin Christ, Speed Vac RVC 2-33 CD, Cooling Trap alpha 2-4 LD plus) over night.

### 3.2.5 Sample Derivatization

In order to enable metabolites to transition into the gas phase without pyrolysis, a chemical derivatization has to be carried out in which certain chemical groups are modified so as to render the resulting product more volatile. To do so, dried tissue, blood serum, and CSF extracts were resolved in 20 µL, 10 µL, and 10 µL of methoxyamine hydrochloride (MEOX), respectively, and shaken at 30 °C for 1.5 hours. N-methyl-N-(trimethylsilyl)-trifluoroacetamide (MSTFA) containing the alcane mixture (see Alcane Mix) was then added to the samples (80 µl for tissues, 30 µL for blood serum and CSF), and shaken at 37 °C for one hour. The samples were then centrifuged at 10,000 rcf for 10 minutes and 30 µL (tissues) or 15 µL (blood serum and CSF) were transferred into glass vials (Th. Geyer) for GC-MS measurement.

### 3.2.6 Alcane Mix

n-decane, n-dodecane, n-pentadecane, n-octadecane, n-nonadecane, n-docosane, n-octacosane, n-dotriacontane, and n-hexatriacontane, together comprising the alcane mix, were dissolved in hexane and combined to a final individual concentration of 2 mg/mL. This alcane mix was added to the MSTFA solvent during the derivatization procedure at a final concentration of 2% v/v.

### 3.2.7 Quantification Mix

The Quant mix is composed of a total of 63 compounds (stock concentration 1 mg/mL in 50 % MeOH). A dilution series of empirically determined concentrations from 1:1, 1:2, 1:5, 1:10, 1:20, 1:50, 1:100 to 1:200 was prepared, aliquoted, dried under vacuum and stored at -20 °C. One set of quantification standard was derivatized in parallel with each batch of torpor samples and measured at the beginning of each measurement batch. For more details, please refer to Matthias Pietzke's dissertation at the Freie Universität Berlin, 2014.

### 3.2.8 GC-MS Configuration

Metabolomic analysis was performed on a gas chromatography coupled to time of flight mass spectrometer (LECO-Pegasus III- TOF-MS-System, LECO), supplemented with an auto-sampler (MultiPurpose Sampler 2 XL, Gerstel). Tissue samples, blood sera, Ident and Quant mixes were injected in split mode (split 1:5, injection volume: 0.8 µL,) and the CSF in splitless mode (injection volume: 0.8 µL) in a temperature-controlled injector (CAS4, Gerstel) with a baffled glass-liner (Gerstel). The following temperature program was applied during sample injection: Initial temperature of 80 °C for 30 seconds followed by a ramp with 12 °C/minute to 120°C and a second ramp with 7 °C/minute to 300 °C and final hold for 2 minutes. Gas chromatographic separation was performed on an Agilent 6890N (Agilent) gas chromatograph, equipped with a VF-5ms-column of 30 meters length, 250 µm inner diameter and 0.25 µm film thickness (Varian). Helium was used as carrier gas with a flow rate of 1.2 mL/minute. Gas chromatography was performed with the following temperature gradient: 2 minutes heating at 70 °C, first temperature gradient with 5 °C /minute up to 120 °C and hold for 30 seconds, subsequently a second temperature increase of 7 °C/minute up to 350 °C with a hold time of 2 minutes. Spectra were recorded in a mass range of 60 to 600 u with 20 spectra/second at a detector voltage of 1750 V. (This method description was

kindly supplied by Matthias Pietzke and Christin Zasada from a methodological paper currently in revision and only slightly modified).

### 3.2.9 Data Analysis and Imputation

Acquisition, pre-processing, and processing of GC-MS data is described in the Materials and Methods and the Results of the Maui-SILVIA section.

The intensities of different derivatization products of individual metabolites were summed. Furthermore, since some bioinformatic analysis, for example principle component analysis, is only possible when a final datamatrix contains no missing values, I have employed the following imputation strategy: For any metabolite that was measured in at least a single biological replicate of any phase within each tissue, the biological replicates of each phase either contained no, one, two, or three missing values. In the case of a single missing value, a value of ½ the intensity of the lowest intensity detected for the metabolite was assigned. For two missing values, each was assigned a tenth, and for three missing values, each was assigned one hundredth of the lowest intensity detected for the metabolite. The imputation was chosen because detecting metabolites in more or fewer biological replicates does give an indication of the abundance of the metabolite in a certain biological state.

### 3.2.10 Statistics and Graphing

All analysis and graphs were produced in R, using the packages ggplot2, reshape2, scales, plyr, doBy, psych, nFactors, GPArotation, PerformanceAnalytics, cluster, rgl, corrgram, and agricolae (see R-References). The correct understanding of the line plots displayed in this dissertation is essential and therefore needs detailed explanation.

All data representations observed throughout are captured in three example graphs (Figure 3.1). The y-axis indicates the $\log_2$ value of the fold change of each torpor phase (for the Campus Run each round) relative to the initial condition (baseline phase for torpor, R0 for the Campus Run). All error bars throughout this thesis represent the 95% confidence interval of the respective data point, so that non-overlapping error bars likely indicate a significant difference. The gray shadow marks the confidence interval of the initial condition for convenience.

Example metabolite A is representative of all metabolites that were detected in all biological replicates of all phases and therefore no imputed values were plotted (Figure 3.1).

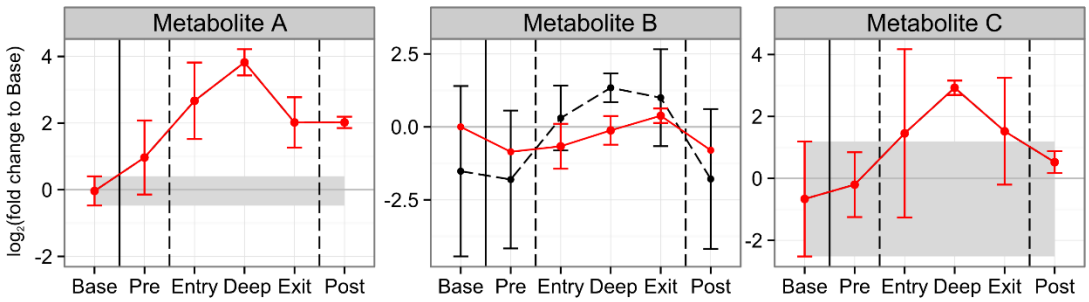


**Figure 3.1 – Examples of metabolite line plots as a guide to the visualizations employed in this dissertation**. Metabolite A is representative of all metabolites that were detected in all biological replicates of all time points. The colored line in metabolite B represents the mean of only those biological replicates that were measured for every time point. Missing error bars indicate that the metabolite was measured in only a single biological replicate. Black long-dashed lines represent imputed data. The unimputed data of the baseline condition plotted in metabolite C is not zero due to high biological variation in the baseline condition. (Base= baseline; Pre=pre entry)

Metabolite B serves as an example where imputed data (always black long-dashed lines) is displayed in addition to unimputed data (always a continuous line colored according to the tissue/fluid displayed) (Figure 3.1). Since the data are plotted relative to the first data point, the shape can vary strongly from the unimputed shape if values in the first data point are imputed. Unimputed datapoints represent the average of all measured data, ignoring those biological replicates where the metabolite of interest was not detected. If the metabolite was detected in only a single biological replicate, no confidence interval is displayed.

Metabolite C represents a special case in that the first data point is not zero as would be expected of the $\log_2$ of a fold change of one (Figure 3.1). This occurs when the initial condition has high biological variation, as all data points correspond to the average of the $\log_2$ of fold changes to the average intensity of the initial condition, rather than the $\log_2$ of the average of fold changes. This allows for the determination and representation of confidence intervals of the initial condition to which all others are compared and provides a more realistic representation of the initial condition.

Kruskal-Wallis statistical analysis was performed using the R package agricolae. It is the rank-based non-parametric equivalent of a one-way analysis of variance (ANOVA) and tests whether samples originate from the same distribution. It does not assume a normal distribution of the residuals and can be employed when group sizes are not equal, which was the case in this dataset as the test was performed using unimputed data only (Kruskal & Wallis 1952). Multiple testing was corrected for by the use of

False Discovery Rate (FDR) correction supplied by the agricolae package (Benjamini & Hochberg 1995). Note that FDR was used for correcting multiple testing only across the torpor phases within each compound and does not account for the total number of metabolites tested.
Hierarchical clustering was performed in R using the average linkage method, unless otherwise specified.

## 3.3 Results

### 3.3.1 Global View

In order to study the metabolic changes occurring during the induction, progression, and termination of torpor, blood serum, CSF, liver, muscle, and WAT were sampled in each of six crucial phases of torpor from three mice each, and the polar component of metabolites analyzed on a LECO GC-TOF mass spectrometer (Figure 3.2). The numbers of total features detected, metabolites identified, and metabolites absolutely quantified using the Quant mix are summarized in Table 2.

| Tissue | # Peaks | # Metabolites | # Unknown | # Abs. Quantified |
|---|---|---|---|---|
| **Liver** | 372 | 88 | 284 | 49 |
| **Muscle** | 354 | 72 | 282 | 41 |
| **WAT** | 265 | 63 | 202 | 34 |
| **Blood** | 313 | 63 | 250 | 38 |
| **CSF** | 432 | 50 | 382 | 19 |

**Table 2.** Overview of the number of peaks detected, metabolites identified, and metabolites absolutely quantified in the torpor study.

Principal component analysis (PCA) of all five tissues revealed the most distinct tissue to be the CSF (Figure 3.3). It is separated from the other tissues by principal component one (PC1), the component containing most of the variation of the dataset. PC2 spreads the liver samples and separates both muscle and liver from WAT and the blood serum samples. PC3 separates the muscle from liver tissue, and PC4 contains mostly the variation within blood samples. PC5 separates WAT from blood samples,

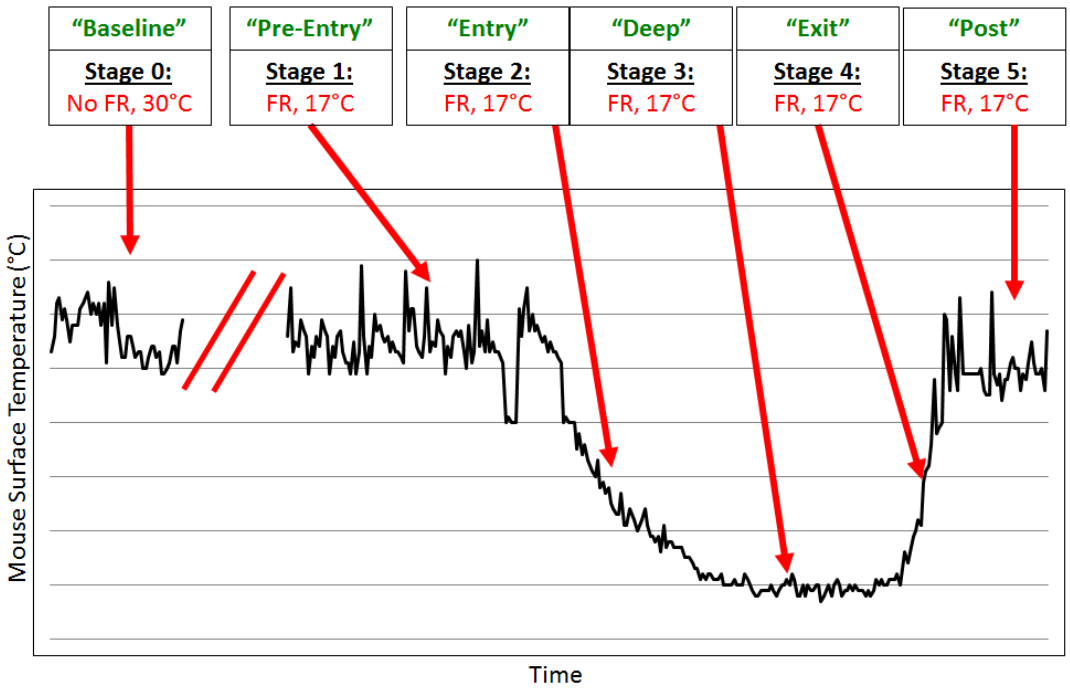


**Figure 3.2 – The torpor phases during which tissues and body fluids were sampled.** An illustrative surface temperature trace of a mouse undergoing torpor is used to indicate the distinct phases of torpor during which samples were collected. Three mice were sacrificed at each of the six sampling points and their tissues and body fluids collected. (FR=Food restricted; ambient temperature was 30°C at baseline, and 17°C in all other phases)

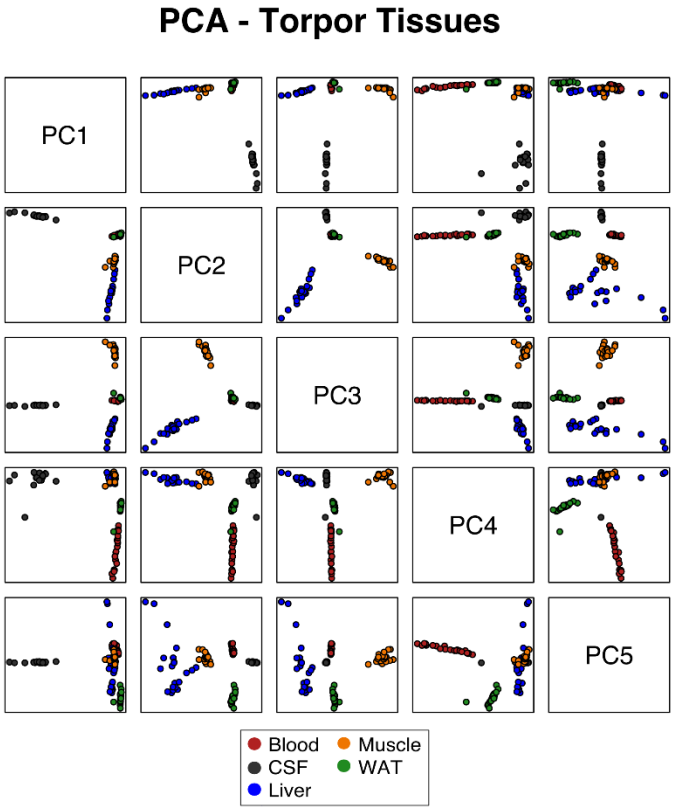


**Figure 3.3 – Principle components of the torpor dataset.** Plotting the first five principle components (PCs) indicates that they contain all information required to distinguish the tissues collected in the torpor study from one another. The tissue most unlike any other is the CSF, which is separated from the other tissues by PC1, the component containing most of the variation in the dataset.

so that all tissues can be distinguished clearly in at least one of the first five principle components, supporting the observation made during annotation of the dataset that there are clear differences between the tissues, especially in respect to unknown peaks but also the behavior and presence or absence of known metabolites.

Hierarchical clustering shows highest relatedness within tissues and clearly separates the CSF from the other tissues in agreement with the PCA. A heatmap of the data provides an overview of the hierarchical clustering result and the overall structure and volume of the data (Figure 3.4).

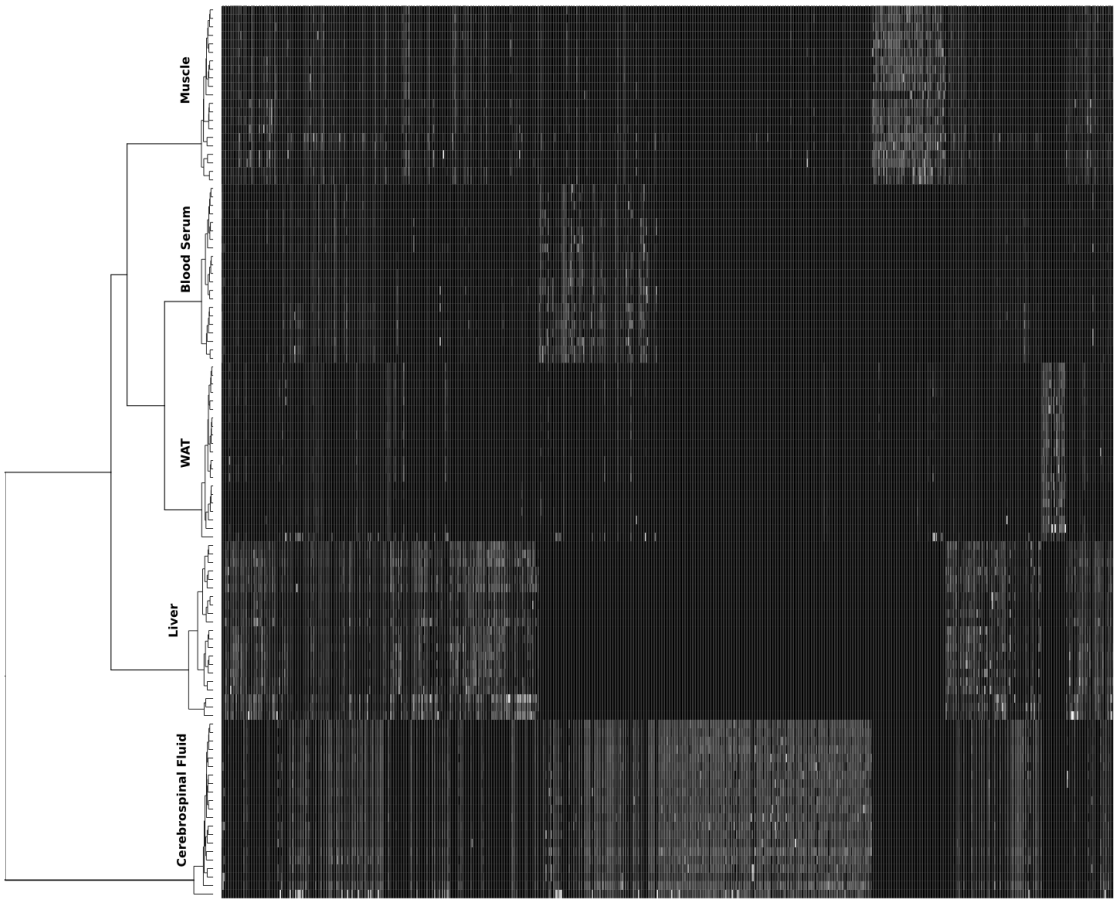


**Figure 3.4 – A heatmap of hierarchically clustered intensity data of all tissues in the torpor study.** Hierarchical clustering indicated that relatedness was highest among samples of the same tissue or body fluid. The CSF is most distinct, containing a large block of metabolites that were either not or only rarely found in the other tissues.

From this global analysis, one can conclude that a good quality data matrix was obtained for the experiment, lending credibility and confidence to the following analyses of the tissues and their metabolic changes during torpor. To decide on a point of entry into the vast dataset, I performed Kruskal-Wallis tests on all known metabolites in all tissues (Figure 3.5). Clearly, the organ undergoing the most significant changes is the liver. Since it is the organ responsible for carbohydrate homeostasis as well as the major site of fatty acid oxidation and ketone body production, as well as the urea cycle, the liver represents a central hub of energy homeostasis. The fundamental goal of torpor is the conservation of energy in times of need, in which it is reasonable to assume the liver to play a central role. Taken together with the evidence of it being the most dynamic of all tissues under investigation, the understanding of its mechanisms of action will likely be required to gain insights into the process as a whole.

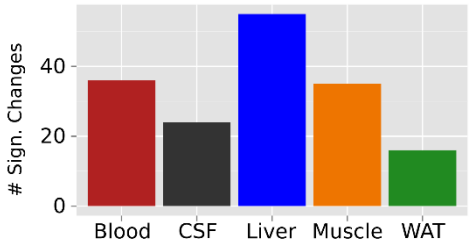


**Figure 3.5 – The number of significantly changed metabolites throughout torpor by tissue.** The number of known metabolites with significant changes in at least one torpor phase as determined by Kruskal-Wallis tests is highest in liver, followed by the blood and muscle. WAT had the fewest significant changes. This pattern holds true when considering also unknown metabolites (not shown).

### 3.3.2 Liver

PCA of liver samples indicates a high similarity of biological replicates of each phase and the distinctiveness of the torpor phases (Figure 3.6). In fact, the phases are arranged in such a way that a movement from one to the next phase through the PC1 and PC2 coordinate system results in a half circle. PC1 clearly separates the baseline phase from the other phases, the deep phase being its extreme opposite. PC2 contains three main groups made of the baseline, pre-torpor, and entry, the deep phase, and the exit and recovery phases.

Both non-deterministic k-means clustering and deterministic hierarchical clustering group the biological replicates of the different torpor phases into distinct clusters (Figures 3.7 and 3.8). As can be seen in the dendrogram of the hierarchical clustering,

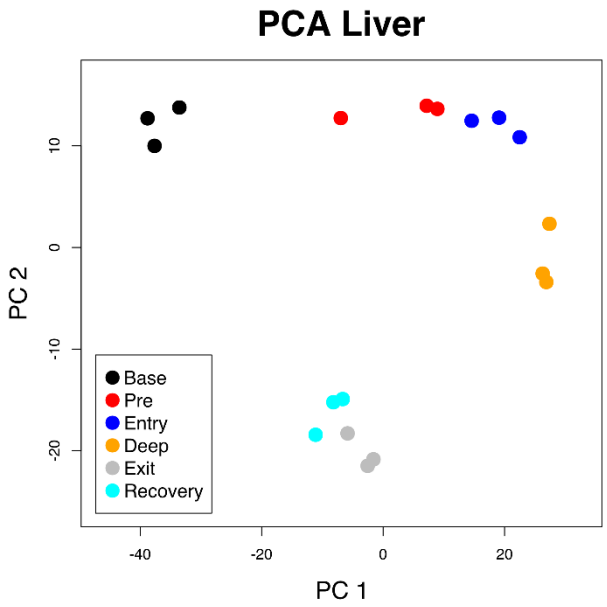


**Figure 3.6 – Principle component analysis of liver samples.**
Plotting the first two principle components of the liver samples results in a strong grouping of biological replicates, with all phases being separated well in the first two principle components. The trajectory of the torpor process through the Cartesian space of PC1 and PC2 is that of a half-circle, starting at the top left and ending in the bottom middle. (Base = Baseline; Pre = Pre phase).

the baseline samples are most distinct from all other phases, likely reflecting the fundamental difference in liver metabolism in the fed versus unfed states already indicated by PC1 of the PCA. As observed when plotting the first two principal components, exit and recovery are closely related to one another, as well as the entry and deep phases.

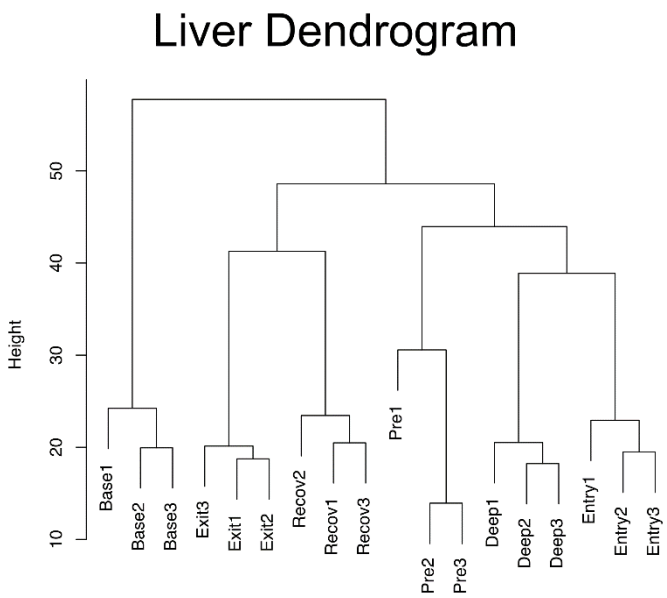


**Figure 3.7 – Dendrogram of the hierarchical clustering of liver samples using the average linkage method**.
All biological replicates of the torpor phases are clustered together. The baseline phase forms a lone branch, the exit and recovery phases form another. In the third branch of pre, deep and entry phases, the deep and entry phases are more closely grouped.

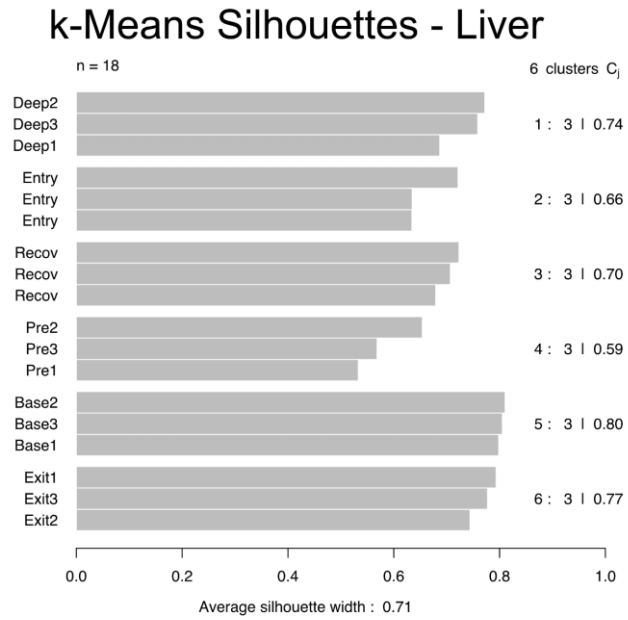


**Figure 3.8 – k-means clustering of liver samples.**
The silhouette plot of k-means clustering of six clusters of the liver samples shows that biological replicates of the torpor phases form strong clusters (the higher the width value, the stronger the cluster), indicating that the distinct physiological states of torpor are also metabolically distinct in the liver.

To understand the mechanistic changes that occur during torpor in the liver which allow for such a clear separation of the torpor phases, I performed a factor analysis of the Pearson correlation matrix of known metabolites measured in the liver, excluding unknown peaks from this kind of analysis as the interpretation of their function is not possible at this time.

Several packages in R exist to predict a reasonable estimate for the number of underlying factors of a correlation matrix. I used the nScree function from the nFactors package, which for the liver samples suggested four factors (see R-References).

The first factor (F1) contains metabolites that increase or decrease relative to the baseline condition, and never return to their baseline levels. While the mechanistic interpretation of this group is difficult as there is no specific pathway enriched in the factor, it is nonetheless informative that there is a group of compounds that differ strongly between the fed and unfed states. This factor corresponds to the PC1 that clearly separates the baseline condition from all other torpor phases. Prominent examples of F1 that make physiological sense in separating the fed and unfed states are:

1) Glycerol, which is known to be produced during fatty acid mobilization from triglycerides, 2) β-hydroxybutyrate, which is the ketone body produced by fatty acid β-oxidation during times of starvation in the liver, as well as 3) maltotriose, which as a trisaccharide indicates an abundance of carbohydrates in the fed state (Figure 3.9).

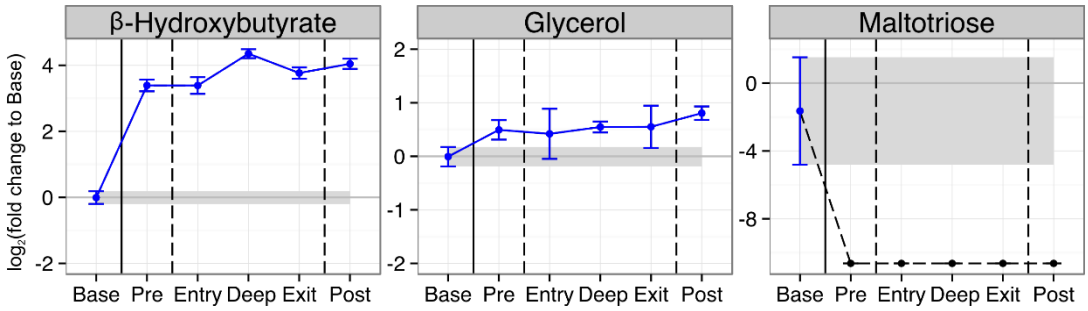


**Figure 3.9 – Selected important members of F1 in liver.** Glycerol and the ketone body β-hydroxybutyrate were elevated in all phases relative to the baseline. Maltotriose, in contrast, was only detectable in the baseline condition, indicating a lower abundance of carbohydrates in times of food deprivation.

The other three factors will be considered together to deduce changes in metabolic state throughout the torpor phases.

F3 contains maltose, a disaccharide of two molecules of glucose, glucose itself, and the two most abundant glycolysis intermediates, glucose-1/6-phosphate and fructose-6-phosphate (glucose-1-phosphate and glucose-6-phosphate are difficult to clearly distinguish on our GC-MS setup in most conditions; however, this does not influence the interpretation and conclusions of the study presented here). Also in F3 is the oxidized form of glucose called gluconate, lactose (a disaccharide of glucose and galactose), and fructose, which is known to enter glycolysis through fructose-6-phosphate directly or by first being converted to fructose-1-phosphate before entering at the level of fructose-1-6-bisphosphate (Leite et al. 2011). Another F3 member, pantothenate, is a vitamin required for acetyl-CoA synthesis, a cofactor required for pyruvate, the last glycolysis intermediate, to enter the TCA cycle. F3 further contains the two TCA cycle intermediates malate and fumarate. Taken together, F3 appears to represent glycolysis and the catabolic TCA cycle (Figure 3.10). Generally, phosphate intermediates like fructose-6-phosphate and glucose-1/6-phosphate are most abundant when glycolysis is "turned on", leading to the interpretation that glycolysis and the

TCA cycle are active in the baseline state and decline during the entry and deep torpor phase. During waking, the pathways are turned back on and remain active afterwards. The evidence for the "off" state of the TCA cycle and its turning back on afterwards might appear weak from malate and fumarate alone, but are further supported by the behavior of citrate and succinate (Figure 3.11). Citrate accumulates towards the deep phase while succinate levels drop, indicating a block of TCA intermediate cycling. This block might be resolved when succinate increases, followed by a decrease in citrate levels, during the exit and post phases, respectively.

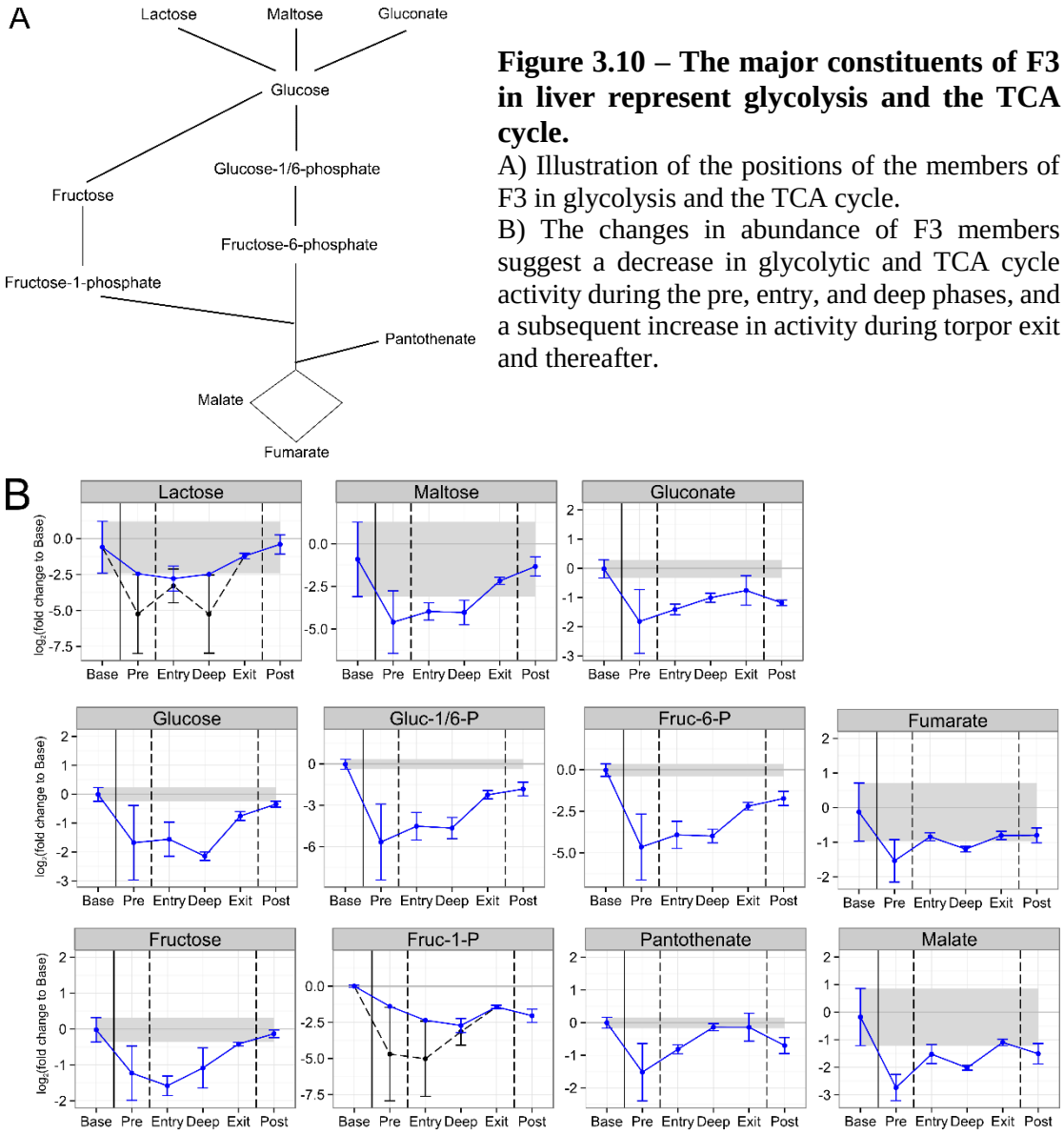


**Figure 3.10 – The major constituents of F3 in liver represent glycolysis and the TCA cycle.**
A) Illustration of the positions of the members of F3 in glycolysis and the TCA cycle.
B) The changes in abundance of F3 members suggest a decrease in glycolytic and TCA cycle activity during the pre, entry, and deep phases, and a subsequent increase in activity during torpor exit and thereafter.

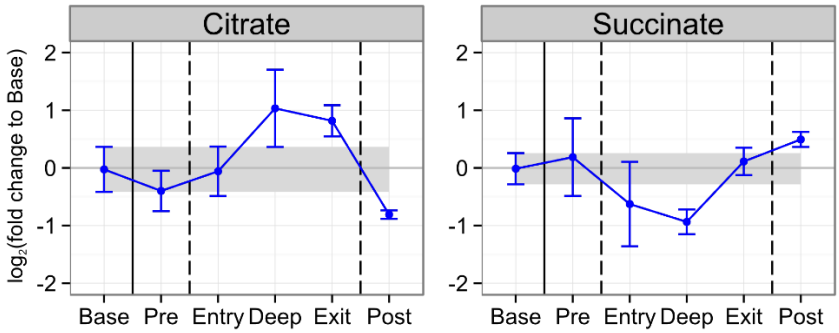


**Figure 3.11 – Citrate and succinate behavior during torpor in liver**. In support of TCA cycle activity suppression during the early torpor phases, an accumulation of citrate and concurrent decrease in succinate levels occured during torpor entry, indicating a lack of carbon flow through the catabolic TCA cycle. The reversal of this observation during the exit and post phases indicate the reactivation of the TCA cycle during arousal.

F4 prominently features the essential amino acids cysteine, phenylalanine, and valine, the amino acid metabolism intermediate hypotaurine, as well as proline and the urea cycle intermediate ornithine (Figure 3.12). F4 therefore indicates an accumulation of essential amino acids, as well as a concurrent increase in urea cycle and other amino acid metabolism intermediates towards the deep phase. Interestingly, threonine, isoleucine and lysine (essential), as well as glutamate, pyroglutamate (to be interpreted as a combination of glutamine, glutamate, and pyroglutamate) and serine also show an accumulation in the deep phase. Asparagine, also a component of the urea cycle, displays an increasing trend similar to ornithine (Figure 3.13). Taken together with urea and putrescine levels increasing during and accumulating after the deep phase, one can conclude that two phenomena might be encoded in this factor:

1) Amino acid accumulation and conversion: Since essential and other amino acid levels increase without food intake, there are three possible sources of these amino acids: a protein synthesis inhibition in liver, an active protein degradation in liver, or the import of amino acids from the blood released, most likely, from muscle tissue.
2) An active metabolizing of amino acids: As indicated by urea cycle components ornithine and asparagine and the following accumulation of urea and putrescine, as well as the production of the processing intermediate hypotaurine (Figure 3.13).

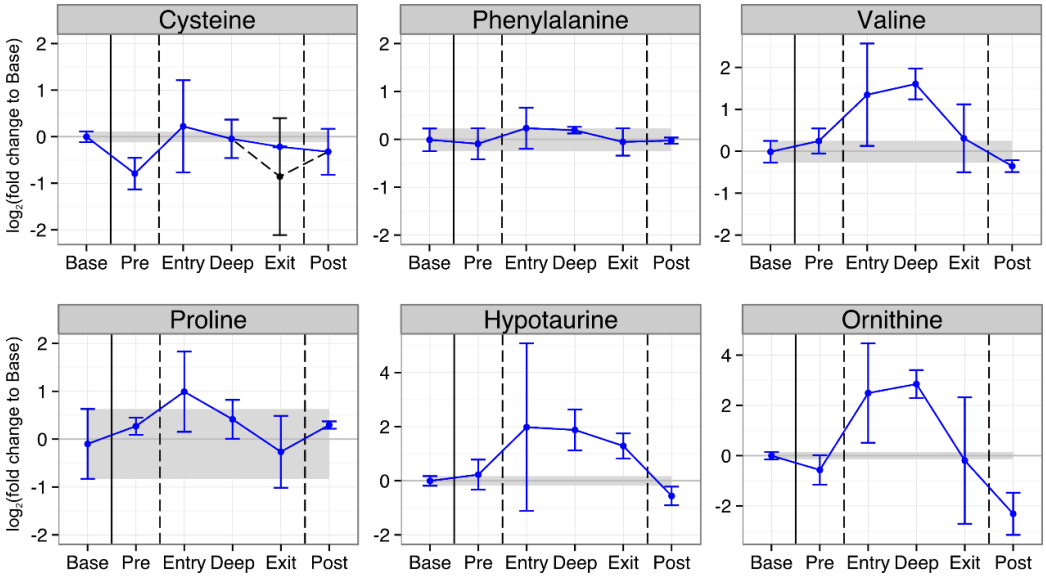


**Figure 3.12 – Members of F4 in liver.** The accumulation of essential amino acids (cysteine, phenylalanine, and valine), an amino acid processing intermediate (hypotaurine), and the urea cycle intermediate ornithine indicated an inhibition of protein synthesis, amino acid uptake from blood, or active proteolysis, as well as active amino acid catabolism during torpor in liver.

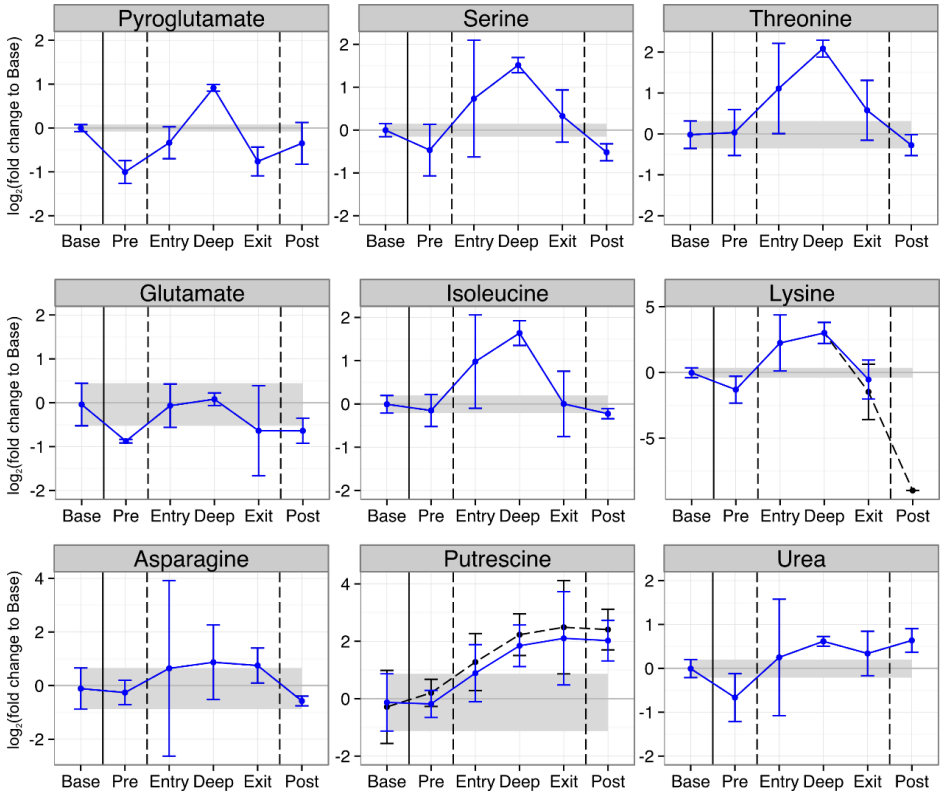


**Figure 3.13 – Amino acid accumulation and urea cycle activity in liver during torpor.** Amino acids not part of F4 tended to accumulate relative to the food restricted non-torporic pre-phase in the deep torpor phase. Furthermore, the urea cycle intermediate asparagine showed a trend of increasing during the deep phase, and both putrescine (urea cycle) and urea itself were elevated in the deep phase and thereafter, lending further support to the notion that amino acids are processed during the early phases of torpor.

The metabolization of amino acids in liver is evident from the data and in accordance with the current state of knowledge. The major site of amino acid metabolism, in fact, has been said to be the liver, the only tissue besides the intestine in which the full complement of urea-cycle enzymes is expressed (Morris 2002). Furthermore, amino acid utilization in the liver, especially alanine, to fuel gluconeogenesis has been observed during both sleep and exercise (Bass & Takahashi 2010; Wagenmakers 1998).

It is, however, considerably more difficult to differentiate between the three possible mechanisms leading to the general amino acid accumulation in liver. On the one hand, it has been found that during prolonged starvation, amino acids, most of which are glucogenic (meaning that they can be used to produce glucose through gluconeogenesis), are released by muscle tissue for uptake by the liver and kidney where they may fuel gluconeogenesis (Brosnan 2003). However, muscle breakdown seems not to be a method of choice for obtaining amino acids for fuel in hypometabolic states. In fact, hibernation is an active field of study for muscle wasting researchers, where clear evidence has shown that hibernators retain most muscle mass and function even after months of inactivity, while much shorter timeframes would render most people strongly debilitated (Lee et al. 2010). Whether or not this argument is applicable to daily torpor has not been investigated and, due to the much shorter periods of inactivity in daily torpor, might not be appropriate.

An inhibition of protein synthesis has been described for both hibernation and daily torpor and the liver is known to be able to carry out proteolysis (Mortimore et al. 1989; Knight et al. 2000; Berriel Diaz et al. 2004). Theoretically, therefore, all three mechanisms of active proteolysis, accumulation due to an inhibition of protein synthesis, and amino acid uptake from blood might contribute to the amino acid accumulation in liver. Even when analyzing the behavior of amino acids throughout torpor in liver, blood, and muscle simultaneously, I could not find any clear pattern of behavior for all amino acids or specific subsets (Supplementary Figure 1). While the source of the amino acids cannot be resolved definitively here, it is clear that amino acids are accumulating in the liver and being metabolized during the early torpor phases.

F2 contains three key metabolites that can fuel gluconeogenesis: Alanine, lactate, and glycerol-3-phosphate. Also part of the factor are sorbitol, a metabolite that can be converted to either glucose or fructose, as well as the two sugar acids galacturonate and glucuronate, one of which can be converted to glucose in few steps. Also part of this factor are succinate and citrate, which instead of directly playing a role in gluconeogenesis more likely reflect the concurrent decrease in TCA cycle throughput, as well as pyroglutamate and threonine that represent the concurrent accumulation of amino acids and their breakdown. The compounds able to provide fuel for gluconeogenesis decrease during the entry into torpor and reach their overall lowest levels in the deep phase, recovering only during the waking and post phases (Figure 3.14). This evidence points towards active gluconeogenesis during the early part of torpor, while the following increase in abundance during the waking and post torpor phases are likely caused by the restarting of glycolysis at that time.

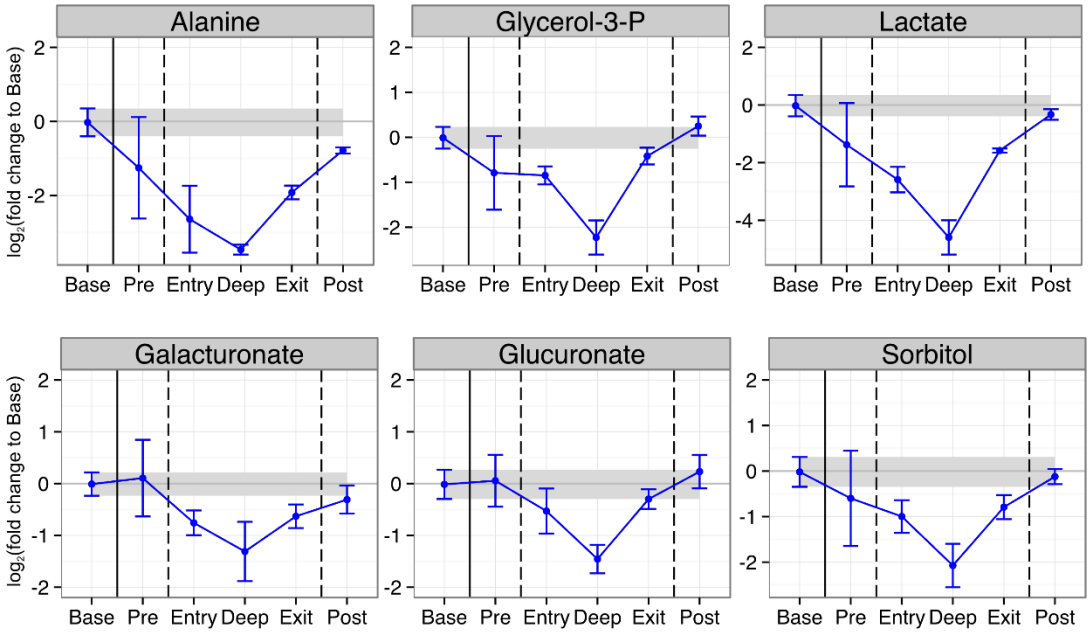


**Figure 3.14 – Members of F2 in liver**. F2 features three gluconeogenesis substrates (alanine, glycerol-3-phosphate, and lactate), their depletion during torpor potentially representing active gluconeogenesis. The other members of F2 displayed a similar pattern and might contribute to glucose production as well.

Combining the evidence of factors F2, F3, and F4, the following picture emerges: Glycolysis and the TCA cycle are active in the fed control states, and are subsequently decreased during the early torpor phases. In these early phases, gluconeogenesis is active, reaching its peak (or endpoint) during the entry and deep phase, concurrent with

amino acid breakdown, the products of which partially fuel gluconeogenesis. As the animals wake, glycolytic activity returns and brings about a decrease in gluconeogenesis and amino acid catabolism (Figure 3.15).

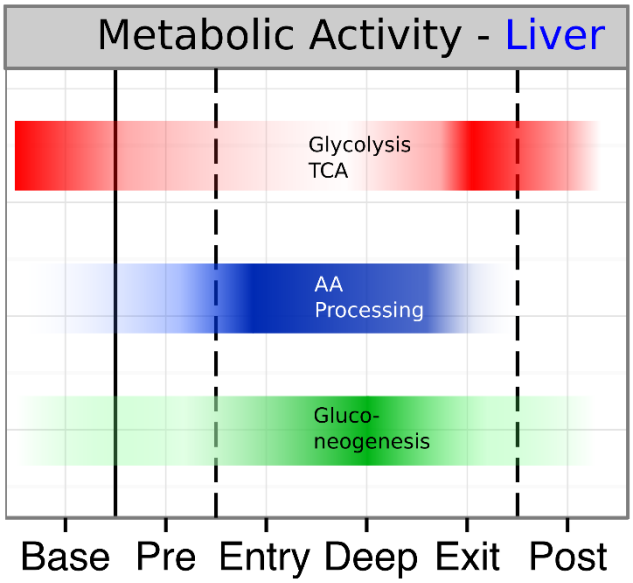


**Figure 3.15 – Metabolic pathway activities in liver throughout the torpor process.** The activity of glycolysis and the catabolic TCA cycle (red), amino acid accumulation and processing (blue), and gluconeogenesis (green) in liver throughout the torpor cycle are illustrated. High activity is represented by high color opacity.

One is most confident in declaring a pathway to be active when one sees the accumulation of intermediates and its end products, like lactate or pyruvate for glycolysis. Similarly, one should see the accumulation of the end product of gluconeogenesis, glucose, in liver or blood serum. Indeed, blood glucose levels rise during the deep torpor phase in blood already (as does glucose in the muscle and WAT, where it seems to be taken up in preparation for the waking phase and after), while liver glucose levels are lowest, indicating an active release of glucose by the liver. In fact, the deep torpor phase has the lowest absolute concentration of glucose in the liver while the ratio of absolute liver to blood glucose concentration is lowest (Figure 3.16). While the kidney is known to be capable of gluconeogenesis as well, it is likely that the liver plays a large, if not the predominant role in producing and supplying glucose during torpor (Mitrakou 2011). To study the involvement of kidney metabolism in torpor, I have also collected kidney tissue in all phases from the same mice as described in this thesis, and will measure and analyze them in the near future.

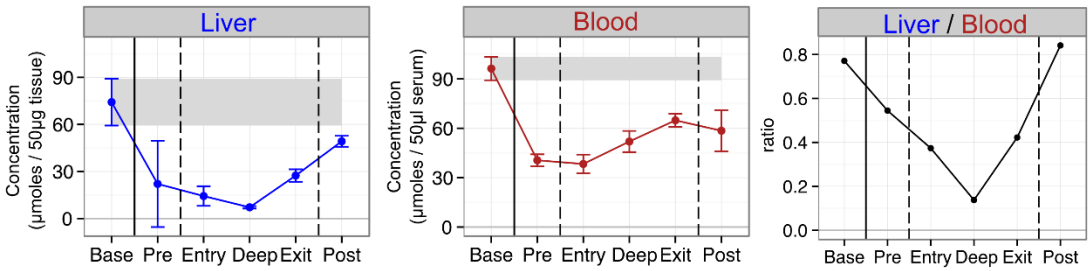


**Figure 3.16 – The ratio of hepatic to blood serum glucose concentration**. Absolutely quantified glucose levels in liver and blood, as well as their ratio show that the lowest liver to blood glucose ratio occurred during the deep torpor phase when the liver seemed to supply the blood serum, and through it, other organs, with glucose to prepare for the energetically demanding process of torpor arousal.

The requirement of a highly active gluconeogenesis during the early torpor phases has several reasonable justifications. For one, waking from torpor means increasing the body temperature by at least 17 °K, which poses a large energetic need. This is mostly accomplished by general metabolic activity, skeletal muscle-dependent shivering, and brown adipose tissue-dependent (BAT) non-shivering thermogenesis (Oelkrug et al. 2011). BAT contribution is likely negligible in this study due to acclimatization conditions that strongly decrease BAT function and abundance (Cannon & Nedergaard 2011). In fact, during the dissection of the mice under study, BAT was usually not visible in the neck region where it is commonly most abundant. While it is possible that the remaining and elsewhere located BAT depots contribute, mitochondrial uncoupling is not necessary for torpor arousal (Oelkrug et al. 2011). A definitive contribution of glucose to fuel the waking process, however, is indicated in increases in lactate in liver, muscle, and blood serum in my dataset (Figure 3.17, see below).

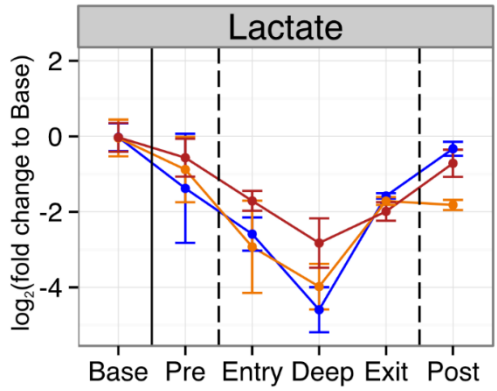


**Figure 3.17 – Relative changes in lactate levels observed in liver, muscle, and blood serum.**
The increase in lactate levels in liver, muscle, and blood serum observed between the deep and exit phases are indicative of significant glucose utilization during torpor arousal.

Glucose levels might therefore be instrumental in signaling when the animal is energetically capable of rewarming. Interestingly, glucose levels in CSF, to which critical brain regions like the energy and thermoregulatory centers in the hypothalamus have access, return already during the exit phase to levels observed in the fed state (Figure 3.55). This makes glucose an ideal candidate for being a permissive exit signal sensed in the brain.

In conclusion, the liver appears to have two distinct phases in torpor. During the early phases, it processes amino acids and uses all available resources (lactate, alanine, glycerol-3-phosphate) for gluconeogenesis, before returning to a glycolytic state during the exit phase and afterwards. Its production of glucose raises blood, muscle, WAT, and CSF glucose levels already during the deep phase, presumably supplying itself and the rest of the body with part of the energy required to fuel rewarming and the reestablishment of the tissues' pre-torpor homeostatic states.

### 3.3.3 Muscle

Muscle tissue metabolism during torpor is of interest because muscle is the major site of amino acid storage of the body and is of crucial function during the rewarming phase, when the animals shiver to raise their body temperature to euthermic levels.

PCA of the muscle samples clearly groups biological replicates of the different torpor phases together, with PC1 separating the fed baseline state from the food restricted torpor stages, similar to what was observed in liver (Figure 3.18). k-means clustering produced the greatest average silhouette width when searching for six clusters, their individual large silhouette widths indicating stable clusters as observed in liver (Figure 3.19). Hierarchical clustering showed greatest relatedness between biological replicates from the different phases, leading to the overall conclusion that similar to the structure of the liver data, the muscle metabolome is distinct in each of the torpor phases (Figure 3.20). Hierarchical clustering showed the baseline to be isolated from the other samples, likely reflecting the difference between fed and unfed metabolism in muscle and mirroring PC1. In fact, the overall structure of the relationships of the phases to one another using hierarchical clustering is nearly identical between muscle and liver.

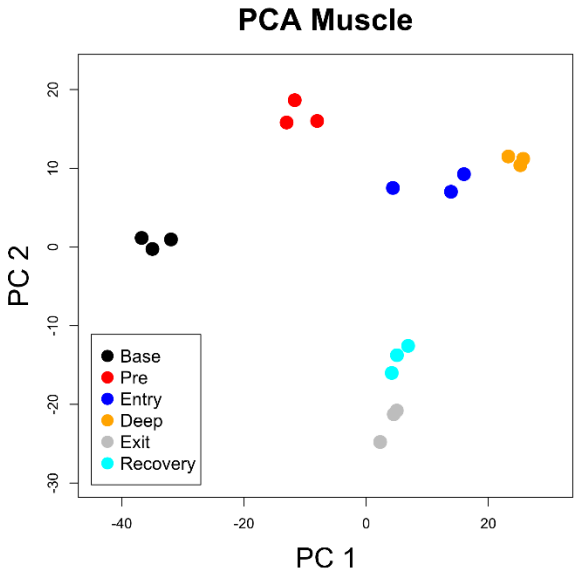


**Figure 3.18 - PCA of muscle samples.**
Plotting of the first two PCs of muscle samples shows strong grouping of biological replicates and all phases being separated well. The trajectory of the torpor process through the Cartesian space of PC1 and PC2 is similar to that observed in liver, but does not so strongly resemble a half-circle. (Base = Baseline; Pre = Pre phase).


**Figure 3.19 – k-means clustering of muscle samples.**
The silhouette plot of k-means clustering of six clusters of the muscle samples shows that biological replicates of the torpor phases form strong clusters, indicating that the distinct physiological states of torpor are also metabolically distinct in muscle.

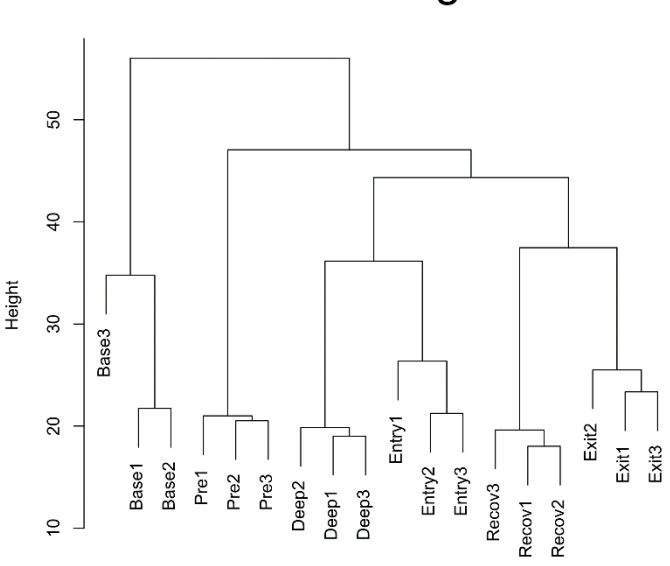


**Figure 3.20 – Dendrogram of hierarchical clustering of muscle samples using the average linkage method**.
All biological replicates of the torpor phases are clustered together. The baseline and pre phases each form a single branch. The exit and recovery, as well as the entry and deep phases are more closely related to one another.

To gain mechanistic insights into the metabolic changes during torpor in muscle, I performed a factor analysis of the Pearson correlation matrix of all known compounds identified in muscle samples. F1 contains the glycolysis intermediates fructose-6-phosphate and

glucose-1/6-phosphate, the fructose glycolysis entry intermediate fructose-1-phosphate, glycerol-3-phosphate, also able to feed into glycolysis, as well as the two glycolysis end products pyruvate and lactate. Also part of the factor, but anti-correlated with glycolytic intermediates, are isoleucine, proline, valine, and α-hydroxybutyrate (not shown), which, as observed in the liver, accumulate towards the deep torpor phase.

The glycolysis-related metabolites in F1 show a pattern quite similar to that observed of glycolysis in the liver, predicting high glycolytic activity in the fed state, decreasing activity towards the deep phase where they reach their lowest abundance, followed by an increased activity during the waking phase and afterwards (Figure 3.21). This pattern likely reflects the fact that muscle is actively in use in both fed and unfed states when the animals are actively moving about (baseline and pre-entry, respectively). During torpor, when the animals do not move, glycolysis is shut down, and starts anew when shivering and metabolic activity is required to rewarm the animal and it becomes mobile again thereafter (exit and post).

The major difference in behavior between glycolytic metabolites in liver and muscle are glucose and pyruvate. Whereas glucose in liver is lowest in the deep phase, its abundance in muscle at that point already begins to increase, excluding it from F1 in the muscle, and likely representing the anticipation of arousal from torpor in muscle when glucose will be needed to fuel rewarming (Figure 3.22). The second difference is that pyruvate levels in the liver are unchanged in the torpor phases while in muscle they behave like lactate and the glycolysis intermediates (Figure 3.22). This difference is likely due to the fact that the liver turns on gluconeogenesis during the early torpor phases, while the muscle does not. Pyruvate is both an intermediate in glycolysis and gluconeogenesis and is the first gluconeogenic intermediate produced out of alanine, which appears to be actively funneled into gluconeogenesis in the liver. Pyruvate levels are therefore constant in all phases in the liver, as it is either produced during glycolysis or, when glycolytic activity is low, gluconeogenesis.

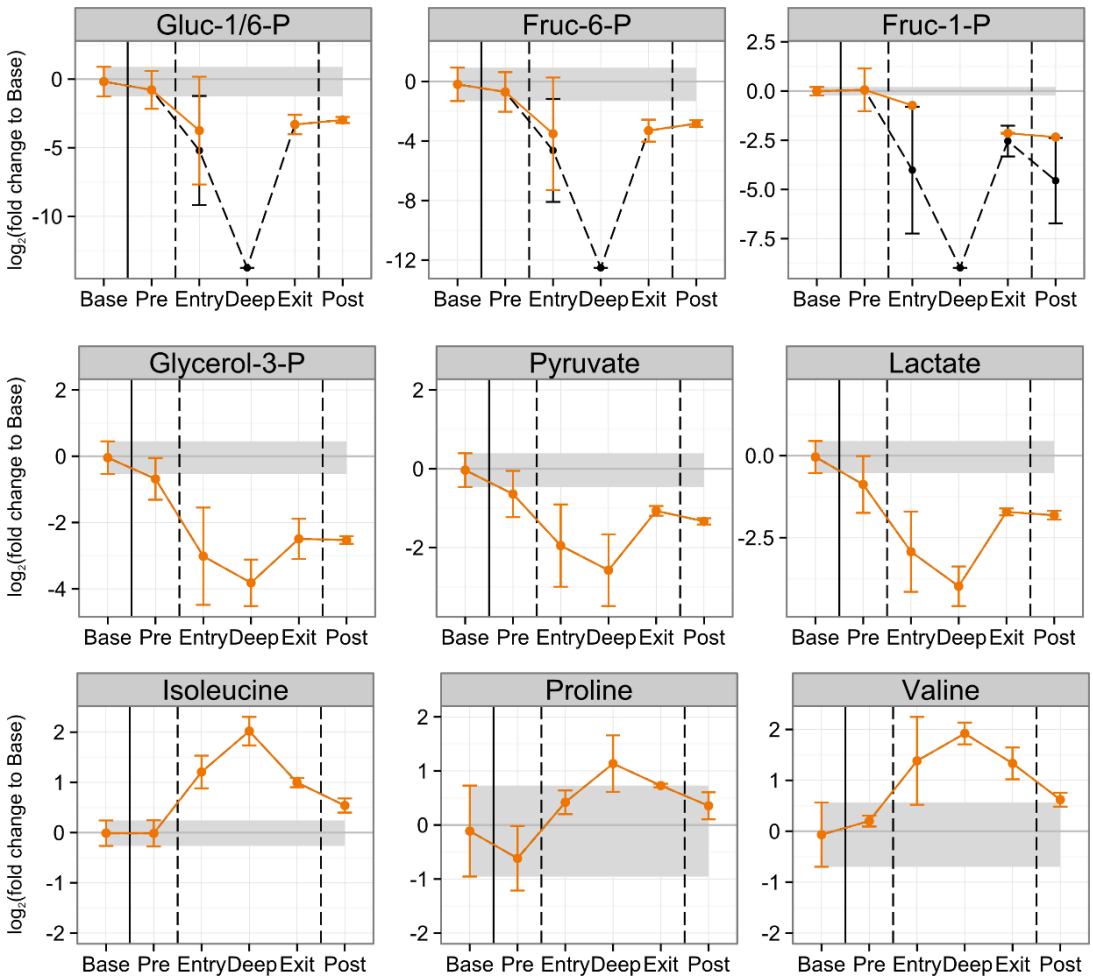


**Figure 3.21 – Members of F1 in muscle.** The members of F1 in muscle are part of the upper glycolysis or serve either as glycolytic substrates or are products thereof. Three amino acids are also included. Together, they indicate glycolytic activity decreasing during torpor and its increase upon torpor arousal. Similar to what was observed in liver, some amino acids also accumulated in the deep torpor phase.

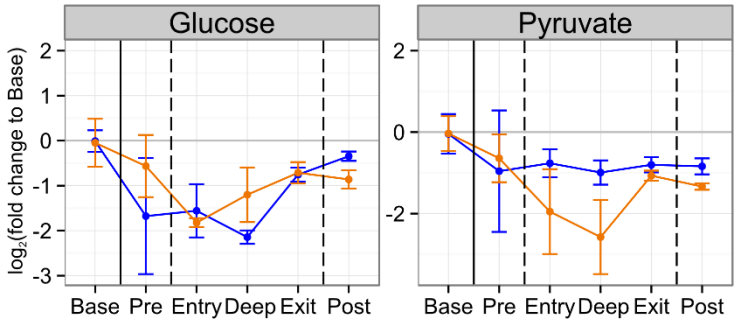


**Figure 3.22 – Differences of pyruvate and glucose behavior in liver and muscle.** Whereas liver glucose levels (blue) were lowest in the deep torpor phase, muscle glucose levels (orange) were observed to increase at that time. Liver pyruvate levels (blue) were constant throughout torpor, likely balanced by glycolytic and gluconeogenic activities. In muscle (orange), levels decreased in accordance with other glycolytic markers, indicating that gluconeogenesis did not occur during torpor in muscle.

It is also likely that TCA cycle activity is decreased in muscle in accordance with glycolytic activity, as especially succinate and α-keto-glutarate, but also malate and fumarate levels are decreased in deep torpor (Figure 3.23). In accordance, one of the primary sources of TCA cycle fuel, pyruvate, is drastically depleted as mentioned above.

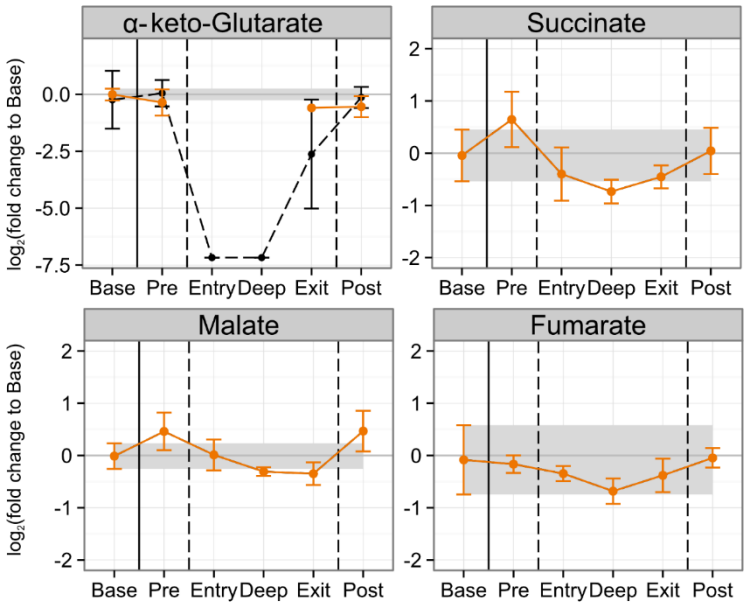


**Figure 3.23 – TCA cycle intermediates in muscle during torpor.** Similar to observations in liver, TCA cycle intermediate abundance, especially α-keto-glutarate (keto-Glutarate), decreased in accordance with low glycolytic activity during torpor.

Furthermore, some essential and non-essential amino acids accumulate also in muscle and are part of F1 (Figure 3.21), whereas many others, including the processing intermediate hypotaurine, either show no significant changes or even decreases in abundance (Figure 3.24). The accumulation could again be interpreted as protein degradation or an inhibition of protein synthesis, and in muscle most likely serves to release amino acids into the blood stream to be taken up by the liver and/or kidney as gluconeogenic fuel. As discussed before, there are several lines of argument to support any combination of possibilities on the definitive source of the accumulating amino acids, and they cannot be conclusively determined in this study. To resolve the possibilities, further studies employing more tailored assays would be beneficial and, in combination with this dataset, may lead to a sound conclusion.

F3 in muscle is composed of a group of metabolites that differentiate the baseline phase from all other phases, either by an increase or decrease in abundance that does not return to original levels. It includes the amino acids lysine, glutamine, tyrosine,

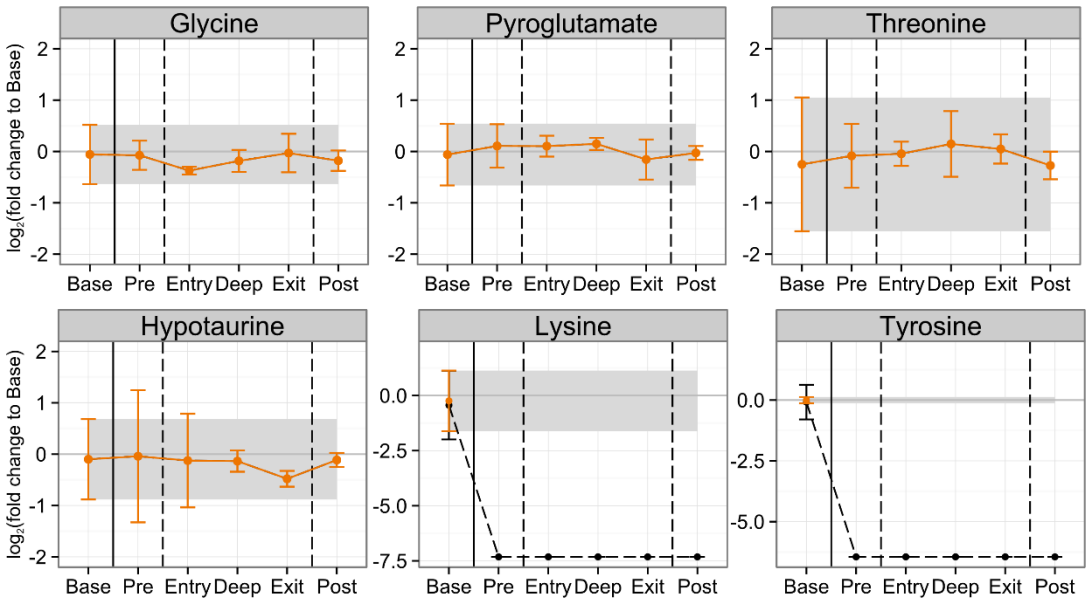


**Figure 3.24 – Amino acid behavior in muscle differs from that observed in liver.** Several amino acids, as well as the processing intermediate hypotaurine, either show no changes or even decrease during torpor in muscle, indicating little if any amino acid accumulation and processing in muscle.

and creatinine, ribose (a five-carbon sugar), sucrose (a disaccharide), as well as triethanolamine and ethanolamine-phosphate (both intermediates of phospholipid metabolism) (Figure 3.25).

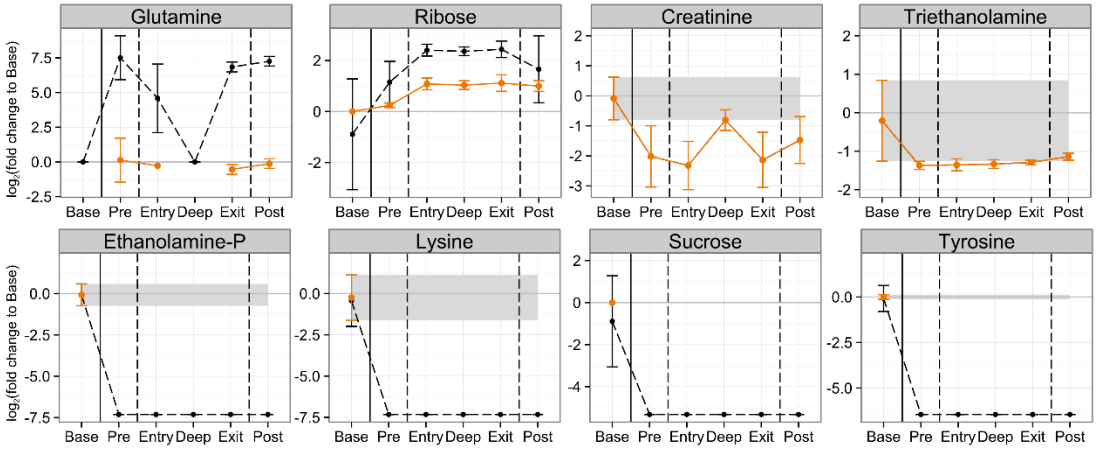


**Figure 3.25 – Members of F3 in muscle are diverse and differentiate the baseline from all other sampling time points.** While the diversity of metabolites in F3 makes it difficult to define an underlying connection, they seem to represent metabolic activities that either decrease strongly or increase as a result of food restriction, differing little throughout torpor (with the exception of glutamine and creatinine in the deep phase only).

While the diversity of the group makes it difficult to deduce a common underlying connection, it is certainly of note that:

1) Creatinine levels are generally decreased in muscle in the unfed states, and seem to sharply rise during the deep torpor phase.
2) Lysine and tyrosine, two metabolically distinct amino acids, are only detectable in the fed state.
3) Glutamine is not detectable in the baseline and deep phase, while having similar levels in the other phases.
4) Ribose is elevated during starvation, an effect that is exacerbated during torpor.
5) Sucrose as well as phospholipid synthesis intermediate abundance is decreased strongly during the unfed states.

F2 is composed of two metabolites that did not significantly change during the course of torpor as well as nicotinamide, phosphoenolpyruvate (PEP), and putrescine, all three of which showed different patterns and have no known relation so that I am unable to interpret F2 (Figure 3.26). However, it is interesting to note that the derivative of the antioxidant vitamin C, dehydroascorbic acid dimer, does not change during torpor, since other antioxidants have been found to accumulate during the deep torpor phase in hibernators in liver (Nelson et al. 2009).

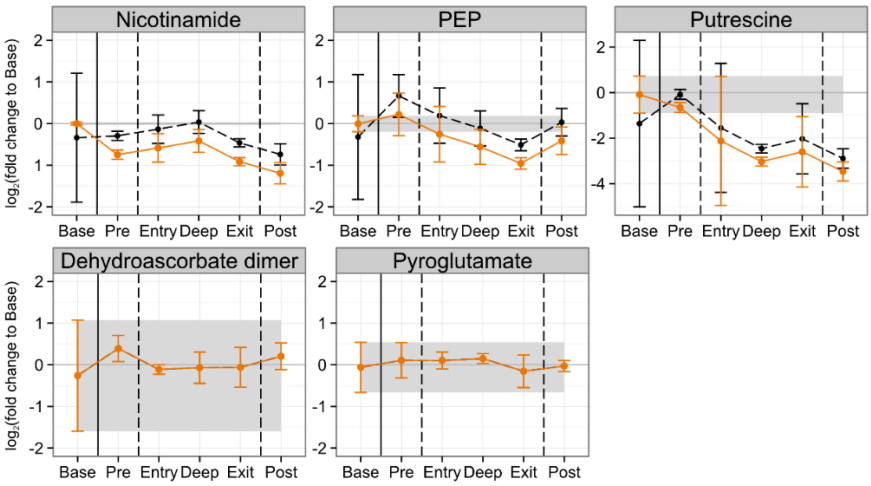


**Figure 3.26 – Members of F2 in muscle.** Although it is difficult to interpret the mechanisms underlying this factor, it is of interest to note that the dehydroascorbate dimer, a derivative of the antioxidant vitamin C, does not change during torpor.

F4 on the other hand contains four metabolites that are of approximately stable levels before, and then increase to a constant level during and after the deep phase. F4 contains the sugar alcohol mannitol and sugar acid glucuronate, as well as urea and phosphoric acid monomethyl ester (PAME). The changes in glucuronate and PAME are not significant, while those in mannitol are significant but minimal in magnitude (Figure 3.27). Urea does significantly increase; however, neither ornithine nor asparagine was detected in any muscle sample, and putrescine levels actually continuously decreased over the course of torpor (Figure 3.26). It is most probable that urea is taken up by muscle from the blood, as the only two tissues known to express the full complement of urea-cycle enzymes are liver and the intestine (Morris 2002).

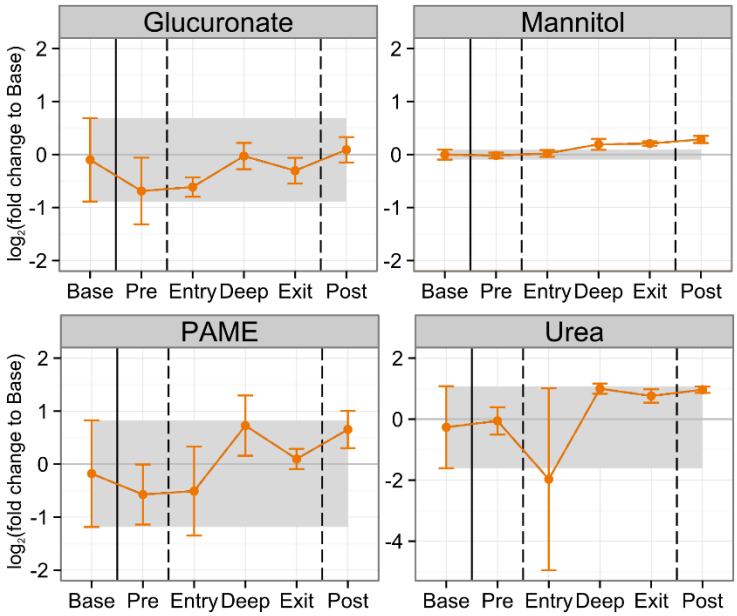


**Figure 3.27 – Members of F4 in muscle**. The fourth factor is defined by metabolites that rise during and remain elevated after the deep torpor phase. Whereas changes in mannitol are significant but minimal, and those in glucuronate and PAME statistically insignificant, increases in urea are difficult to attribute to urea cycle activity in muscle as the tissue does not express a full complement of urea cycle enzymes and none of the urea cycle intermediates displayed a pattern in accordance with its activity.

In conclusion, the muscle shows two glycolytic phases, similar to the liver. During the pre phase when animals may still move about, glycolysis is at a level comparable to that observed in the baseline phase. As the animals enter torpor, glycolysis decreases and seems to stop during the deep phase, at which point glucose levels rise, together with certain amino acids. In contrast to the liver, gluconeogenesis does not appear to be active while glycolysis is inhibited, as evidenced by pyruvate levels decreasing during

the entry and deep phase and in line with the liver and kidneys being the only gluconeogenic organs (Figure 3.22). The reduction of the gluconeogenic source lactate is most likely caused by its release into blood which is common muscle behavior and part of the Cori cycle (Brooks 1998). Whereas some amino acids accumulate, others are unchanged or show the opposite behavior. While urea does accumulate towards the end of torpor likely due to passive uptake, the urea cycle intermediates themselves are either not detected or decrease over time in accordance with the urea cycle being unavailable to muscle tissue.

### 3.3.4 White Adipose Tissue

WAT represents the fat storage of the body in the form of triglycerides that are released during food restriction when glycogen stores in the liver are depleted. It is therefore of interest during torpor since the process occurs in times of starvation during which fats form the basis of the main source of energy. Fatty acids and glycerol are released by WAT and taken up by the liver, where fatty acids undergo β-oxidation to produce acetyl-CoA and the ketone body β-hydroxybutyrate and glycerol may enter gluconeogenesis (Wu & Windmueller 1979; Lass et al. 2011; Quiroga & Lehner 2012). Furthermore, WAT seems to play an essential role in torpor regulation, as it is the site of leptin secretion and its genetic near-ablation strongly alters the torpor phenotype (Gavrilova et al. 1999).

PCA of WAT did not so clearly separate the different phases from one another as seen in liver and muscle, although there appears to be some grouping (Figure 3.28). This is in agreement with the observation that WAT had the lowest number of significantly changed metabolites throughout torpor (Figure 3.5). PC1 appears to separate the baseline and pre phases from the other torpor phases, while PC2 is skewed by a single biological replicate of the deep phase. k-means clustering produced the largest silhouette width when allowing the formation of seven clusters, in which one biological replicate each of the baseline and the deep phase formed a separate group, and the deep and exit phases belonged to a single cluster (Figure 3.29).

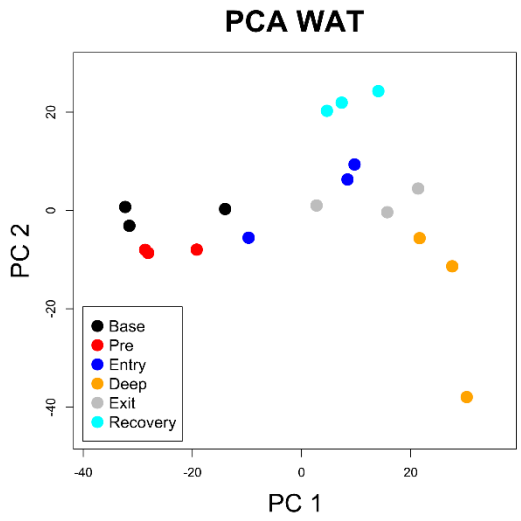


**Figure 3.28 – PCA analysis of WAT samples.**
Plotting the first two PCs of WAT samples shows a less distinctive grouping of biological replicates than observed in liver and muscle. This is in accordance with the WAT containing the least number of metabolites having significantly changed in at least one torpor phase. (Base = Baseline; Pre = Pre phase).

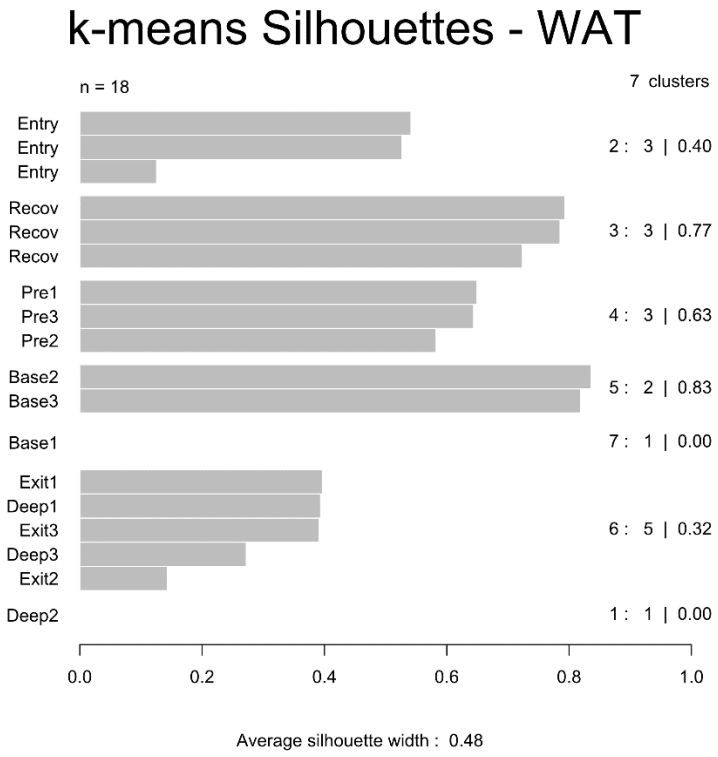


**Figure 3.29 – k-means clustering of WAT samples.**
The silhouette plot of k-means clustering of seven clusters of the WAT samples shows that biological replicates form strong clusters only for the pre and recovery phase, and a weaker one for the entry phase. One replicate of the baseline and deep phases each form singlet clusters, the other deep replicates being grouped with those of the exit phase, indicating a strong similarity of the deep and exit phases in WAT that was not found in liver or muscle.

Hierarchical clustering mirrored the observations made in the k-means analysis, in that one baseline and one deep phase were distant from the other replicates (Figure 3.30 A). However, if the "Ward" method was used, which favors the formation of equally-sized clusters, all biological replicates were assigned appropriately (Figure 3.30 B) (Ward 1963).

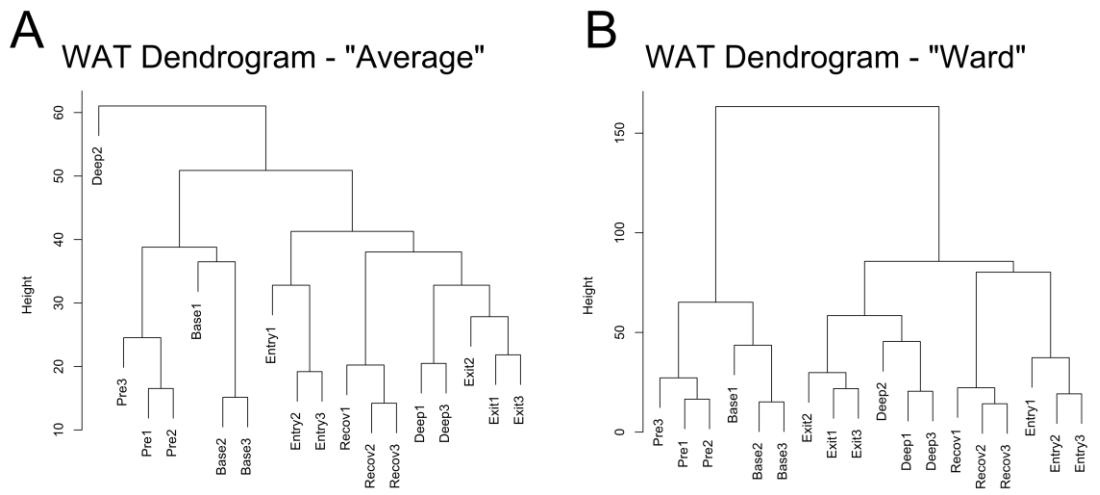


**Figure 3.30 – Dendrograms of hierarchical clustering using the average and Ward linkage methods.** A) Despite the weak k-means clustering and PCA result, hierarchical average linkage clustering grouped most biological replicates appropriately, with the exception of an outlier deep phase. B) Using the Ward linkage method, which favors the formation of equally-sized clusters, all biological replicates clustered together. The pattern of relationships between the phases is distinct from liver and muscle: baseline and pre, exit and deep, as well as entry and recovery phases were most related.

In contrast to both liver and muscle, the baseline phase did not form a lone branch, but instead was grouped with the pre phase as separate from the other torpor phases. Another interesting difference is the closer relation on the one hand of the entry and recovery phases, and on the other hand the exit and deep phases. While the phase relationships in liver and muscle indicated that consecutive phases were most alike during torpor and that strong changes occurred in the metabolome between baseline and the pre phase, pre phase and entry, as well as the deep phase and the exit, WAT appears to be more symmetrical, in that the baseline and pre phases, the entry and recovery phases, as well as the deep and exit phases are more similar. Detailed interpretation of global clustering is always precarious, but at the very least the conclusion that the WAT behaves quite differently from both liver and muscle might be safely made.

The comparatively fewer changes in WAT are further reflected by the fact that factor analysis of the Pearson correlation matrix of metabolites measured in WAT samples produced only two factors, whereas four were suggested for liver, muscle, blood serum, and CSF.

F1 represents compounds that are similar in baseline and the pre phase, but then increase in abundance and thereby differentiate the first two phases from the others. Most metabolites in F1 are unfortunately measured with high variability, and the majority of them are either statistically insignificant or contain many imputed values, thereby reducing the confidence of interpretation (data not shown). The few exceptions are urea, which, as in muscle, increases towards the deep phase and remains elevated at a constant level throughout the rest of the phases; glycerate, which has no significant changes; and threonate, whose role in mammalian metabolism to my knowledge is entirely unclear (Figure 3.31).

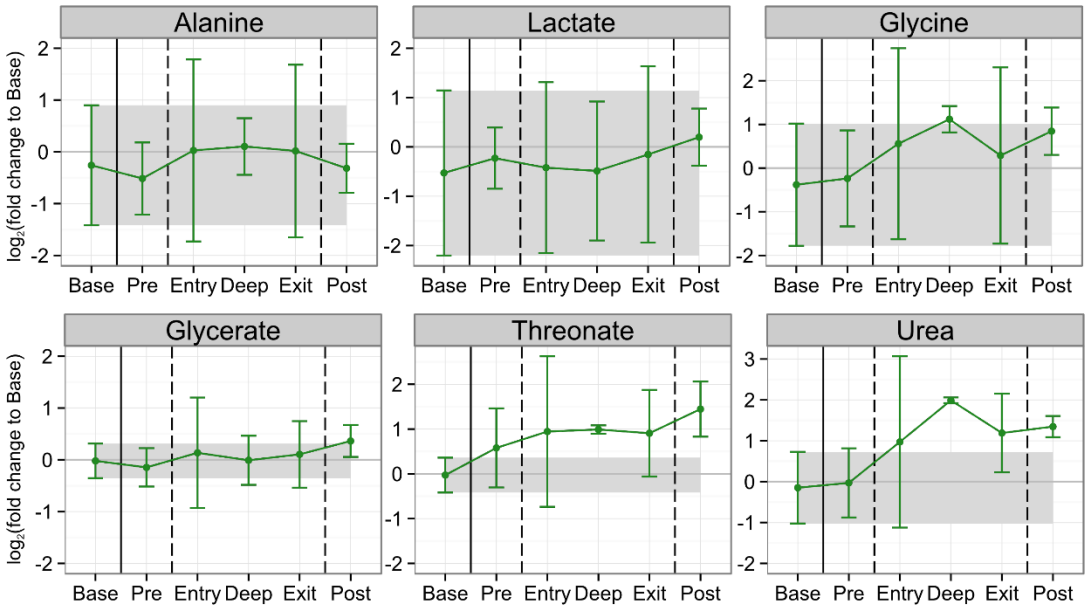


**Figure 3.31 – Members of F1 in WAT.** The strongest contributors to the factor showed increased abundance after the pre phase and remained elevated thereafter. The underlying mechanism is not discernable at this time, and most changes are statistically insignificant. The exceptions were threonate, whose role in mammalian metabolism is unclear, and urea.

F2 contains metabolites that are highest during the entry, deep and exit, or during deep and exit phases only. Unfortunately, interpretation of most of these is again hampered by many imputed values and high biological variation (Figure 3.32). However, three exceptions are α-hydroxybutyrate, citrate, and valine, all three of which rise during entry, peak during the deep phase, and then fall off again during arousal. Citrate accumulation was observed in the liver as well; however, interpretation of its levels in the WAT are complicated by the disagreeing levels of other TCA cycle intermediates. Malate and succinate are elevated from the entry

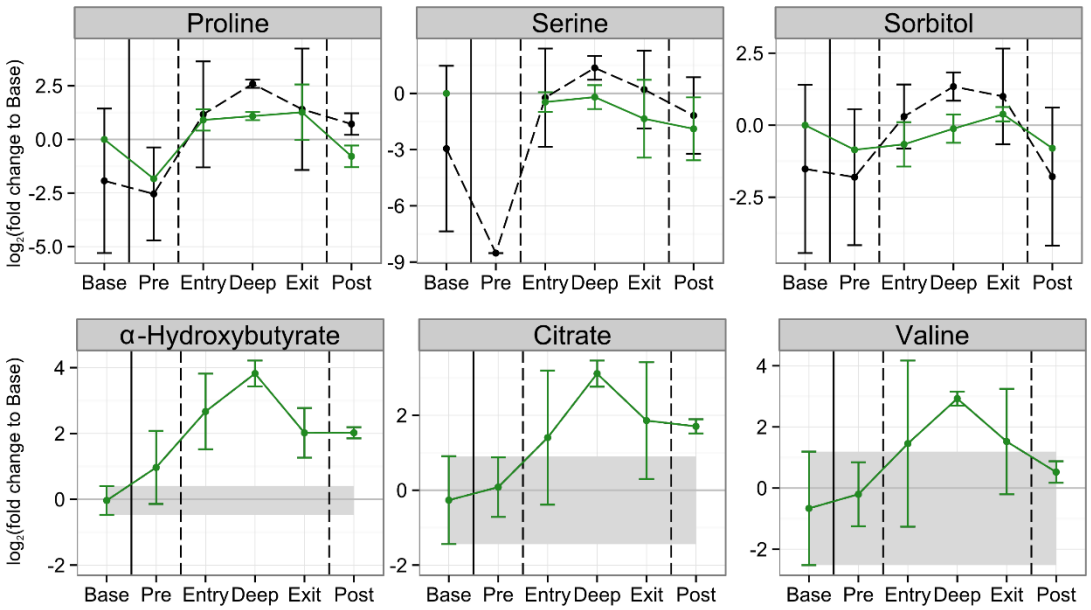


**Figure 3.32 – Members of F2 in WAT.** F2 is characterized by metabolites that accumulated towards, peaked in, and decreased after the deep phase. Unfortunately, half the metabolites contain many imputed values. However, α-hydroxybutyrate, citrate, and valine accumulated strongly in the deep phase.

phase onward, while fumarate, which was measured with the least biological variation, appears unchanged with a trend of slightly decreased levels (Figure 3.33). Assuming the hypothesis of the WAT being a rather passive tissue, the observed pattern of TCA intermediates, which is reflected also in pyruvate and other members of F1, might simply be one of a tissue that is neither regulating an active inhibition, nor a selective activation of any particular pathway. Rather it might represent a tissue in which metabolites accumulate and are converted in accordance with enzyme kinetics chiefly influenced by the changing body temperature.

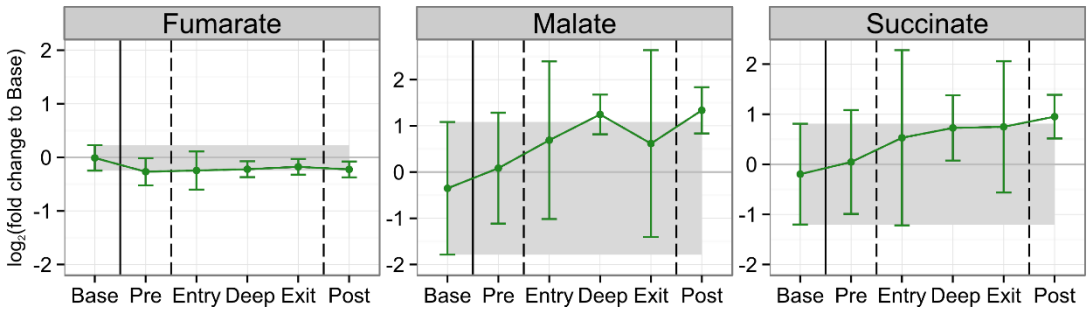


**Figure 3.33 – TCA cycle intermediates do not decrease in WAT.** Unlike in liver and muscle, malate and succinate levels did not decrease during torpor, but showed high biological variation throughout. Fumarate was slightly decreased relative to baseline, but did not change between any of the torpor phases.

Since the factor analysis in WAT was not as successful as in liver and muscle, an examination of metabolites grouped by known pathways or chemical characteristics was undertaken to discern mechanistic insights. While most amino acids did not significantly change and many contained imputed values, the general trend was one of accumulation towards the deep torpor phase, with the exception of alanine and phenylalanine (Figure 3.34), mirroring the general amino acid trend in liver and muscle but being much less pronounced, mostly statistically insignificant, and likely biologically entirely irrelevant.

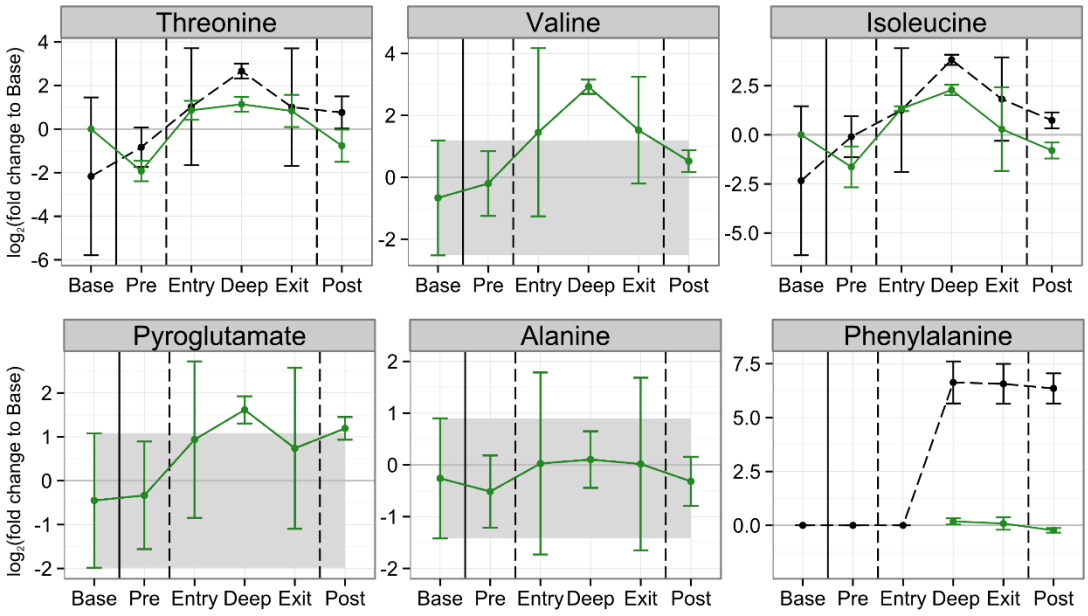


**Figure 3.34 – Amino acids in WAT during torpor.** While most amino acids contained imputed values and showed high biological variation, a trend of accumulation towards the deep phase was discernible in some.

Metabolites involved in lipolysis, such as the ketone body β-hydroxybutyrate and glycerol, are of considerable interest especially in WAT as it is the source of the triglycerides whose breakdown produces them. β-hydroxybutyrate strongly increases in the pre phase and remains elevated throughout the rest of torpor (Figure 3.35). Glycerol, which in blood is frequently used as a marker for triglyceride breakdown, is highest during the pre phase, decreases during the entry and deep phase, before increasing again during exit and the post phase. Although of low magnitude in WAT, this behavior is mimicked by glycerol in blood, validating it as a lipolysis marker and lending support to the hypothesis that fat mobilization occurs during the starvation phase in which animals are active, is suspended during torpor, and begins anew when

the animals become active again (Figure 3.36). This fits well with fatty acids and their products representing the main fuel source during starvation, and torpor arousal requiring both glucose and fatty acids as suggested by this dataset and other investigations (Viscarra & Ortiz 2013).

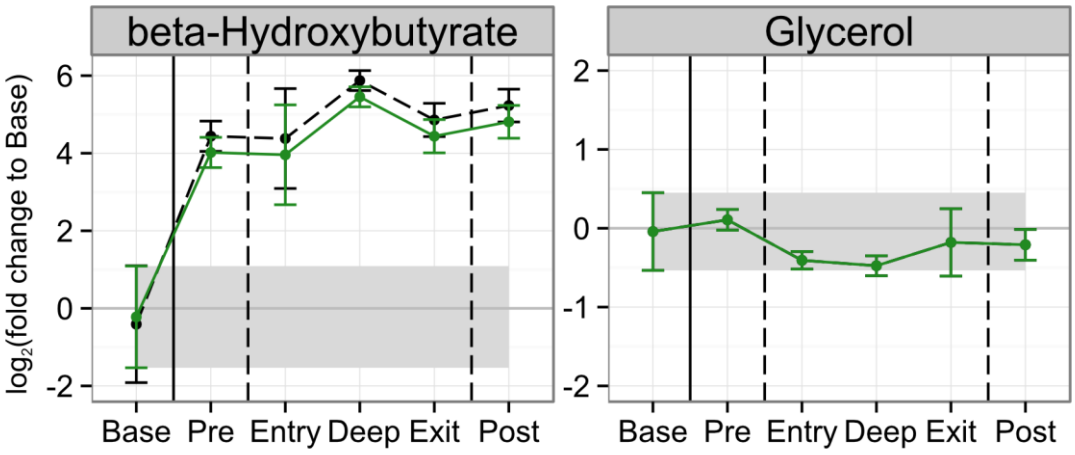


**Figure 3.35 – Lipid store mobilization and indicators of lipolysis in WAT.** Similar to what was observed in the other tissues, β-hydroxybutyrate levels were strongly increased in all food restricted time points. Glycerol levels were elevated relative to baseline during the pre and exit phases when fatty acid release is known to occur.

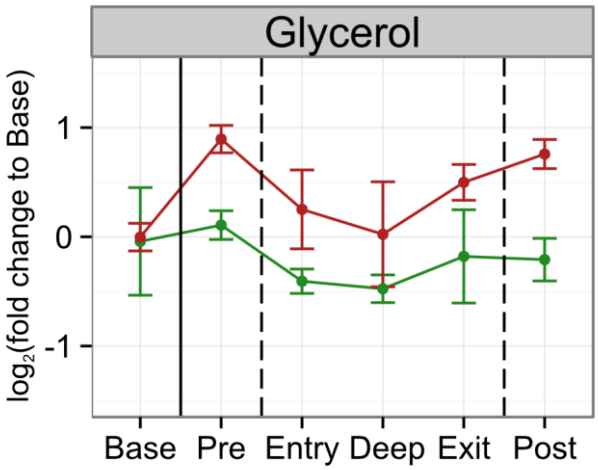


**Figure 3.36 – Glycerol behavior in WAT is mimicked in blood.** Glycerol levels in blood (red) closely mimic the behavior observed in WAT (green), validating it as a marker of lipid mobilization during torpor.

Another curiosity observed in WAT is that glucose levels do not change between the baseline and pre phase, unlike in any of the other tissues. Glucose actually increases in abundance above baseline levels during the deep torpor phase and remains elevated even in the post phase (Figure 3.37). Similarly intriguing is the fact that glycolysis intermediates are only observed, even if only in two and four out of six animals for

glucose-1/6-phosphate and fructose-6-phosphate, respectively, during the deep and exit phase (Figure 3.37). Their levels either passively increase due to the higher availability of glucose, or indicate glycolysis actually being activated during those time points, the energy gained possibly required for the increase in lipid mobilization during the exit and post phase. PEP and pyruvate, on the other hand, are most abundant during the entry and deep torpor phase, which could reflect an accumulation due to an inability to enter the TCA cycle (Figure 3.37).

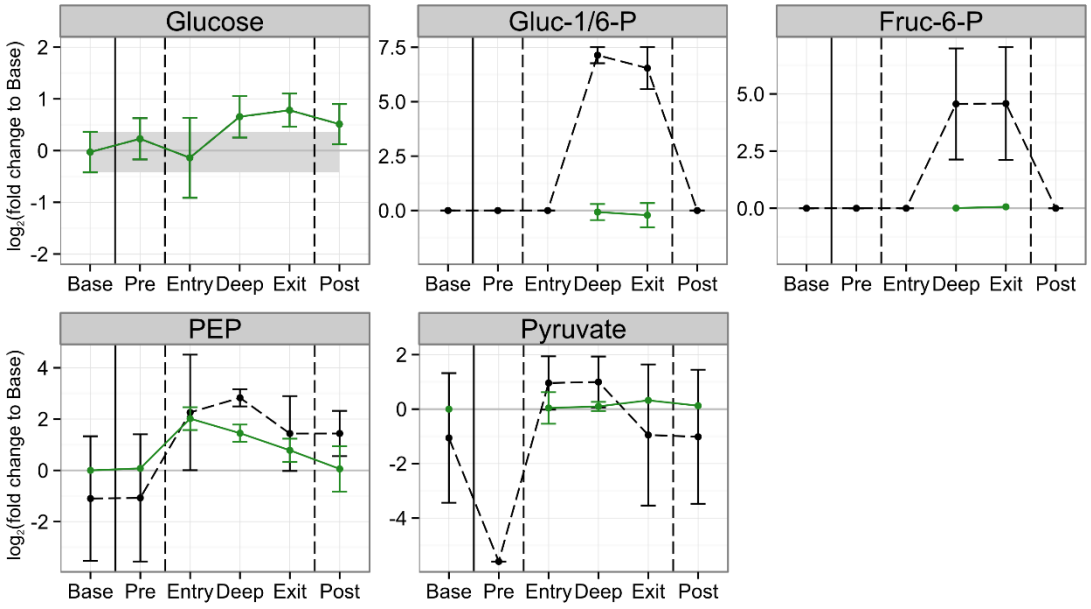


**Figure 3.37 – Glycolysis behaves unexpectedly in WAT.** Whereas glycolytic intermediates are decreased in liver and muscle during torpor, glucose, upper glycolysis intermediates, as well as PEP and pyruvate appear to be elevated in WAT. Whether this is a passive thermal effect or of biological significance cannot here be determined.

It is also quite possible that most of the interpretation attempted beyond that of triglyceride, glycerol, and fatty acid release is biologically insignificant as much of the data is imputed or statistically insignificant. The main purpose of WAT during torpor, in terms of the central carbon metabolism, might simply be the mobilization of triglycerides and fatty acids during the pre and exit phases, the degree of which being strongly correlated with glycerol abundance in both WAT and blood. Its crucial involvement in torpor, for example by controlling leptin levels, is unquestioned; this involvement, however, might simply occur predominantly outside the scope of the central carbon metabolism that was investigated here.

### 3.3.5 Blood Serum

The blood serum metabolome is of great interest during torpor and any other physiological process, and of course particularly in the context of the theme of this dissertation, because it is the direct path of communication between the different tissues of the body. It is both a means of signaling and a way to deliver metabolites from their site of production to where they are required. It is therefore crucial to read its metabolomic changes not from the perspective of an organ consuming or producing, but rather a tissue that takes up, delivers, and buffers metabolite pools.

PCA of blood serum samples showed a good grouping of biological replicates of the different phases when plotting the first two PCs, with only one pre phase being separated from its other two biological replicates (Figure 3.38). k-means clustering produced a maximal average silhouette width when six clusters were allowed to form, with pre and recovery phases forming two mixed clusters, implying a close relation between the two phases already indicated in the PCA (Figure 3.39). Hierarchical clustering successfully grouped all biological replicates together and stands in agreement with both k-means clustering and PCA (Figure 3.40).

The relatedness of the torpor phases in blood serum is different from liver, muscle, and WAT. The baseline is clearly separated from the other phases, representing the blood metabolome difference between the fed and unfed state, similar to liver and muscle. Interestingly, the entry phase forms an individual branch, whereas in the other tissues it was either grouped with the deep phase (liver/muscle) or the recovery (WAT). I would argue that the entry phase being distinct, and being both in PCA and hierarchical clustering distant from the pre phase, is indicative of an abrupt change that would be expected if its composition encoded the decision or required preparation to enter torpor. If the pre and entry phases were very similar, it would seem that the pre phase is used to establish a permissive state, and once reached to completion, would allow torpor entry. While this might still be the case, the dominant effect is one of great changes between two consecutive phases that likely represent the cumulative effect of many small changes in the metabolomes of organs. While the changes in liver, muscle, and WAT individually might be small between the pre and entry phase, they can signal a major physiological state change in blood if the

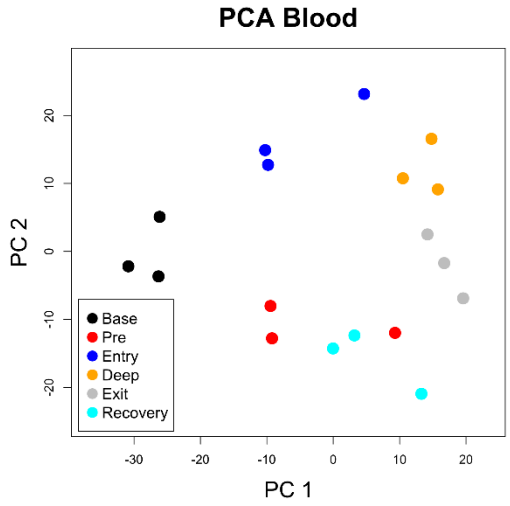


**Figure 3.38 – PCA analysis of blood serum samples.**
Plotting the first two principle components of the blood serum samples results in the strong grouping of biological replicates, with all phases being separated in the first two principle components with the exception of a single pre phase.

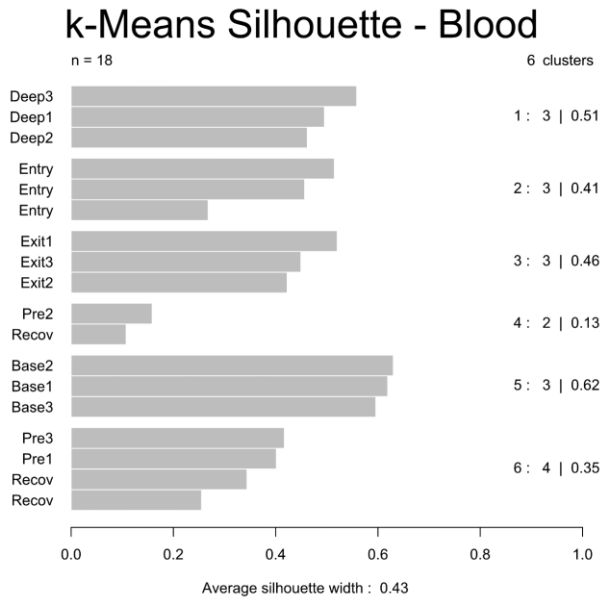


**Figure 3.39 - k-means clustering of blood serum samples.**
The silhouette plot of k-means clustering of six clusters of blood serum samples shows that biological replicates of the individual phases form strong clusters. The exceptions are the pre and recovery phases that form two mixed clusters, and therefore appear to be very similar.

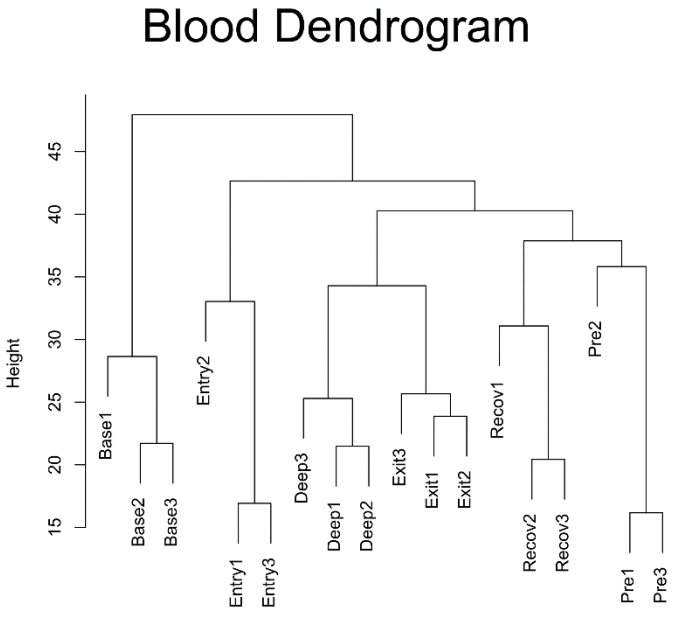


**Figure 3.40 - Dendrogram of the hierarchical clustering of blood serum samples using the average linkage method.** All biological replicates of the torpor phases are clustered together. The baseline phase forms a lone branch as observed in the liver and muscle. The entry phase surprisingly forms another lone branch despite being closely related to others in liver, muscle, and WAT. The high similarity of the pre and recovery phases observed in k-means clustering is also reflected.

intraorgan changes are composed of different metabolites that are representatively released into circulation.

Alternatively, when strong physiological changes occur that are not distinguishable in the blood serum metabolome, some tissue must compensate another tissue's needs by balancing its demand, rendering the blood a "buffering system". Philosophically speaking, one would assume those components that are most crucial for organ function to be buffered, while those allowed to vary strongly might either serve a signaling role or are of lesser importance but nonetheless useful as passive biomarkers.

Considering the blood serum from a perspective of a buffering system allows for a reasonable explanation of why the pre and post phases are more closely related to one another than to any other phase. The pre phase represents the stable starvation state in blood serum, and it is reasonable to assume that the mice, once they have completed the torpor cycle, will attempt to quickly recover to the fundamental starvation state. In order to do so, re-establishment of blood metabolite levels should occur quickly so as to supply the organs with what they need to return themselves to their respective food-restricted homeostasis. The return to blood homeostasis should therefore occur more quickly than the re-establishment of the starvation state within the organs, which either still produce to compensate the demand of others, or yet are in a state of strong demand.

Furthermore, the relationship between the deep and exit phases is closer in blood than in liver and muscle, not displaying the strong separation that occurs between the other two phases in which a crucial decision, that of entry between the pre and entry phase, has to be made. While the data clearly show functional changes in both liver and muscle between the deep and exit phase, the blood appears to be a buffer that has already been established during the deep phase through the accumulation of, for example, both glucose and several amino acids (see below). It seems that the organs load the blood with metabolites required for exit during the torpor phases, the blood metabolome thereby anticipating the metabolic requirements in crucial organs to exit torpor.

Factor analysis of the Pearson correlation matrix of all known metabolites measured in blood serum produced four factors.
F1 contains metabolites that decreased from the baseline to the deep phase and then increased towards baseline levels, as well as three that showed the anti-correlated pattern. Among the first group are alanine, lactate, and pyruvate, three of the endpoints of glycolysis and entry points of gluconeogenesis; malate and fumarate, two TCA cycle

intermediates; as well as uracil and uridine, α-hydroxybutyrate and ethanolamine (Figure 3.41). Alanine, lactate, and pyruvate show patterns that are in accordance with glycolytic and gluconeogenic activity as outlined in the previous sections, their levels high during glycolytic periods, and their levels dropping strongly when they fuel gluconeogenesis in the liver. Malate and fumarate patterns in blood seem to represent the general, although in the tissues less pronounced TCA cycle inhibition during torpor. Similarly, blood citrate levels mirror its accumulation in liver and WAT towards the deep phase, but behave opposite the tissues in the pre and post phase (Figure 3.42). It is interesting to note that many of these metabolites show clear differences in levels between the pre and entry phases.

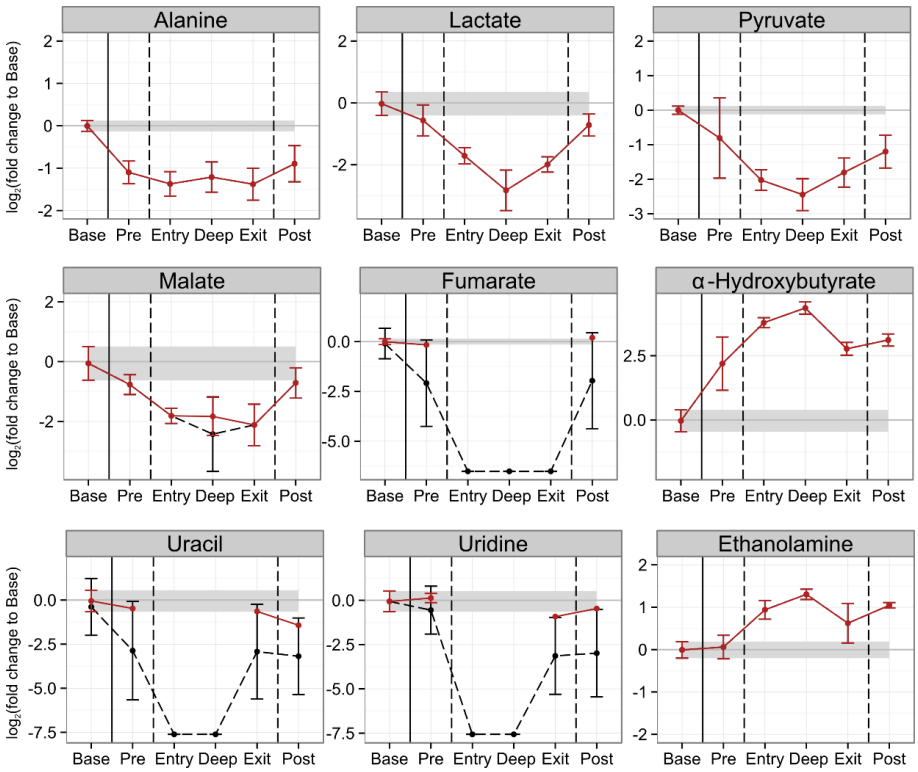


**Figure 3.41 – Members of F1 in blood serum.** Alanine, lactate, pyruvate, malate, and fumarate behavior in blood serum represent the glycolytic inhibition and depression of the TCA cycle during torpor in liver and muscle. Lactate rising in the exit phase indicates the return of glycolytic activity during torpor arousal. α-hydroxybutyrate levels behaved similarly in blood serum, liver and muscle (data not shown). Uracil, uridine, and ethanolamine are also part of F1 but their contributions to the torpor phenotype are at this time unresolved.

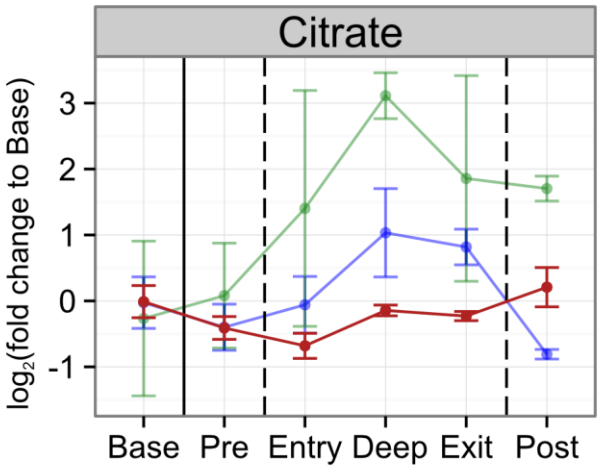


**Figure 3.42 – Citrate levels in blood serum, liver and WAT.** Citrate levels in blood serum (red) increase in accordance with the accumulation observed in the deep phase in liver (blue) and WAT (green).

F2 contains metabolites that are decreased in the pre and entry phases when compared to baseline, but then accumulate in the deep phase to below, above, or original baseline levels and remain relatively constant thereafter. This factor contains glucose, glucuronate, mannitol, pantothenate, cytosine, and the amino acids methionine, proline, pyroglutamate, and threonine (Figure 3.43). It is representative for the amino acid accumulation seen primarily in liver and to a lesser extend in muscle, as well as the buffering hypothesized before. It appears to be stocked with metabolites necessary to support the exit from torpor like glucose, and more generally contains metabolites that are similar in deep and exit phases with the exception of pyroglutamate and threonine that are quickly cleared in the exit phase. An alternative to the hypothesis of preemptively enriching metabolites required for arousal is the possibility of metabolite accumulation or depletion, the re-establishment of original levels of which necessitating arousal, an idea previously proposed for hibernation (Epperson et al. 2011). Most likely is a combination of both.

F3 contains compounds that are similar in both the pre and post phase like 2-hydroxyglutarate and the sugar acid threonate, but also contains with glycerol the primary indicator for the mobilization of fatty acids, the second major fuel source aside from glucose (Figure 3.44). The behavior of glycerol in blood serum is mimicked in WAT, leading to the conclusion, as mentioned before, that lipolysis is active during the pre phase, turned off during torpor, and resumes upon exit.

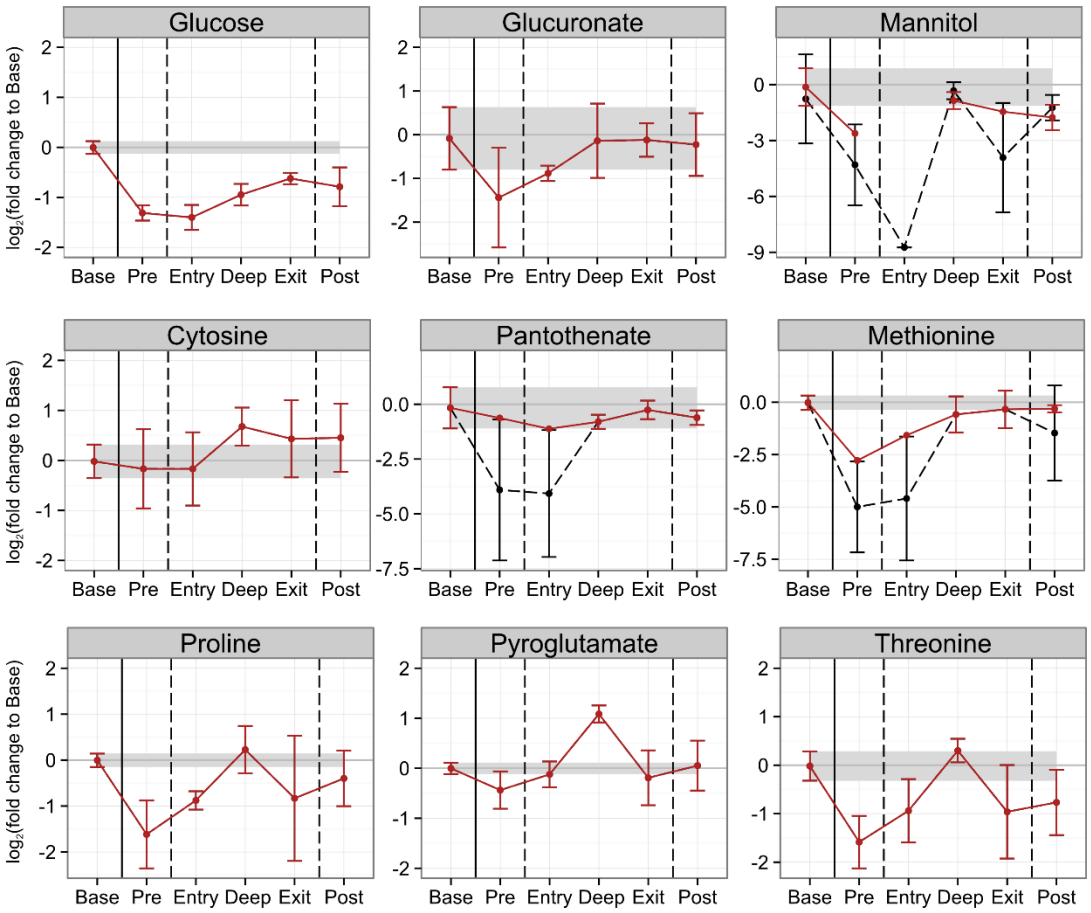


**Figure 3.43 – Members of F2 in blood serum samples.** The factor contains metabolites that decreased initially and then recovered during the deep phase to or above baseline levels. While detailed interpretation is difficult, it is interesting to note that glucose abundance increased already in the deep phase. Similarly, several amino acids accumulated in the deep phase in agreement with an accumulating trend observed in the tissues.

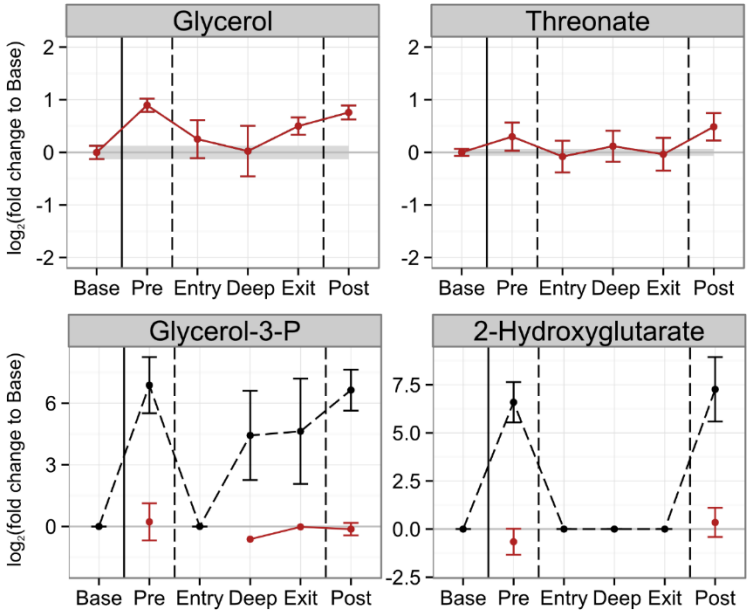


**Figure 3.44 – Members of F3 in blood serum samples.** This factor contains only two metabolites that were not largely imputed, namely glycerol and threonate. Whereas the function of threonate in mammalian metabolism is unclear, glycerol levels in blood corresponded to known phases of lipid mobilization (pre, exit, and post).

F4 contains only three metabolites, two of which are largely imputed, but generally represents those metabolites that render the exit phase distinct from all others. In the case of glycerate, the only metabolite in the factor measured reliably, the exit phase features its lowest abundance that recovers to near pre phase levels in the post phase (Figure 3.45).

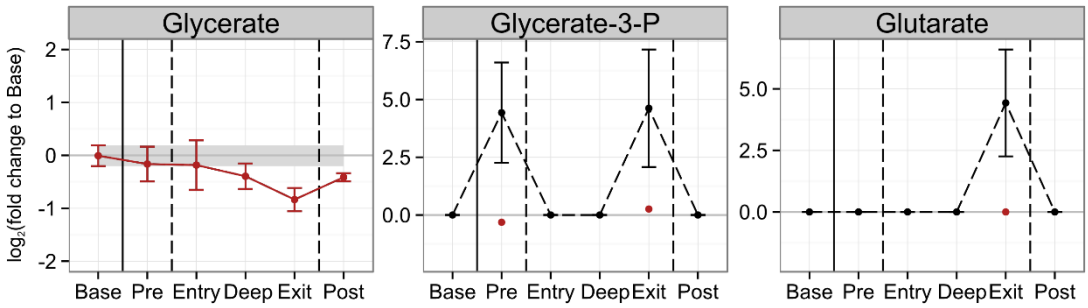


**Figure 3.45 – Members of F4 in blood serum samples.** The fourth factor contains only a single metabolite without largely imputed values, namely glycerate. Its abundance decreased during the exit phase and its functional significance is unclear at this time.

In conclusion, the blood serum is powerful in representing the overall physiological state of an animal. The TCA cycle suppression in tissues is represented in lowered TCA intermediates (Figure 3.41, see malate/fumarate), and the general amino acid accumulation observed in both muscle and liver is at least partially reflected (Figure 3.43). Most apparently mirrored, however, is the use and management of the primary fuel sources glucose and fatty acids. The mobilization of fat stores is indicated clearly by glycerol levels, which correspond strikingly with glycerol levels measured in WAT (Figure 3.36). Similarly, both glycolytic activity of muscle and liver is reflected in serum glucose, lactate, and pyruvate levels, which also serve to discern periods of gluconeogenesis (Figure 3.46). Especially the ability to infer fuel source regulation, but also the general sense of being able to draw reasonable conclusions about organ function based on their reflection in the blood serum metabolome served as motivation for the Campus Run experiment, and represents the first successful systematic study of how organ physiology is reflected in the blood serum metabolome.

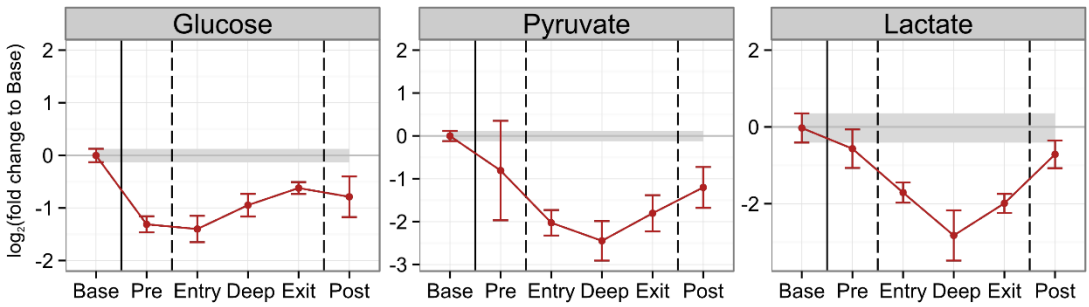


**Figure 3.46 – Glucose, pyruvate, and lactate levels in blood serum reflect times of gluconeogenic and glycolytic activity observed in liver and muscle.** Decreasing glucose, pyruvate, and lactate levels during the early torpor phases indicated the depression of glycolytic activity in liver and muscle. Further lactate depletion and concurrent glucose level increases in the deep phase indicated hepatic gluconeogenesis. The resumption of glycolysis during torpor arousal was reflected in pyruvate and lactate levels increasing in the exit phase.

### 3.3.6 Cerebrospinal Fluid

The CSF is of interest in the study of torpor because it can be sensed by and released into by key areas of the hypothalamus that contain, among other crucial homeostatic centers, those that control body temperature and energy expenditure. It is known to maintain appropriate concentrations of neurotransmitters and considered to play an active role in brain state and general neuronal communication and likely contains immense diagnostic and mechanistic information for both physiological and pathophysiological processes (Zappaterra & Lehtinen 2012; Smolinska et al. 2012).

Plotting the first two principal components of PCA of CSF samples displayed an interesting pattern that is unlike any of the other tissues (Figure 3.47). The exit, deep, and recovery phases are in close proximity to each other, while the baseline and pre phases are furthest removed from each other and the conglomerate of aforementioned phases. The entry phase is located between the pre and the deep/exit/post phase cluster. k-means clustering produced the maximal silhouette width when six clusters were allowed to form, correctly clustering all biological replicates of distinct phases together (Figure 3.48). Hierarchical clustering failed to group one recovery replicate appropriately when using the average linkage method, but was able to do so successfully when employing the Ward linkage method of hierarchical clustering (Figure 3.49). I found the pre and baseline phases to form one of the two major branches. The deep and exit phases are closely related in congruence with k-means

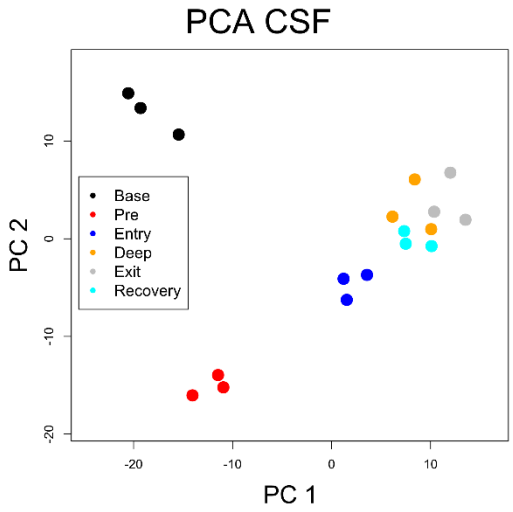


**Figure 3.47 – PCA analysis of CSF samples.**
Plotting the first two principle components of the CSF samples results in a strong grouping of biological replicates; however, the deep, exit, and recovery phases are in very close proximity.

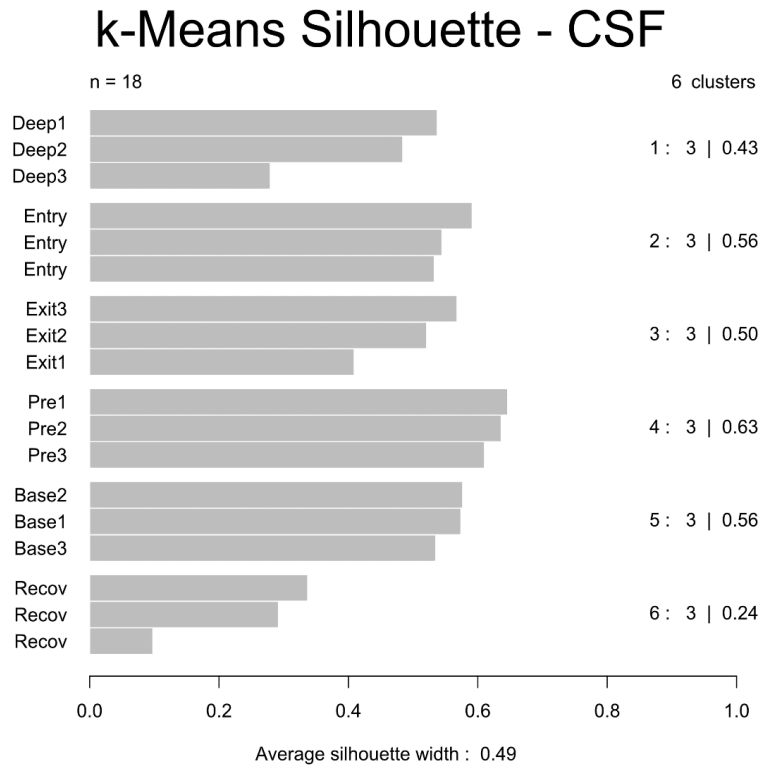


**Figure 3.48 – k-means clustering of CSF samples**.
The silhouette plot of k-means clustering of six clusters of CSF samples shows that biological replicates of the torpor phases form reasonably strong clusters, despite the deep, exit, and recovery phases appearing quite similar in PC1 and PC2.

clustering and PCA, with the recovery and entry phases located between them and the pre/baseline branch. An interesting observation is that the CSF and blood serum show clearly different structures of relatedness among the torpor phases. Whereas the baseline and pre phases are quite similar in the CSF, they are least related in blood serum. Similarities in blood serum between baseline and entry and pre and post phases are not observed in CSF, the only commonality between the two tissues being the relatedness of the deep and exit phases.

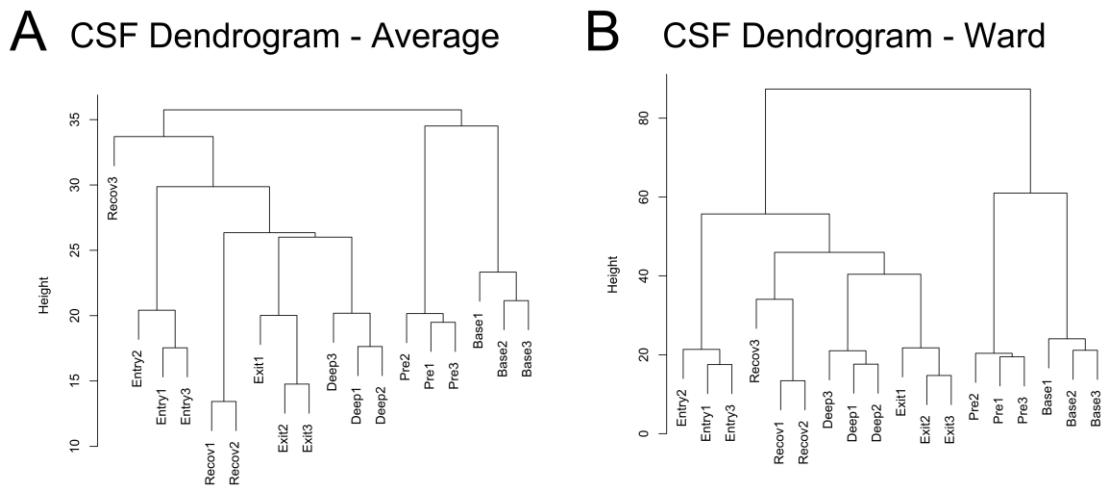


**Figure 3.49 – Dendrograms of hierarchical clustering of CSF samples using the average and Ward linkage methods.** A) In accordance with the k-means clustering and PCA, hierarchical clustering using average linkage grouped all biological replicates together, with the exception of a single recovery phase. B) Using the Ward linkage method, which favors the formation of equally-sized clusters, all biological replicates clustered together. Baseline and pre phases form one branch, the entry another, and the deep, exit, and recovery phases appear closely related as indicated by the plotting of PC1 and PC2.

Factor analysis of the Pearson correlation matrix of all known metabolites measured in CSF revealed four factors. F1 contains metabolites that distinguish the first or the first two phases from all others. It is composed entirely of nucleotide derivatives and amino acids, their abundance either strongly decreasing or dropping below detection limits in the entry torpor phase and never recovering thereafter (Figure 3.50). Three members of the factor, adenine, uracil, and pyroglutamate (a mixture of glutamine, glutamate, and pyroglutamate), are of special interest, as they themselves or their derivatives may function as neurotransmitters or signal by interaction with cell surface receptors in the central nervous system (Dalziel & Westfall 1994; Ciana et al. 2006; Zhou & Danbolt 2014). Proline, which shows a similar pattern and curiously peaks during the exit phase, has also recently been described as an active neurotransmitter (Takemoto 2011).

F2 contains metabolites in which the exit phase has similar abundance levels as observed in the fed baseline state. This factor contains glucose, glycerate, mannose, triethanolamine, and uridine (Figure 3.51). As hypothesized earlier, the brain is an ideal site for sensing when it is energetically possible to exit torpor, and therefore metabolites that peak before or during the exit qualify as candidates to carry that information. Since the decision is likely based on energy availability, a direct sensing

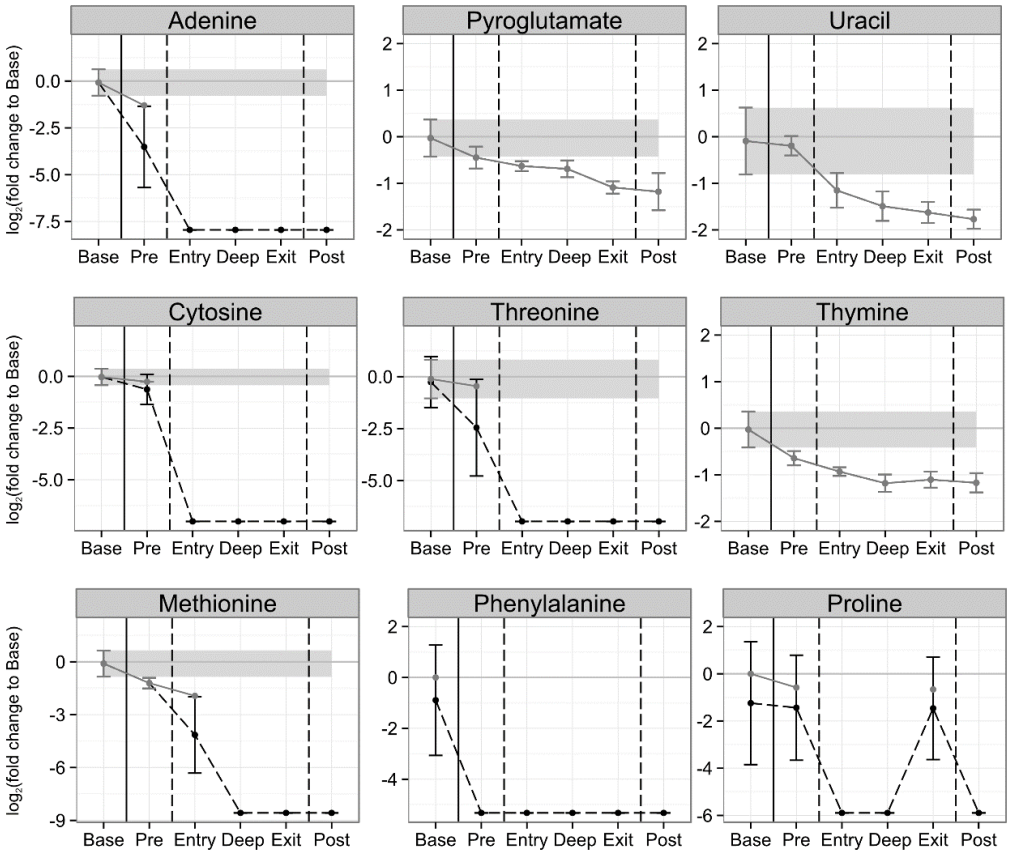


**Figure 3.50 – Members of F1 in CSF samples.** F1 is characterized by metabolites that decreased in abundance steadily between baseline and pre, and then more strongly during the entry phase, and never recovered their original levels thereafter. Of special interest here are adenine, pyroglutamate, uracil, and proline, as they have known signaling functions and/or serve as neurotransmitters in the central nervous system.

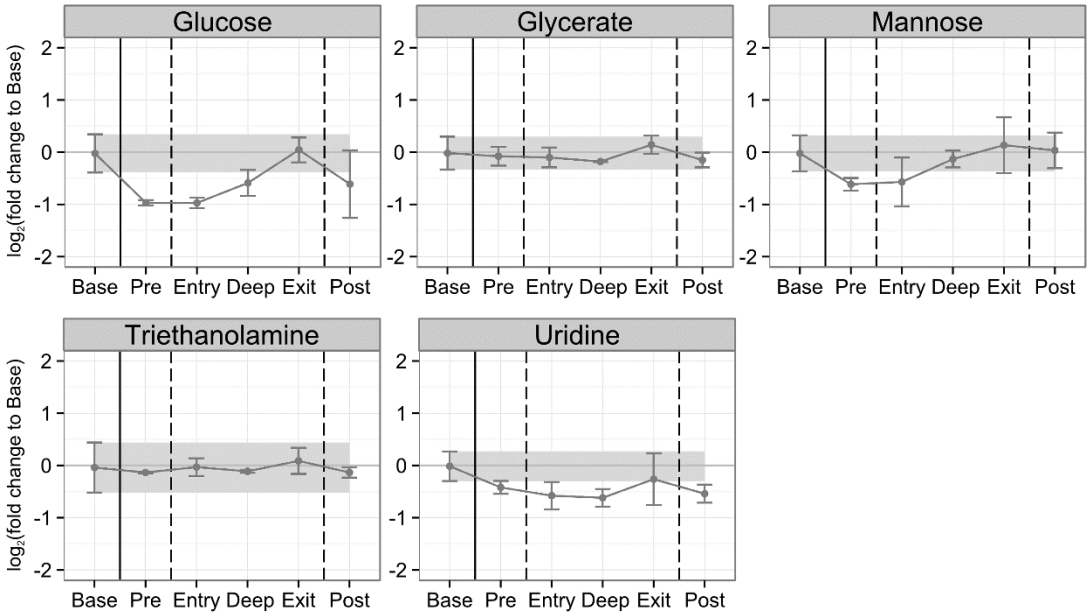


**Figure 3.51 – Members of F2 in CSF samples.** Metabolites in F2 showed an initial decrease in abundance but recovered to baseline levels during the exit phase of torpor. Of special interest here is glucose, which may serve as an indicator of sufficient carbohydrate stores to allow for initiation of torpor arousal.

of glucose levels might be sufficient for the decision to be made. In this second factor, glucose also shows the highest dynamics, its levels dropping the lowest and recovering entirely in the exit phase before decreasing again in the post phase, its range having the potential to encode more information than other metabolites in the factor. In this line of argument it is of note that there are two other compounds that show a distinct peak in the exit phase but are not part of F2, namely fructose and an unknown compound (Figure 3.52). It would be interesting to see in future studies if glucose, fructose, or the unknown compound (once identified) levels are able to influence torpor exit timing.

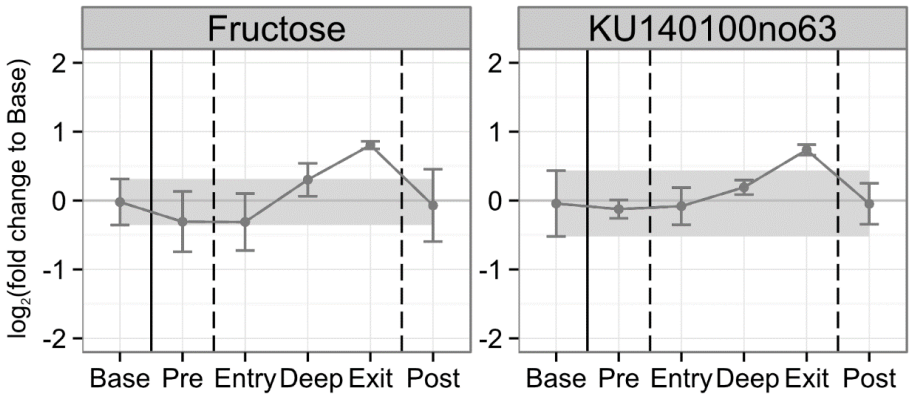


**Figure 3.52 – Fructose and an unknown metabolite peak during the exit phase.** Of special interest are compounds that peaked during the exit phase in the CSF, as they could prove instrumental in mediating arousal from torpor. Fructose and an unknown metabolite shown here displayed such behavior.

F3 contains the sugar alcohols arabitol and ribitol, as well as citrate, their commonality being a sharp drop in abundance in the post phase. Anti-correlated but also in the factor are putrescine, hypoxanthine, and α-α-trehalose, all of them measured at the detection level threshold and containing many imputed values (Figure 3.53). The only reasonable conclusion that can be drawn from this factor is a requirement of arabitol and ribitol during the exit phase or immediately after waking, the reasons for which, however, are not obvious at this point in time. F4 is made up of only two compounds whose values are largely imputed, so that its in-depth consideration is of little conclusive power.

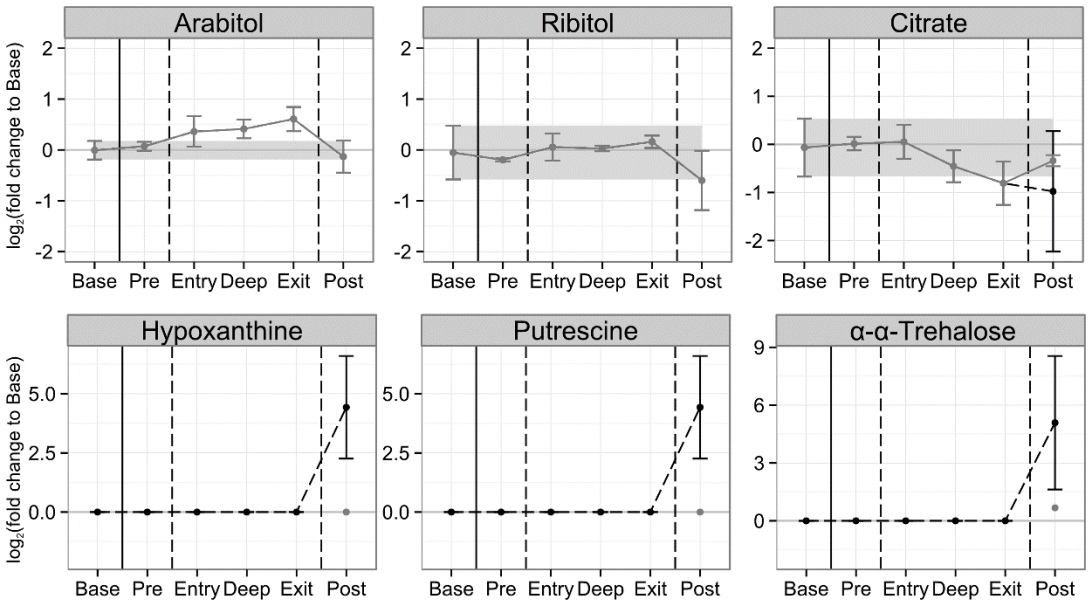


**Figure 3.53 – Members of F3 in CSF samples.** F3 is characterized by metabolites that differentiate the post phase from all others. Of interest here is the disappearance of arabitol and ribitol between the exit and post phases, which might indicate their requirement as substrates for some metabolic pathway in order to facilitate torpor exit.

The brain is an organ with a high energetic demand, and while other tissues might largely be at rest, certain areas of the brain maintain activity even during the deepest torpor phases when overall metabolism is lowest. One example of this constant vigilance is the observation that animals even in deep torpor are in full control of their body temperature, as local brain temperature changes elicit compensatory heat-generating responses (Heller et al. 1977).

While textbook knowledge states that glucose is the favored and primary energy source for the brain, ketone bodies have received much attention recently because of their apparent involvement in and beneficial contribution to brain metabolism (Nugent et al. 2014; Yifan Zhang, Kuang, LaManna, et al. 2013; Yifan Zhang, Kuang, Xu, et al. 2013; Woolf & Scheck 2014). One of the surprises of this study was that ketone bodies are already present in high concentrations during the fed baseline state, and only mildly increase during starvation when compared to other tissues (Figure 3.54). Similarly, while glucose abundance does decrease in starvation, its levels never drop as much as in blood or other tissues, and recover to baseline levels already during the exit phase, whereas they never recover in blood, liver, and muscle (Figure 3.55). It appears therefore that the CSF is regulated quite separately

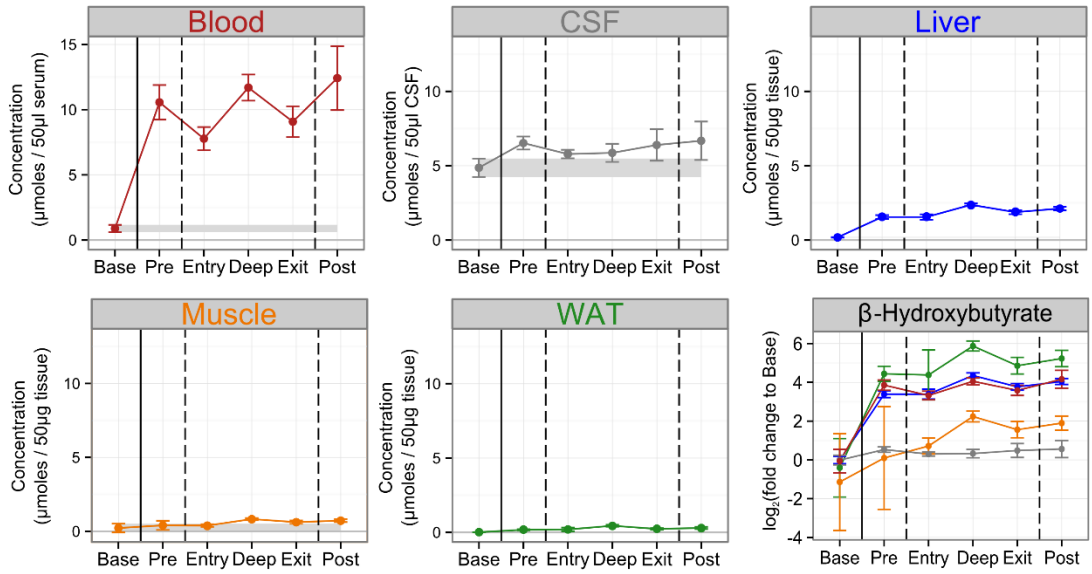


**Figure 3.54 – Absolute concentrations of β-hydroxybutyrate across tissues during torpor.** While ketone bodies commonly serve as markers of food restriction and starvation, and are only detected during such times in blood, muscle, liver, and WAT, high concentrations of β-hydroxybutyrate were found in CSF in the fed state with the subsequent starvation causing only a mild increase in its abundance. This indicates that ketone bodies are in abundant supply in the CSF at, presumably, all times.

from the rest of the body, likely due to the fact that many metabolites have active signaling roles in the central nervous system but not in the periphery. Additionally, the metabolic demands of the brain even during torpor might require a higher level of energy supply, as evidenced by both glucose level decreases being blunted and ketone bodies being available at all times. It is therefore the relative abundance and ratio of glucose to ketone bodies that changes during times of starvation and the torpor phases, and might be more useful to determine fuel availability and selection in CSF rather than the presence or absence of β-hydroxybutyrate (Figure 3.56).

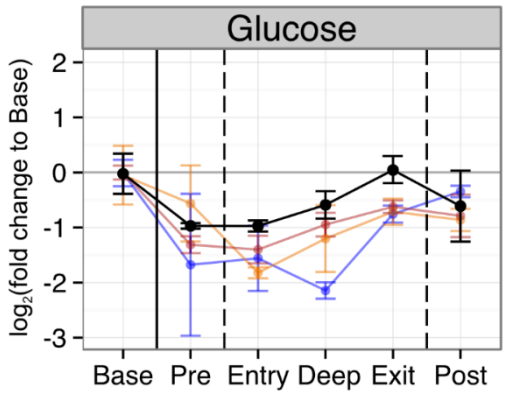


**Figure 3.55 – Glucose levels in CSF vary less strongly and recover to baseline levels during torpor exit.** In addition to glucose levels dropping lower in liver (light blue), muscle (light orange), and blood serum (light red) than CSF during torpor, glucose levels in CSF (black) recover to those observed in the fed state already in the exit phase of torpor.

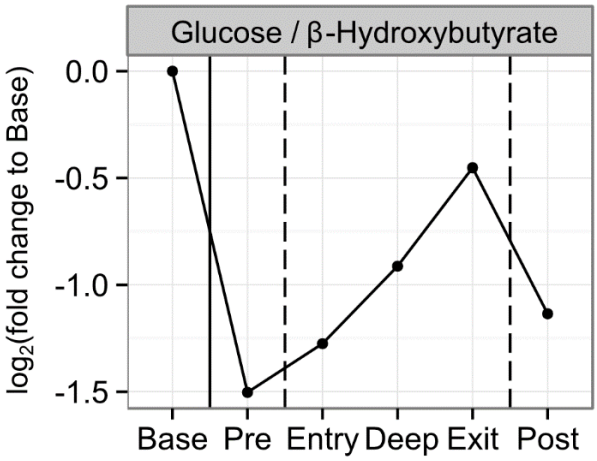


**Figure 3.56 – Glucose and β-hydroxybutyrate ratios throughout torpor in CSF.** Since both glucose and ketone bodies were present in CSF at all time points sampled in this study, a ratio between their absolute concentrations might be more indicative of fuel source selection. Indeed, the ratio of glucose to β-hydroxybutyrate is highest in the fed state, returning towards similar values during the exit phase. This could be indicative of glucose playing an important role in the brain during torpor arousal.

Similarly to the glucose level differences in CSF and blood serum, many other metabolites that vary in accordance throughout torpor do so to a lesser degree in CSF (Figure 3.57). Furthermore, many metabolites that are cellular intermediates without known signaling mechanisms in the brain show either completely different behaviors in blood serum and CSF, or differ drastically in specific torpor phases (Figure 3.58). The blood-CSF differences can have three potential causes: 1) brain-specific production, 2) brain-specific consumption, or 3) a selective transport between the blood and CSF in the blood-cerebrospinal-fluid barrier, which is maintained by choroidal cells of the choroid plexus.

In accordance with the choroid plexus, which produces CSF from blood in the first place, being "one of the most understudied tissues in neuroscience", specifics about metabolite filtering or selection between blood and CSF have not been systematically studied (Lehtinen et al. 2013). It is therefore extremely difficult to interpret the observed differences, because the choroid plexus and in addition the numerous astrocytes, known to be metabolically versatile and supportive of the neuronal populations, are likely major contributors to metabolite level regulation (Rossi et al. 2007; Sonnewald et al. 1994). The choroid plexus, for example, is involved in the maintenance of neurotransmitter levels (i.e. glutamate (measured as pyroglutamate), glycine, adenosine/adenine, proline, etc…), compounds that in the rest of the body would be considered from a metabolic rather than a signaling perspective.

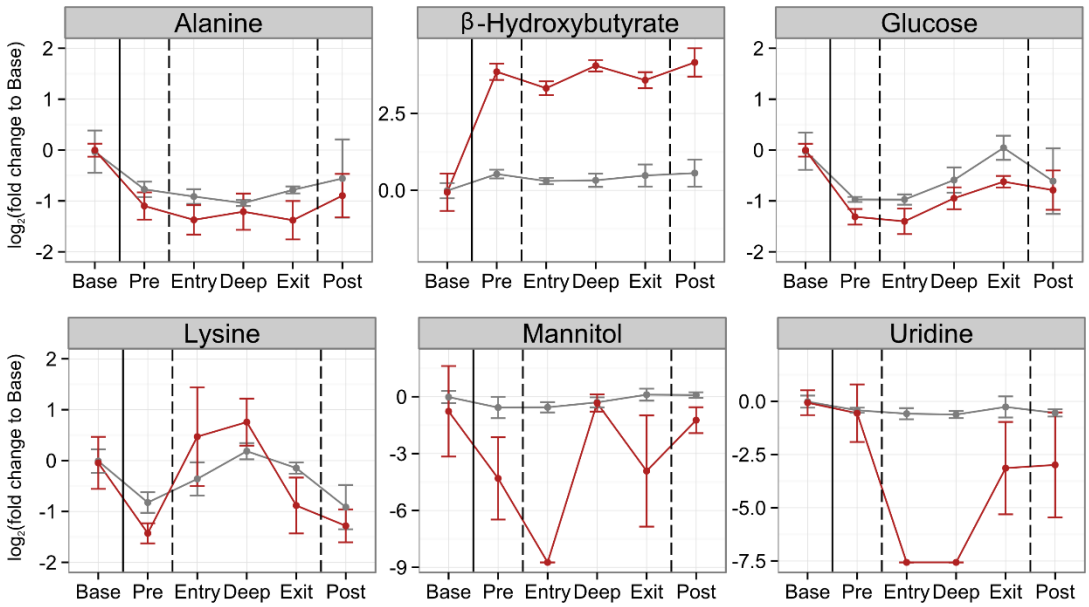


**Figure 3.57 – Metabolite abundance changes are less pronounced in CSF when compared to blood serum.** CSF (gray) and blood serum (red) levels of many metabolites vary similarly, but do so to a lesser degree in CSF. This difference is best exemplified by the six metabolites displayed.

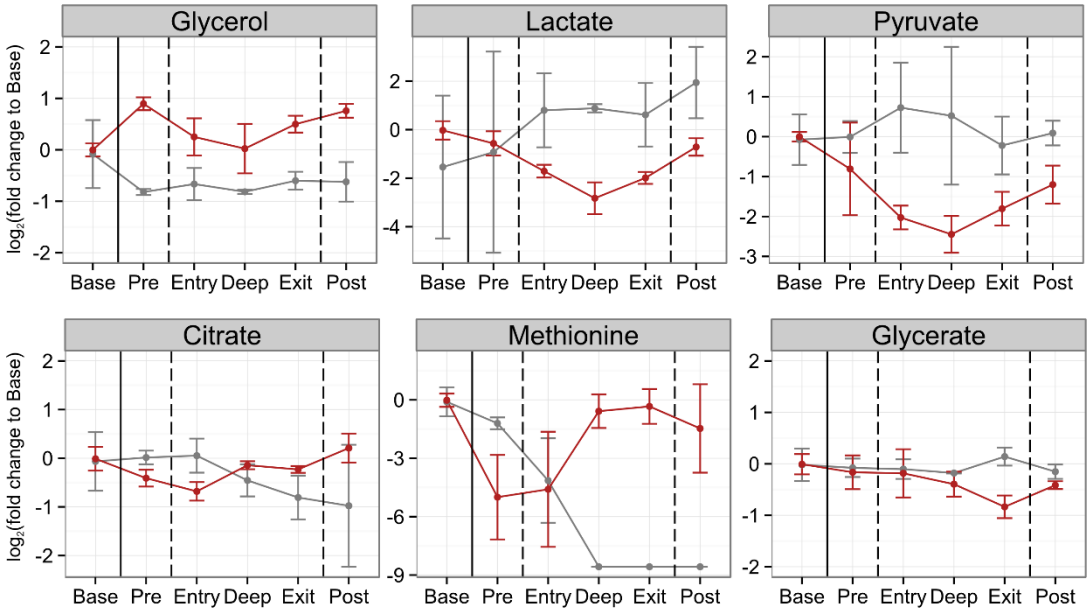


**Figure 3.58 – Metabolite behavior in CSF and blood serum are in disagreement in most instances.** CSF (gray) and blood serum (red) levels of several metabolites either behave entirely differently throughout torpor (glycerol, lactate, pyruvate, citrate, methionine), or vary only in specific phases of the torpor cycle as exemplified by glycerate.

These data suggest and are in congruence with the choroid plexus and glial cells acting as regulatory organs for the central nervous system-specific circulatory fluid CSF. Similar to what the liver accomplishes for the rest of the body (with contributions from

other organs), they appear to control fuel source availability and other important metabolite levels quite independently from the blood serum, creating a milieu in the central nervous system that can be considered metabolically separate from the rest of the body.

In conclusion, one of the most striking observations made during the torpor study was the strong difference between the blood serum and CSF metabolomes. In the general overview section both PCA and hierarchical clustering indicated the CSF to be the most distinct tissue (Figures 3.3 and 3.4). While the CSF contains many new unknown peaks that certainly separate it from other tissues, many metabolites that were found in both blood serum and CSF either behaved utterly different or their amplitudes of change were lower in CSF. While differences in composition are known, this study the first to track a dynamic process like torpor in both blood serum and CSF and shows the true extend of their dissimilarity. Particularly interesting from an energetic point of view were the behaviors of glucose and β-hydroxybutyrate in the CSF, the former potentially signaling that enough energy is present to facilitate rewarming by its levels increasing to fed-state levels during the exit phase, and the latter being already present in high concentrations during the fed state, when it is below detection threshold in all other tissues and commonly considered as a marker of starvation only.

## 3.4 Discussion

In this study, I have monitored metabolic changes in liver, muscle, WAT, blood serum, and CSF that occur throughout the full torpor cycle to gain insight into the mechanisms regulating entry into, maintenance of, and arousal from torpor. Furthermore, the size of the dataset allowed for the first time a systematic investigation of how the blood serum and CSF metabolome compositions differ, and how the blood serum metabolome reflects organ physiology throughout a metabolically diverse biological process.

The dataset can be judged to be of high quality due to the fact that hierarchical clustering was able to separate the individual tissues from one another, as well as the biological replicates of the distinct torpor phases in each of the individual tissues. Clustering of the torpor phases within each tissue, in combination with correlation

matrix-based factor analysis and study of specific crucial pathways allowed for the first time the formulation of mechanistic hypotheses regarding the metabolic changes occurring in liver, muscle, WAT, blood serum, and CSF.

Generally, metabolic mechanisms of entry into and arousal from torpor are of greatest interest, as they represent the two crucial decision points of torpor. Marking both the beginning and end of the process, they are each accompanied by drastic metabolic changes. Torpor entry is suspected to be mediated by a mechanism, or multiple mechanisms, of active metabolic suppression. Arousal from torpor is an energetically demanding process as animals need to raise their CBT by almost 20 °C, which is accomplished by a combination of shivering thermogenesis, non-shivering thermogenesis in the form of uncoupled mitochondrial activity in BAT, and passive heat generation as a result of general metabolic activity throughout the body. While the exact contribution of these factors to the process of rewarming is unknown, shivering and passive heat generated from an active metabolism likely contribute most in our study as BAT is not required for torpor arousal and our acclimatization protocol minimized BAT mass (personal observation) and thermogenic potential (Cannon & Nedergaard 2011; Oelkrug et al. 2011). It is of interest to note that wild torporic animals have frequently been observed to expose themselves to sunlight to aid in the rewarming, saving even more energy by minimizing shivering and BAT-dependent thermogenesis (Geiser & Drury 2003). The animals in this study were observed to shiver extensively, and without significant contributions from BAT or sunlight, the only other contributing factor to rewarming was likely passive heat generated by overall metabolic processes. Metabolic changes during torpor and their relation to the current state of knowledge, as well as the insights gained into the organ-derived metabolic signatures in blood serum will be discussed in detail in the following sections.

### 3.4.1 Liver

I found two distinct metabolic phases in the liver, one occurring during the earlier phases of entry and deep torpor, and the other occurring during the exit and after waking.

Because of the decrease and disappearance of glycolytic intermediates and lactate during the early phases, as well as an accumulation of citrate relative to succinate, both glycolytic and TCA cycle activities appeared to be diminished. There are several lines of evidence supporting both glycolytic and mitochondrial suppression during daily torpor in liver. Respiratory retention of carbon dioxide just prior to torpor entry causes a significant acidosis in blood and several tissues, with strongest effects on the brain and muscle, but nonetheless possible effects on liver (P. Bickler 1984; Nestler 1990b; Nestler 1990a). In support of this, several enzymes in upper and lower glycolysis, most notably pyruvate dehydrogenase (PDH), were found to be significantly less active in deep torpor when compared to euthermic controls (Heldmaier et al. 1999). Mitochondrial activity was similarly found to be decreased by both active suppression and passive temperature effects in both dwarf Siberian hamsters and three strains of laboratory mice, including C57/Bl6, comparing deep torpor and euthermic controls (Brown & Staples 2010; Brown et al. 2007). It is therefore a reasonable conclusion that a combination of active and passive metabolic suppression, both at the level of glycolysis and mitochondrial activity, plays a key role in mediating the entrance into and possibly maintenance of daily torpor in liver.

Due to lactate, alanine, and glycerol-3-phosphate disappearance, concurrent amino acid accumulation and processing, as well as the rise of glucose levels in blood and other tissues, gluconeogenesis appears to be active in torporic livers in mice. While there have been no investigations focusing on gluconeogenesis to provide a conclusive and comprehensive sense of its activity, several indications exist which are, at least, not contradictive to this novel finding. First, the activity of two out of four gluconeogenic enzymes, when compared to euthermic controls, showed an increasing trend, though neither was statistically significant. The other two enzymes were neither statistically significant nor indicated a trend, in the least indicating that the gluconeogenic potential of the liver is maintained during deep torpor. Other authors have mentioned that carbon dioxide accumulation in tissues during torpor might potentiate gluconeogenesis (Walker et al. 1983). While the gluconeogenic potential does not seem to change, the drastic reduction in glycolysis and mitochondrial activity might contribute, or in a sense "allow", for gluconeogenesis to take place.

The competing hypotheses of active protein degradation, protein synthesis inhibition, or amino acid acquisition from blood serum could not be differentiated by this dataset. Amino acid metabolism has received no attention in the study of daily torpor, except that both transcription and translation appear to be suppressed, as indicated by decreases in polysome complexes during the deep phase compared to euthermic levels (Berriel Diaz et al. 2004). The study is in accordance with an almost identical study with identical results carried out in hibernating squirrels, leading to the conclusion that the energetically demanding processes of transcription and translation are repressed during both hibernation and torpor (Knight et al. 2000).

Since, to my knowledge, autophagy has never been investigated in daily torpor or hibernation, studies of proteasome-mediated proteolysis in hibernation provide the only indications on the activity of protein degradation during torpor. Two studies from the same group were able to show an accumulation of ubiquitinylated proteins, as well as a depression of proteasome-dependent proteolysis in liver during hibernation, the effect being mostly due to the low CBTs of hibernators. Nonetheless, even at torporic temperatures, the inhibition was significant (Velickovska et al. 2005; Velickovska & van Breukelen 2007). While this at first appears to argue against active proteolysis, the inhibition was not total. In fact, a group specifically studying the maintenance of muscle mass and contractility after months of immobility in hibernation showed evidence in hibernating bats that the maintenance of muscle mass is mediated by a constant, low level of proteolysis that is counterbalanced by short periods of amino acid and protein homeostasis being reestablished during the interbout arousal (Lee et al. 2010). Since the post torpor phase in this dissertation is quite similar to the hibernation interbout arousal, the same mechanism might be at play in daily torpor in both liver and/or muscle, as we observe most amino acid levels return to pre phase levels after accumulation in both tissue and blood serum. It is therefore possible that active proteolysis, even if partially suppressed at the level of the proteasome as compared to euthermia, is nonetheless less suppressed than protein synthesis, causing an accumulation of amino acids in the deep torpor phase. Additionally, the accumulation could be caused by autophagic mechanisms that are yet to be investigated in the context of hypometabolism.

It is of note also that an accumulation of modified amino acids has been observed in blood plasma from hibernating squirrels in the only other extensive metabolomic study (Epperson et al. 2011). Amino acids in liver in our study showed comparable behavior in the NMR and LC-MS metabolomic studies of liver from hibernators, given the caveat that far fewer phases were sampled (NMR study), and comparability between summer active ground squirrel and fed or starved mouse metabolism is not guaranteed. One clear difference between the datasets are the branched-chain amino acids valine, leucine, and isoleucine, which accumulated in the deep phase of torpor, and decreased significantly in the deep hibernation phase when compared either to hibernation entry or the summer active control (Serkova et al. 2007; Nelson et al. 2009). The reasons for this difference are unclear. Nonetheless, strong and indisputable evidence from my study indicates urea cycle activity during early torpor with a subsequent accumulation of urea in both liver and the blood, which to my knowledge represents the first report supportive of amino acid catabolism being crucially involved in daily torpor.

Glucose, alanine, succinate, and lactate are of mechanistic interest and showed similar patterns in my and the NMR dataset. Inosine and uridine, which were found in the LC-MS study, are also in agreement with my dataset.

The second phase of liver metabolism begins in the exit and continues into the post phase. It is marked by an increase in the glycolysis product lactate, a rise in glycolytic intermediates, as well as the removal of the TCA cycle block at the level of citrate, indicating that the inhibition of glycolysis and the TCA cycle that allowed for gluconeogenesis is alleviated and a glycolytic metabolic signature established. Curiously, none of the studies cited above measured changes in enzymatic or mitochondrial activity during torpor exit, focusing mostly on metabolic suppression as a mechanism of torpor entry. It is suggested, considering the rise in metabolic rate and respiratory quotient information, that mainly lipids fuel rewarming, but glycogen reductions are seen both in liver and muscle, an observation consistent with our results indicating the restart of both glycolysis and mitochondrial activity during arousal from daily torpor (Nestler 1990b; Nestler 1991; Heldmaier et al. 1999). It is also interesting to note that glucose and glycogen appear to play a crucial role in heart metabolism throughout torpor, lending further support that the major gluconeogenic tissue of the body, the liver, has to meet a known glucose demand during torpor (Nestler 1991).

Because of the possibility of the kidney playing a role in gluconeogenesis during torpor, I have planned to measure kidney samples from the mice used in this study for all phases in the nearest possible future. It is my hope to then be able to attribute the relative contribution of liver and kidney gluconeogenesis to the observed increases in glucose levels in blood serum, WAT, muscle, and the CSF.

While the liver is generally considered to obtain its energy from fatty acid oxidation, glycolytic activity might be required to contribute to the various energetic demands during torpor exit. The liver needs to reestablish pre-torpor homeostatic levels of cellular components; for example, it has to return to a protein composition that has been depleted to provide amino acids to fuel gluconeogenesis during the entry and deep torpor phase.

Taken together, the metabolomic analysis of liver has revealed glycolytic and TCA cycle inhibition at the beginning of and during torpor in accordance with reports in the literature. Novel findings are an active period of gluconeogenesis fueled by lactate, glycerol-3-phosphate and alanine, with evidence of concurrent protein degradation and active amino acid catabolism during torpor, as well as glycolysis being active in support of fatty acid oxidation and ketone body use during torpor exit. The liver appears to be crucial to supply sufficient carbohydrates to the rest of the body during torpor to allow for the glycolytic contribution to rewarming especially in muscle. I also hypothesize that glucose production and secretion of the liver might contribute to rising glucose levels in the CSF, which may contribute to signaling that sufficient energy is available to fuel the arousal from torpor.

### 3.4.2 Muscle

The muscle most likely contributes to torporic physiology by being the largest potential source of amino acids, and by contributing most of an animal's body mass, thereby representing the largest potential source of heat generation. As discussed before, heat generation during the warming phase in our study is likely a combination of shivering

and passive heat produced by general metabolic activity, the muscle likely contributing much, if not most, even to the latter.

In this study, skeletal muscle underwent two major phases of metabolism, analogous to those observed in the liver. During the early phases, both glycolysis, because of low glycolysis intermediate, lactate, and pyruvate abundances, and the TCA cycle, seem to be suppressed. This idea is supported by muscle experiencing the strongest acidosis during daily torpor and a report describing the specific inhibition of the glycolytic enzyme phosphofructokinase (PFK) in hibernating ground squirrel muscle in torporic conditions (Nestler 1990a; Somero 1981). Furthermore, a study of glycolytic enzyme binding of substrates in daily torpor in deer mice provided evidence for decreased binding capacity in glyceraldehyde-3-phosphate dehydrogenase, pyruvate kinase, as well as PFK (Nestler et al. 1997). Using $^{14}C$ glucose as substrate and measuring $^{14}C$-containing carbon dioxide release, muscle glucose oxidation was shown to be inhibited by lowered temperature, acidosis, and substrate availability reminiscent of torpor (Nestler 1992). Muscle mitochondrial respiration capacity, however, was found to be unaffected by daily torpor in the Djungarian hamster in a study that was able to confirm liver mitochondrial suppression (Kutschke et al. 2013). Taken together, previous studies are therefore in accordance with our results showing a more subtle decrease in TCA cycle intermediates than in the liver, not contradicting, however, a TCA cycle suppression and intermediate decrease due to a lower substrate availability (pyruvate) as evident in my dataset, caused by a strong glycolytic inhibition during the early phases of daily torpor.

The second major phase begins in the exit and continues into the post phase, where glycolytic intermediates, lactate, and pyruvate increase, concomitant with TCA cycle intermediate abundances recovering to levels observed before torpor entry. As described for the liver, I suggest that both glycolysis and the TCA cycle, fueled both by glycolytic substrates and the available ketone bodies and fatty acids, contribute to increased general metabolic activity as well as the fueling of the intense shivering of animals observed during rewarming (in accordance with this hypothesis, shivering appears to make use of both glycolytic and oxidative muscle fibers (Haman et al. 2004)). While the arousal from torpor has received as little attention in the literature in muscle as in liver, one line of evidence supports the observation of the glycolytic

inhibition being lifted immediately before the beginning of the exit phase. A quick rise of respiratory quotient just prior to the stark increase in metabolic rate fueling torpor exit is said to release carbon dioxide, thereby lifting tissue acidosis and, presumably, partially the glycolytic inhibition in muscle, which should progressively lessen as CBT increases (Nestler 1990b). In accordance with glycolytic activity contributing to rewarming is the observation that muscle glycogen stores are significantly depleted between the deep and exit phase in deer mice (Nestler 1991).

The only unresolved observation, as described in the liver section of the discussion, is the amino acid accumulation during the deep torpor phase. Further studies are required to attain a final conclusion.

### 3.4.3 White Adipose Tissue

WAT is the tissue in which the fewest significantly changed metabolites were observed, and displayed high biological variation in compounds that appear to be tightly regulated in the other tissues examined. Its metabolic role in daily torpor has so far been reduced to glycerol and fatty acid release into the blood stream, from where the liver takes them up and processes them to ketone bodies and glucose for the rest of the body.

Interestingly, no metabolic studies have been conducted on WAT in daily torpor, and very few in hibernation research. The hibernation studies have mostly focused on the mechanisms and timing of fat accumulation (Wang et al. 1997; Baumber & Denyes 1963; Cochet et al. 1999). However, two studies considering lipolysis in WAT described an inhibition of WAT lipolysis during the deep hibernation phase and provided evidence for release of triglyceride stores during arousal from hibernation (Spencer et al. 1966; Dark et al. 2003). Despite the many metabolites identified in WAT, the two conclusions of the papers are identical with the only two conclusions that can be confidently drawn from this dataset. Considering glycerol abundances in both blood serum and WAT, WAT fat store mobilization is active during the pre phase, interrupted during the entry and deep phases, and reactivated during the exit and maintained in the post phase. No conclusive evidence for an active inhibition of the central carbon metabolism during torpor was obtained, and there is no literature on the

topic. If anything, there appears to be a paradoxical glycolytic activation during the deep torpor phase. This finding could be interesting in itself but is at this point inexplicable, or might be representative of peak detection and identification uncertainties at the mass spectrometer's detection threshold.

In conclusion, despite WAT being of great importance to torpor as the site of triglyceride storage and leptin secretion, its CCM appears to be metabolically passive apart from triglyceride release in the pre, exit, and post phases, the process being inhibited towards and during the deep torpor phase, indicating that its regulatory involvement in torpor might not be reflected in the central carbon metabolism.

### 3.4.4 Cerebrospinal Fluid

It was the intention to use the CSF metabolome to understand brain metabolism, just like sampling blood would provide information about organ metabolism. However, brain tissue in this screen was handled in a way that optimized the stability of neuropeptides and their extraction from the hypothalamus, a protocol that is incompatible with metabolomic analysis. The project investigating neuropeptides during torpor is conducted independently of this dissertation. It was my hope that the metabolite levels in CSF would be in general very similar to those found in blood, so as to be able to attribute strong differences to brain metabolism. However, nearly all metabolites measured in both CSF and blood behaved differently, so that the lack of metabolic information from brain tissue is extremely unfortunate. The simultaneous effects of neuronal metabolism, glial cell metabolism, and apparently very selective exchange with the blood as determinants of CSF composition render me careful and hesitant to avoid overinterpretation in the face of too many unknown factors.

Despite being unable to uncover detailed mechanisms of brain metabolic changes during torpor from the CSF, some intriguing observations were made. CSF contained the second fewest significantly changed metabolites, and the changes in those metabolites that corresponded well in behavior with the blood metabolome were of a smaller magnitude. Furthermore, many metabolites behaved very differently, altogether

indicating that metabolite levels in CSF are actively and independently controlled (Figures 3.57 and 3.58).

Interestingly, β-hydroxybutyrate, which is detected in blood only during food restriction and starvation, was present in significant levels in the fed state, increasing less upon food restriction than observed in blood and other tissues. Another potential significant observation is that glucose levels initially drop in the pre and early phases and begin to rise in the deep phase, as observed in the blood, but then actually recover to be identical to those observed in the fed state. While there is no evidence in the literature of glucose playing a signaling role during the waking phase in daily torpor, a reasonable suggestion is that glucose levels in the CSF are sensed, and when sufficiently high, presumably indicating sufficient carbohydrate reserves, provide a permissive signal for the arousal phase to begin. In accordance with this idea is a report that tanycytes, which line the third ventricle of the brain, can sense glucose concentration similar to pancreatic β-cells and may play a role in T3 availability in the hypothalamus to drive metabolic rate (Bechtold et al. 2012).

Although I have found no reports on cerebral metabolism in daily torpor, an *in vivo* metabolomics study has been performed in hibernating squirrels with the use of NMR (Henry et al. 2007). The authors analyzed animals in fall, spring, deep hibernation and interbout arousals. They found an increased phosphocreatine to creatine ratio in deep hibernation, indicating stored energy, and observed no significant changes in myo-inositol and lactate levels, the latter two corresponding to what I have observed in CSF (Figures 3.58 and 3.59). Constant levels of lactate are in stark contrast to those observed for blood in my and other datasets, but make sense in light of glycolytic enzyme activity being unchanged in brain from hibernating squirrels despite significant brain acidosis (Heldmaier et al. 1999). Glucose concentrations were highest during interbout arousals, but even in deep hibernation elevated when compared to both fall and spring animals. While glucose levels rose during the deep and exit phase relative to the entry phase, glucose never increased above the fed control in any torpor phase in CSF. It is therefore possible that the brain levels of glucose are elevated relative to the CSF during both torpor and hibernation, but this remains to be validated by a study measuring both CSF and brain metabolites simultaneously. The most significant finding of the study were

decreased levels of both glutamine and glutamate, which was interpreted as a means to suppress excitatory neuronal transmission by neurotransmitter depletion. Similarly, I observed reduced levels of pyroglutamate (to be interpreted as a combined representation of glutamine, glutamate, and pyroglutamate levels) in CSF throughout torpor, with a first decrease occurring between the pre and entry phases, and a second between the deep and exit phases (Figure 3.50).

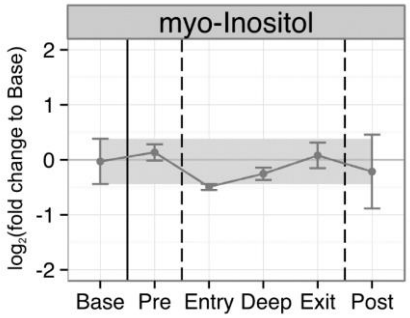


**Figure 3.59 – Myo-inositol in CSF.** There occurred no significant changes in myo-inositol levels in CSF throughout the torpor study.

In conclusion, despite the limiting circumstance of the lack of brain metabolome data, the little information obtainable from the literature seems to be in line with the CSF metabolomes acquired in this study. The CSF does not correlate with behavior of the blood metabolome in any meaningful way, and it remains to be seen if the greatest diagnostic potential for brain metabolism lies in the metabolomic analysis of CSF or blood, or requires a combination of both.

### 3.4.5 Blood Serum and Perspectives

The blood metabolome is of special interest to the study of any physiological process as it contains a conglomerate of information from all tissues of the body. Demands of a tissue can be reflected by sudden depletions of required metabolites, whereas the accumulation of others may signal increased activity of specific pathways. As suggested in the title of this dissertation, the goal of this and future research is to understand the blood metabolome in such detail that it becomes possible to judge

metabolic imbalances of organs, allowing for the diagnosis of pathologic physiology and gain hints as to the molecular mechanisms of diseases in human patients.

In this context, this metabolomic study of daily torpor provided the means to monitor extreme metabolic changes in relevant tissues, as well as their reflection in the blood serum. Since torpor is mainly an energetic phenotype, fuel availability and fuel selection were of primary interest. One intention was to study how the torpor blood metabolomes would reflect both the demands and supply of metabolic fuel, as well as relative activities of CCM pathways of the organs at specific times of the torpor cycle.

Indeed, both gluconeogenesis in liver and fat store release from WAT were faithfully represented in blood glucose and glycerol levels. Similarly, glycolytic activity in muscle and liver before torpor and during the waking phases, as well as its inhibition during the early phases of torpor, were reflected in levels of lactate, alanine, and pyruvate. TCA cycle repression in liver and muscle correlated with malate levels and the disappearance of fumarate in blood, and amino acid accumulation, observed both in liver and muscle to varying degrees, correlated with similar increases in blood for many of the amino acids. Lastly, urea levels in blood rose in accordance with those in liver, so that in conclusion, all major metabolic pathways and their activity assessable using GC-MS technology were at least partially represented in the blood metabolome. These observations inspired and motivated the second part of this thesis and have determined the direction of my future research undertakings.

To my knowledge, only one study has monitored metabolite levels in blood during daily torpor, finding patterns identical to those observed in this dissertation for glucose, β-hydroxybutyrate, and lactate (Nestler 1991). However, the study failed to capture the dynamic nature of lactate and glucose within torpor phases, as only the pre, deep, and post phases were assessed.

Blood serum has been the subject of two metabolomic studies in hibernating ground squirrels, using LC-MS and a combination of LC-MS and GC-MS (Nelson et al. 2010; Epperson et al. 2011). The LC-MS-only study mainly measured fatty acids and derivatives thereof. Only three metabolites were detected in common: tyrosine,

methionine, and pantothenate, all of which behaved differently in the torpor and their dataset.

These differences were replicated in and are explicable under consideration of the much more extensive second study which employed both LC-MS and GC-MS. Several amino acids, among them tyrosine and methionine, showed behavior either opposite or simply different from that observed in this dissertation, while others (leucine, isoleucine, alanine, glycine, valine, and others) similarly accumulated during the deep torpor/hibernation phase. Likewise, one of the major findings of the study was a strong accumulation of modified amino acids, most of them essential, which was suggested to be a salvaging mechanism to ensure reestablishment of muscle mass and protein homeostasis during the interbout arousal in hibernation.

It therefore seems that one major and novel difference between daily torpor and hibernation is the behavior of amino acids. While some do not correspond in the two processes, others are specifically modified in hibernation. Amino acids in general appear to be "protected" because urea levels, an indicator of amino acid metabolization, remained unchanged throughout hibernation. Conversely, amino acids do appear to be utilized in daily torpor, as urea cycle activity in liver, as well as urea accumulation in both liver and blood serum were observed. Curiously, artificially raising urea in the blood of hibernating squirrels provokes premature arousal, providing a mechanistic justification for the observed difference (Fisher 1964).

Pantothenate (vitamin $B_5$) is required for acetyl-coA synthesis, a cofactor involved in many biochemical reactions, among them facilitating the entry of ketones and fatty acids into the TCA cycle for energy production. Its high availability during hibernation arousal might indicate a reliance on lipolysis products to fuel rewarming, the predominant hypothesis in hibernation research (Nestler 1991; Nestler 1990b). This is further supported by the TCA cycle intermediate succinate specifically increasing during hibernation arousal, which was not observed for daily torpor. Furthermore, the observation of increased glucose levels in the deep, and pyruvate and lactate levels in the arousal phase in my dataset were not observed in the hibernation study. Taken together, the evidence indicates a potential second novel major difference between daily torpor and hibernation, in that daily torpor appears to use a combination of glycolysis

and lipolysis during waking, while the hibernating phenotype seems to be nearly exclusively using lipolytic fuel.

Fatty acid levels behave similarly in studies of daily torpor and the metabolic studies in hibernators, just like the major ketone body, β-hydroxybutyrate, and the lipolysis indicator in blood plasma, glycerol (Nestler 1991; Epperson et al. 2011; Nelson et al. 2010). It can therefore safely be concluded that lipolysis is inhibited in the deep phases of, and turned back on during arousal from both torpor and hibernation, in accordance with WAT lipolytic activities characterized in hibernation and my own dataset.

In conclusion, the blood serum data revealed for the first time strong evidence of metabolic differences between hibernators and animals that employ daily torpor to conserve energy. Firstly, amino acid abundance and their metabolism appear to be differentially regulated, and the urea cycle significantly active only in daily torpor. Secondly, while hibernators appear to rely exclusively on lipid species and ketone bodies to fuel rewarming, the data provided strong evidence for the additional use of glucose in the arousal from daily torpor in mice and its prior production through hepatic gluconeogenesis. Only ketone body behavior and the lipolytic activity of WAT were identical between hibernators and mice, its suppression during deep torpor being lifted in the arousal phase. Crucially, only the concurrent monitoring of organs and blood serum as well as the extensive metabolite coverage allowed for insights into the coordinated interplay of organs, such as the anticipatory gluconeogenesis and glucose release by the liver in preparation for the glycolytic demand of muscle, and likely other tissues, during torpor arousal.

Beyond the study of daily torpor, the simultaneous metabolomic analysis of organs and blood serum throughout a metabolically dynamic process has for the first time demonstrated the degree to which metabolic states of organ physiology are reflected in metabolite abundances in blood serum. Inspired by the encouraging results obtained in mice, I decided to investigate the human blood metabolome throughout a metabolically dynamic process to take another step towards medical diagnostics. The experiment has been named “Campus Run” and its results will be described in the next section.

# 4. Campus Run

## 4.1 Introduction

In light of the mechanistic insights obtained by determining metabolic states in consecutive stages throughout the torpor process, as well as the strong reflection of pathway-specific organ metabolism in the blood, a study that similarly sampled many stages of a process to assess its dynamic metabolic character was performed. In the context of translational systems biology, this study was to complement the animal-model based study of torpor by investigating a human volunteer directly so as to translate the molecular lessons learned from mice into interpretations of the human blood metabolome.

Working with human patients or volunteers brings about new challenges; for example, the sampling procedure becomes of paramount importance. Ideally, the sampling site should be easily accessible the sampling itself minimally invasive, fast, and simple so as to minimize variation. It was therefore decided to make use of full capillary blood obtained by finger lancing devices that are well known to diabetic patients. After a short pricking sensation, a droplet of capillary blood is obtained (between ten and twenty microliters) that is sufficient to perform all analyses described in this section. This kind of sampling is extremely fast, simple, convenient, and tolerable. Thus, it will greatly facilitate dynamic monitoring of metabolic processes in humans.

The intent of the study was not to fully understand a physiological process, but to create a proof-of-principle dataset. We decided to track the metabolomic changes in full capillary blood during an exercise regime for the following reasons:

1) The general metabolic response to physical exercise has been studied extensively and is, to a certain level of detail, textbook knowledge.
2) We were unable to find metabolomic studies on a short timescale throughout exercise from full capillary blood; rather, most studies focus on before/after or athlete/non-athlete comparisons or measure only a few metabolites (Romijn et al. 1993; Krug et al. 2012; Banfi et al. 2012).
3) There is great interest in the beneficial effects of sports and it is one of the most effective preventative measures against metabolic and other diseases.

4) Elsewhere reported and commonly known as “hitting the wall”, I have often experienced a strong physical discomfort during exercise which, when continuing in spite of it, paradoxically turns into a feeling of elevation before abating into an “average” state that continues until the end of exercise (Stevinson & Biddle 1998; Rapoport 2010). It was of interest to determine whether this phenomenon would be reflected in the blood metabolome.

This dataset can be viewed as a realization of a simple, convenient sampling procedure that has been made compatible with a technological platform with which detailed hypothesis-driven research can address specific hypotheses in human patients the future. The detailed monitoring of effects of dietary regiments, catabolic states as experienced in cancer, and the extensive physiological changes occurring in many intensive care patients are only a small number of possibilities.

The study described in this section was carried out in collaboration with Tobias Opialla, a PhD student under supervision of Prof. Dr. Simone Spuler and Dr. Stefan Kempa. He contributed equally to this project. The initial conception of the experiment arose from a conversation between Tobias, Stefan, and myself, with my having pitched the initial idea. I served as the volunteering subject in the “Campus Run”, whereas Tobias was responsible for collecting, biochemically processing, and measuring the samples on the GC-MS. The annotation of the polar phase metabolites was performed by me, whereas Tobias annotated the lipid phase. The data analysis, figure preparation, and conclusions were acquired through a tight collaborative effort with equal contributions in all respects.

## 4.2 Materials and Methods

### 4.2.1 Sample Collection

Full capillary blood was obtained by puncture of fingertips using a lancetting pen (BD OneTouch comfort, 0.2mm, 33G). 10 µL were collected and immediately added to ice-cold MCW. The extraction, derivatization, and GC-MS measurement procedure for both polar and lipid phases was identical to the one used for blood serum samples in

the torpor study. Polar phase metabolites were measured in technical duplicate, fatty acids in the apolar phase only once.

### 4.2.2 Data Analysis and Imputation

Data was acquired and preprocessed as described in the Materials and Methods section of the torpor study, and processed using Maui-SILVIA. Data was not imputed, as there were no biological replicates measured. Samples where a metabolite was not found were assigned the default value of 0 to allow for principle component analysis and clustering using full data matrices. The Campus Run samples were normalized by the sum of intensity of all peaks contained in each sample instead of CA. This normalization by overall intensity was employed here because the human volunteer did not take in fluids during the exercise regime and the blood was notably "thicker", meaning more concentrated, in some phases when compared to others, leading to observations of nearly all metabolites strongly increasing or decreasing in accordance in certain samples. All analysis was carried out using R and the packages referenced in the R-References section.

### 4.2.3 SINQ - Isotope Standards and Sample Preparation

A full list of isotope standards used for the SINQ study (see Campus Run discussion) can be found in the supplementary section. 50 µL of blood serum samples were added to 1 mL MCW containing the isotope standard compounds in appropriate concentrations (Supplementary Table 1). Samples were extracted, derivatized, and measured on the GC-MS like the blood serum samples of the torpor study, and analyzed using Maui-SILVIA as described earlier. Graphs were generated using R and referenced packages.

## 4.3 Results

### 4.3.1 Experimental Design

To assess the dynamic changes in the full blood metabolome during exercise in a human subject, the following experimental design was employed. After an overnight fast (12 hours), the first sample was taken as a pre-exercise (R0) control. I then ran around the MDC campus, the distance of one round being 2.2 kilometers, collecting samples after each round for a total of six rounds. The one exception was round three (R3), in which the "hitting the wall" feeling was experienced and I took a shortcut in fear of missing this crucial time point (Figure 4.1 A). The R6 sample represents the sample immediately after completion of the last round, and a final sample was taken after lunch (a salad and two wiener sausages) about an hour after the exercise as a representation of post-exercise recovery (post lunch, or PL). Please note that each round took a little over ten minutes, the entire run of six rounds having lasted about one hour and ten minutes. The experiment was designed not for reproducibility (a single volunteer), but rather to allow for flexibility to sample at crucial time points.

At the time of every sampling event, I reported my personal feeling of well-being (Figure 4.1 B). I experienced a strong feeling of discomfort (or "hitting the wall") after exercising for roughly twenty-five minutes (R3). This feeling occurred much earlier than I expected, likely due to the overnight fast. The immediately following "high" occurred in R4, after which the rest of the run was classified as "average" from an energetic standpoint of feeling, although muscle fatigue began to be felt in R5 and more strongly in R6.

We measured a total of ninety key metabolites of glycolysis, the TCA cycle, the urea cycle, ketone body production, amino acid metabolism, and fatty acid species, as well as 124 unknown features. Thirty-nine of the known metabolites were absolutely quantified using the Quant mix. While most blood markers for exercise currently in use are proteinaceous and indicate different levels of muscle, liver, kidney, or heart damage and/or function, blood metabolites measured are usually restricted to glucose, global free fatty acids, glycerol, lactate, and creatinine (Banfi et al. 2012). This is, to our knowledge, the first metabolomic analysis of full capillary blood in ten-minute intervals

during exercise in humans, although similar studies with less frequent sampling have been performed using blood plasma and different MS technologies (Krug et al. 2012).

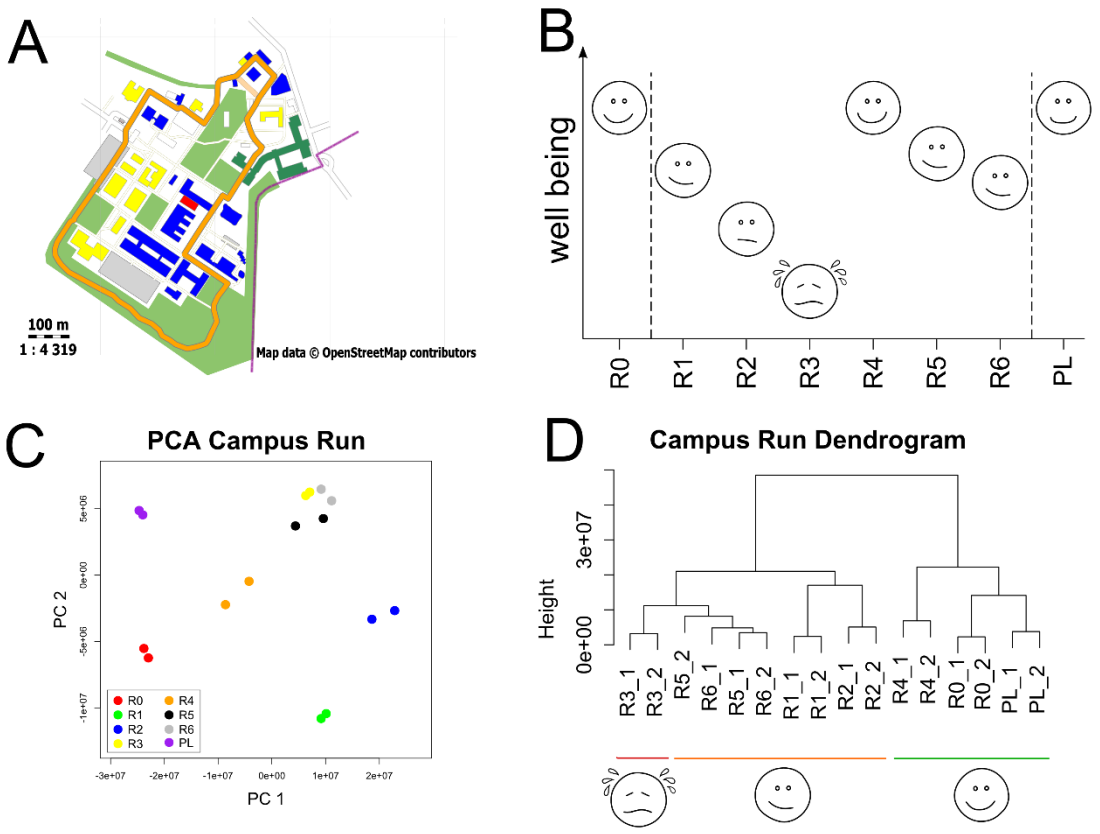


**Figure 4.1 – States of physiological well-being are reflected in the metabolome of human capillary blood.** A) A map of the MDC campus, made by Tobias Opialla using OpenStreetMap, shows the running trail in orange and the shortcut used in R3 in light orange. B) An illustrative diagram displaying the reported feeling of physical well-being throughout the exercise regime. C) PCA of the technical replicates of the Campus Run shows a clear separation of most sampling time points from one another when plotting the first two PCs. D) Hierarchical clustering using the average linkage method grouped the sampling time points into clusters that correspond with the reported feeling of well-being.

### 4.3.2 States of Well-Being are Reflected in the Blood Metabolome

To investigate the degree of relation between the different sampling time points, each technical replicate of each time point was treated as an individual sample. This is not a statistical trick, as we have refrained from any kind of statistical analysis in this single subject dataset. It merely serves to show that technical replicates are more similar to one another than to other sampling time points (with the exception of R5 and R6, which appear to be nearly identical), underlining our technical reproducibility and ability to resolve biological differences in the samples of distinct sampling points.

As can be clearly observed in PCA and hierarchical clustering, technical replicates are most alike to their counterpart (Figures 4.1 C and D). When considering the different sampling time points in relation to one another (hierarchical clustering), a surprising picture emerges: The time points in which personal well-being was perceived to be most similar are more closely related. The R0 control, the "high" phase (R4), and the PL sample formed one branch. The second major branch was made of all other time points of the run, with R3 being the least related to those during which I felt best. Incredibly, the individual feeling of well-being appeared to be reflected in the metabolomic signature obtained from a single drop of capillary blood.

### 4.3.3 Fuel Utilization and Mobilization

Glucose is considered the most important fuel source in muscle during strenuous exercise, but remains important even in exercise conditions that optimize the mobilization and use of fat reserves. It stems from a combination of internal muscle glycogen stores and plasma glucose that is taken up mainly via GLUT4 transporters (Rose & Richter 2005).

Tracking glucose dynamically, we have observed an initial decrease in blood levels occurring in R1, likely corresponding to muscle glucose uptake and its concurrent utilization as indicated by lactate production upon exercise initiation (Figure 4.2). Glucose levels increased in R2 and then minimally overshot R0 levels in R3, representing the release of glucose after its mobilization from glycogen stores in the liver. During R3 and R4, lactate was cleared from the blood, which is in accordance with the activation of the Cori cycle in which lactate produced in muscle is taken up by the liver to fuel gluconeogenesis (Brooks 1998). Glucose levels then reached a plateau in R4, R5, and R6, while lactate accumulated in R5 and R6 as muscle fatigue became noticeable. In PL, the levels of glucose returned to those observed at R0. This behavior is in agreement with the current literature (Goodwin 2010; Zinker et al. 1990).

Glycerol levels were found to increase during R1, indicating fatty acid release at exercise onset, but immediately decreased in R2. They reached their maximum in R4 and R5 (Figure 4.3). The two most abundant fatty acids (palmitate and stearate)

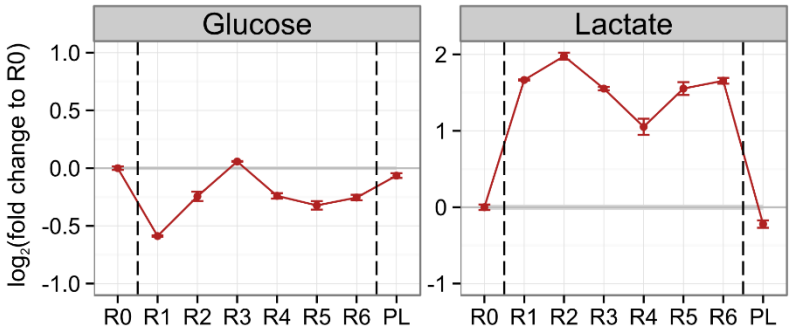


**Figure 4.2 – Glucose and lactate behavior during the Campus Run.** Glucose levels initially dropped in R1, likely due to muscle uptake, recovered by R3, and then settled to an intermediate level in R4, R5, and R6, before returning to R0 levels in PL. Lactate levels increased abruptly at exercise onset, decreased towards R4 before increasing again in the last two rounds where muscle fatigue was felt, and dropped to R0 levels after exercise completion.

showed a corresponding pattern, with two periods of blood level increases in accordance with glycerol in R1 and R4 (Figure 4.3). One exception was the PL phase, where the fatty acid abundances rose without a concurrent increase in glycerol levels. This post-exercise phenomenon has been observed in other exercise regimes and likely does not indicate fatty acid uptake from food (Romijn et al. 1993; Bahr et al. 1990; Yuen et al. 2012). Interestingly, in the first phase of glycerol and fatty acid release in R1, glycerol levels dropped in R2 but fatty acids remained elevated, whereas the second release in R4 showed the reverse, with fatty acids decreasing between R5 and R6 and glycerol levels remaining elevated in R6. This observation is in line with improved fatty acid uptake into muscles due to FAT/CD36 transporter translocation as exercise progresses (Jeppesen & Kiens 2012). It is also of note that between R2 and R3, when fatty acid levels decreased, β-hydroxybutyrate levels rose and remained elevated before accumulating extensively at the PL sampling time point (Figure 4.3).

Taken together, a picture emerges in which the very start of exercise relies heavily on muscle and blood glucose and the glycolysis thereof as indicated by glucose and lactate behavior. The initial glucose uptake is overcompensated by the liver through mobilization of its glycogen stores. Concurrent with the glucose depletion, an initial burst of fatty acid release is immediately followed by ketone body production during a time when lactate serves as a substrate for gluconeogenesis. By R4, glucose levels stabilize, likely balanced by gluconeogenic output from the liver, glycolysis in the

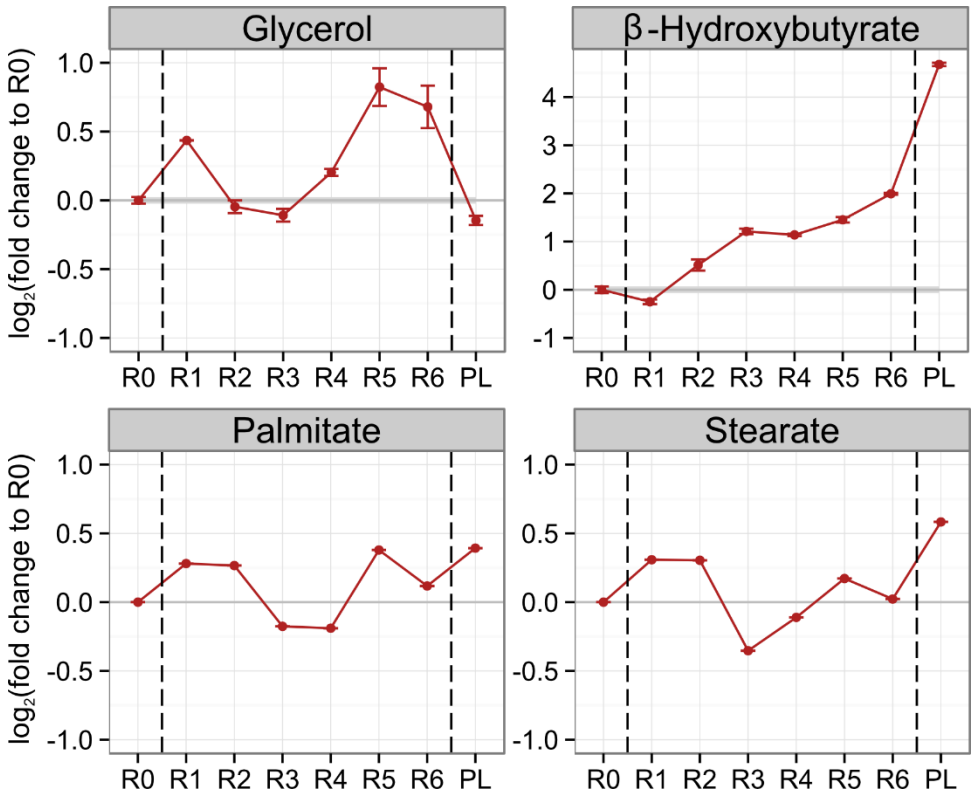


**Figure 4.3 – Lipolysis during the Campus Run.** Based on glycerol, palmitate, and stearate (the two most abundant fatty acids measured) levels, two phases of fatty acid mobilization occurred during the Campus Run (R1 and between R4 and R5). The ketone body β-hydroxybutyrate was produced following the initial lipolytic wave in R1 and remained elevated thereafter, accumulating vastly once the physical activity was concluded.

active muscle, and additional energy being available in the form of fatty acids and ketone bodies. The switch from a strongly glycolytic to a state in which lipolysis actively contributes to satisfying energy requirements is also mirrored in the abundances of TCA cycle intermediates, whose increase in blood likely corresponds to increased TCA cycle activity in muscle. While intermediates are lowest in R0 and R1 samples, they increase rapidly in R2 and remain elevated thereafter until PL (Figure 4.4).

### 4.3.4 Amino Acids

The third potential fuel source for the body are amino acids. However, amino acid metabolism in muscle during exercise has been considered to contribute minimally to meeting energetic demands (Hargreaves 2000; Wagenmakers 1998). Two important roles that amino acids could play are the replenishment of TCA cycle intermediates and provision of alanine and glutamate to the blood stream, which in the liver can be used to fuel gluconeogenesis (Wagenmakers 1998). The degree to which amino acid

metabolism of muscle and liver are reflected in blood were not entirely clear in the torpor study and have not been systematically studied in sufficient detail in exercise to provide a simple explanation of amino acid behavior observed in the Campus Run.

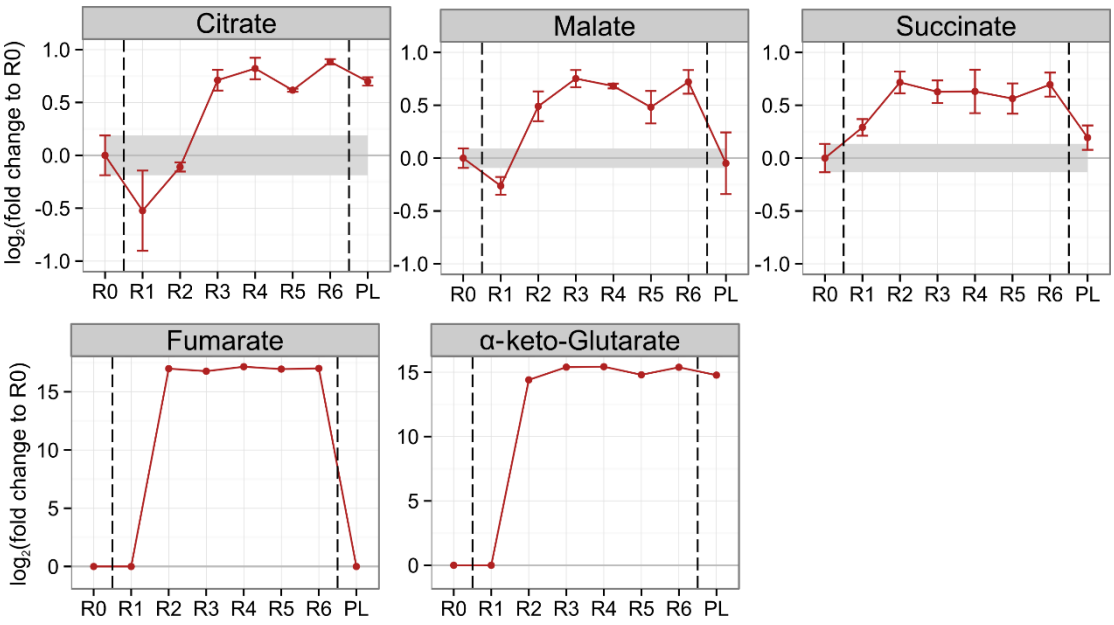


**Figure 4.4 – TCA cycle intermediates during the Campus Run.** TCA cycle intermediates rose in the blood after the initial wave of fatty acid release in R2, and remained elevated thereafter until exercise completion. This is in accordance with the initial phase of physical exercise being fueled mostly by glucose and glycogen stores, after which a combination of fatty acids and carbohydrates are metabolized in muscle.

Nonetheless, it is worth reporting the observed changes in amino acid abundance as well as urea cycle intermediates to gather a first impression. Urea levels first dropped and then recovered to R0 levels in R3, after which a continuous but minor increase was observed until PL (Figure 4.5). Muscle proteolysis and amino acid breakdown can occur after glycogen stores are depleted in muscle, and urea and ornithine levels became concurrently elevated shortly after the major wave of glucose release and the activation of the TCA cycle, whose intermediates amino acids are known to produce (De Feo et al. 2003; Wagenmakers 1998).

The two major amino acid species secreted from muscle to be taken up by the liver are alanine and glutamine (Wagenmakers 1998). Alanine increased in R2, peaked in R4, and returned to R0 levels at PL, whereas pyroglutamate (a combination of

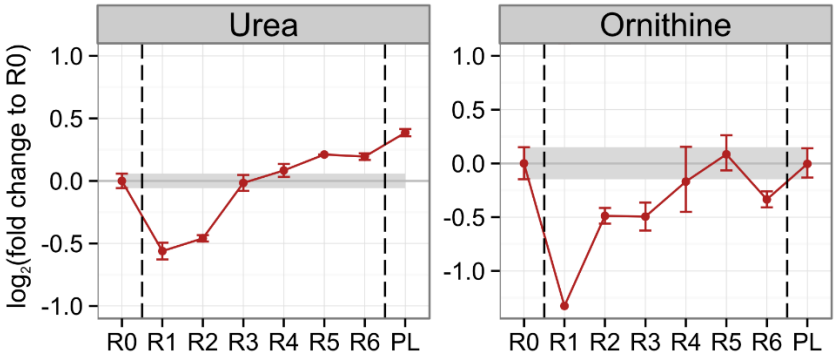


**Figure 4.5 – Amino acid metabolism during the Campus Run.** Urea levels first decreased, then recovered to baseline levels in R3, and increased mildly thereafter. Ornithine, an important urea cycle intermediate, showed a similar behavior.

glutamine, glutamate, and pyroglutamate) remained stable at R0 levels after a transient drop in R1 (Figure 4.6). Interestingly, alanine behaved differently in the Campus Run than during torpor, where its clearance from blood was interpreted as it being used for gluconeogenesis. In the Campus Run, lactate could be the primary metabolite used by the liver to produce new glucose, with alanine either playing a less or no significant role. Alternatively, it is possible that alanine was secreted in such abundance that the rate of liver uptake was insufficient to significantly deplete blood alanine levels.

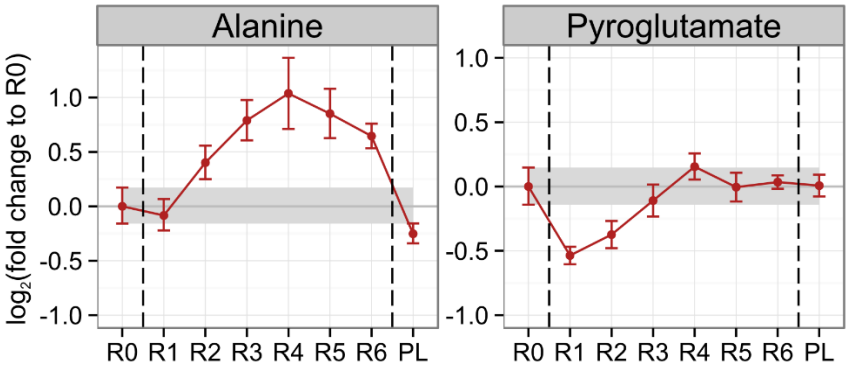


**Figure 4.6 – Alanine and glutamine during the Campus Run.** The two major amino acids released by muscle to fuel gluconeogenesis in the liver and kidney are alanine and pyroglutamate (a combination of glutamine, glutamate, and pyroglutamate). Alanine levels increased and peaked in R4 before falling back to baseline levels after exercise completion. Pyroglutamate first decreased in R1, recovered to baseline levels in R4, and remained stable thereafter.

Branched-chain amino acids (BCAA) and aromatic amino acids showed a similar behavior, in that their levels first decreased in R1, and then recovered or overshot in R3 after which they remained fairly stable (Figure 4.7 A and B). The one exception

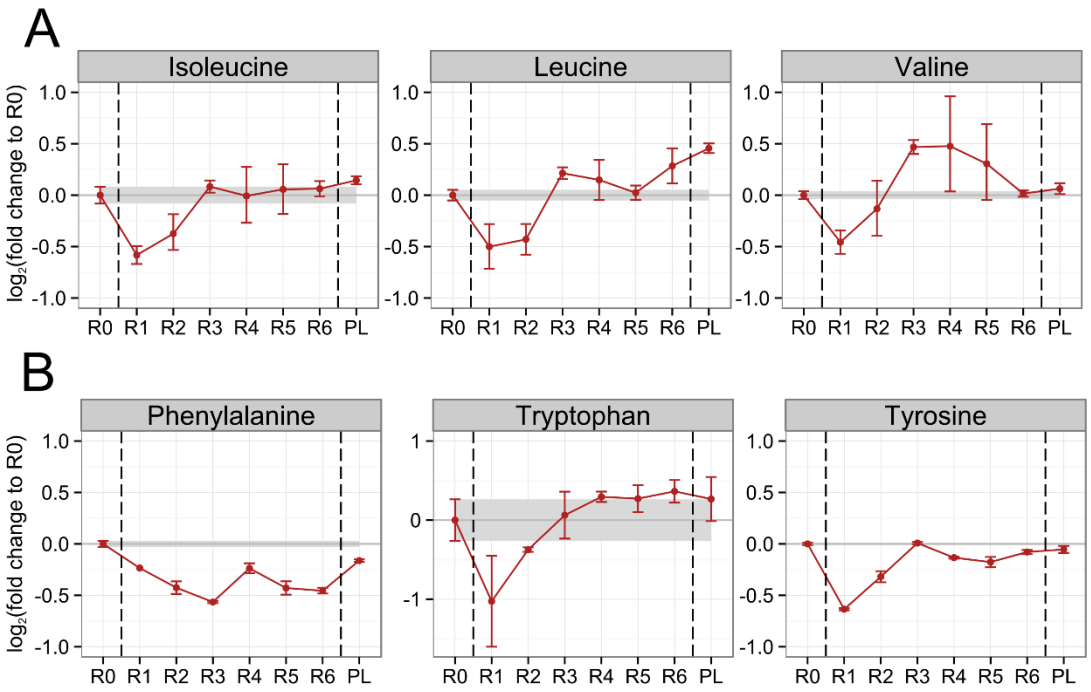


**Figure 4.7 – BCAA and aromatic amino acids in the Campus Run.** A) BCAAs uniformly decreased in R1, recovered or overshot baseline levels in R3, and remained fairly stable thereafter. B) A similar behavior was observed for tryptophan and tyrosine. Phenylalanine decreased initially, its lowest level observed in R3, increased shortly in R4, decreased in R5 and R6, and rose again after exercise completion.

was phenylalanine, which displayed a behavior unlike any other amino acid. Generally, it appears that many amino acids were decreased in R1 and then recovered to differing degrees, either reaching R0 levels, overshooting them, or remaining slightly lower, but generally displaying stable levels from R3 and R4 onwards (Figure 4.8).

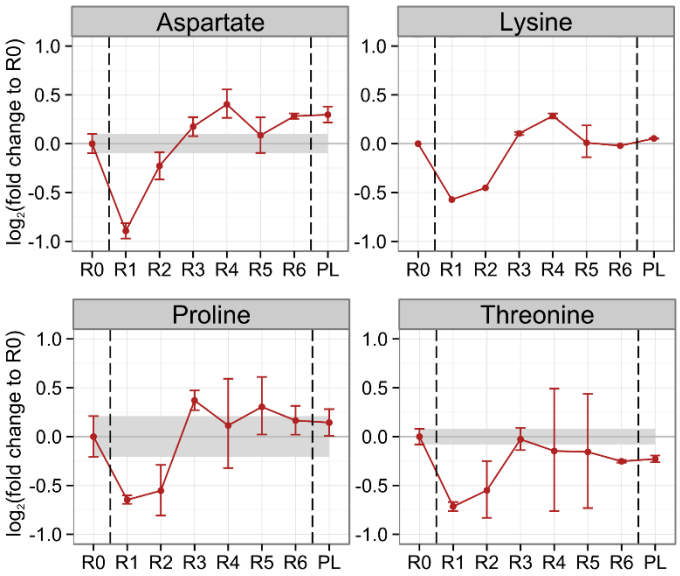


**Figure 4.8 – Other amino acids in the Campus Run.** Amino acids displayed here represent the most common amino acid trend in the Campus Run, in that their abundance decreased in the first two rounds after which they recovered and remained fairly stable thereafter.

As a validation of our dataset and especially amino acid behavior, we have found a correlation between certain amino acids and glucose abundance as described in a report using a similar physical exercise regime and measuring metabolites with a MS-based kit (Figure 4.9) (Krug et al. 2012).

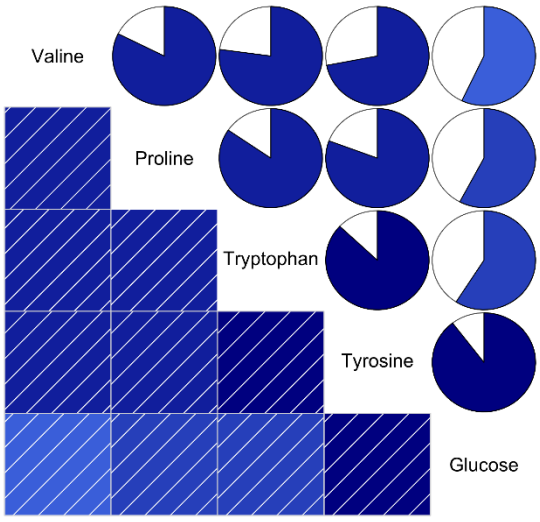


**Figure 4.9 – Glucose correlates with a selection of amino acids in the Campus Run.**
Pearson correlations of glucose with certain amino acids reported in a study using a similar exercise regime and metabolomics approach was replicated in the Campus Run. (Blue indicates a positive correlation; the color depth and circle area colored correspond to the strength of correlation).

In conclusion, most amino acids followed the trend of an initial depletion in R1 and subsequent recovery to R0 levels in R3. At that time, ornithine and urea levels rose, indicating urea cycle activity. This evidence is reminiscent of amino acid and urea cycle behavior during the early phases of torpor in liver, muscle, and blood serum, and will be considered in more detail in the discussion below.

### 4.3.5 Hypoxia

Metabolite levels measured from full blood, as used in this study, are a combination of those found in erythrocytes and other blood cells and those freely circulating. While there have been no systematic comparisons between metabolite levels in full blood and serum, some metabolites are known to be found nearly exclusively in a certain tissue or, as in the case of 2,3-bisphosphoglycerate (2,3-BPG), in erythrocytes. It has been established as a marker for hypoxia, its accumulation causing an increased affinity of hemoglobin for oxygen, thereby enhancing oxygen delivery to tissues in need (Benesch & Benesch 1967). Interestingly, 2,3-BPG was absent in R0, R1, and R2 samples, but measured in high abundance in R3 before it decreased in R4, disappeared in R5, and detected in lower abundance in R6 and after exercise completion (Figure 4.10).

Hypoxia in erythrocytes therefore occurred during the time of strongest physical discomfort, its subsequent decrease coinciding with improved well-being.

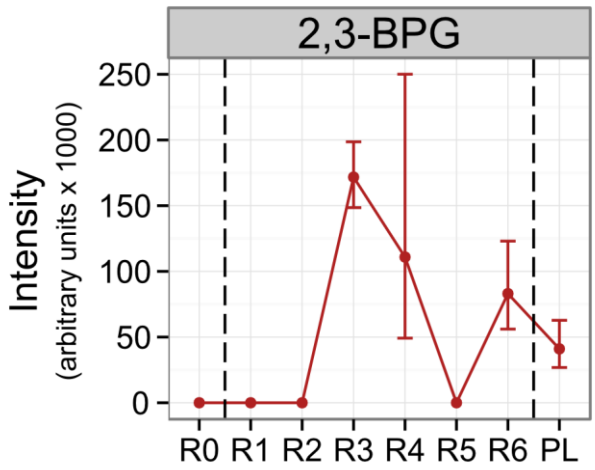


**Figure 4.10 – Hypoxia in erythrocytes during the Campus Run.**
2,3-BPG was undetectable until peaking in R3, the round of greatest physical discomfort, after which it decreased to disappearance in R5. It was detected again in the final round and to a lesser degree after exercise completion.

## 4.4 Discussion

### 4.4.1 The Campus Run

The Campus Run experiment has served well as a proof-of-principle study to show that the dynamic investigation of physiological processes with our convenient sampling method and metabolomic analysis has immense potential to provide mechanistic insight into human metabolism. Future studies with higher numbers of volunteers and concurrent monitoring of muscle and blood metabolism are already planned in collaboration with ECRC researchers at the MDC, the ethics application for the proposed experiments having already been approved by the Charité. In fact, the feedback to the Campus Run was so positive and encouraging that a manuscript is in preparation and will be submitted for publication at the time of completion of this dissertation.

While I am timid to interpret in detail a study with a single volunteer, several interesting observations have been made.

Glycolytic activity, plasma glucose uptake, and fatty acid mobilization that have been described or hypothesized to occur during exercise have been observed in the Campus Run with a greater time resolution than ever before. An increase of mitochondrial activity, as indicated by TCA cycle intermediate abundance, immediately followed the initial burst of lipolysis, and the major ketone body β-hydroxybutyrate was produced in response to the energetic challenge of exercise after fasting, its appearance usually considered indicative of starvation.

The hypoxia marker 2,3-BPG appeared and peaked during the sampling time point of greatest physical discomfort in R3. This was also the time point during which the body seemed to try to establish a balance of many metabolites and reach a new equilibrium of fuel source management, the success of which in combination with a reduction in experienced hypoxia was reflected in a brief feeling of elevation. The behavior of amino acids that were measured in both the Campus Run and a different but comparable study was similar (Krug et al. 2012). Overall, the information of physical well-being was encoded in the metabolome of a single drop of capillary blood throughout exercise,

indicating that the decoding of blood metabolome composition and its dynamics might provide biologically meaningful insights into human physiology.

Beyond the consideration of exercise physiology and the medically relevant hypometabolic state of daily torpor, this dissertation aimed at the translation of model system-based systems biology into clinical applicability. This transition is never trivial and often not overcome. There are two principle difficulties: 1) the translation of biological insights from model systems to humans and 2) the level of maturity required for a technology to transcend basic research, where it is employed successfully by virtue of few highly trained individuals that ensure reproducibility and high data quality. Both are addressed in the following two sections.

### 4.4.2 Translational Systems Biology – From Mouse to Man

Mechanistic insights into metabolism are most easily obtained when tracking a process dynamically, as exemplified by both the torpor and Campus Run studies. While it might be possible to draw diagnostic insight from a single metabolomic measurement in the future, the elucidation of human physiology at this time might therefore be most successful by studying physiological responses to defined challenges. One challenge common to both mice arousing from torpor and the human volunteer during the Campus Run was the initiation of muscle activity in a starved state. It occurred as shivering thermogenesis between the deep and exit phase of torpor and in the form of exercise initiation between R0 and R1 of the Campus Run.

The comparison of the two datasets are complicated by the difference in the species of origin, unknown differences in blood serum and full capillary blood metabolomes, and the times of sample measurement being separated by many months. These difficulties are exemplary for attempts at translating model system studies into the human context. To circumvent them, a measure independent of absolute metabolite intensities is required to remove technical and inter-species variation (there is no way at present to correct for the full blood to blood serum differences).

Metabolite intensity ratios are independent of the absolute intensities and may react more sensitively than changes in abundance of single metabolites. Since fuel source selection and glycolytic activity were strongly reflected in both the torpor and Campus

Run studies, ratios of metabolites that are routinely detected in both blood serum and full capillary blood with relation to these processes of interest were formed between the deep and exit phases, as well as the R0 and R1 sampling time points (Figure 4.11).

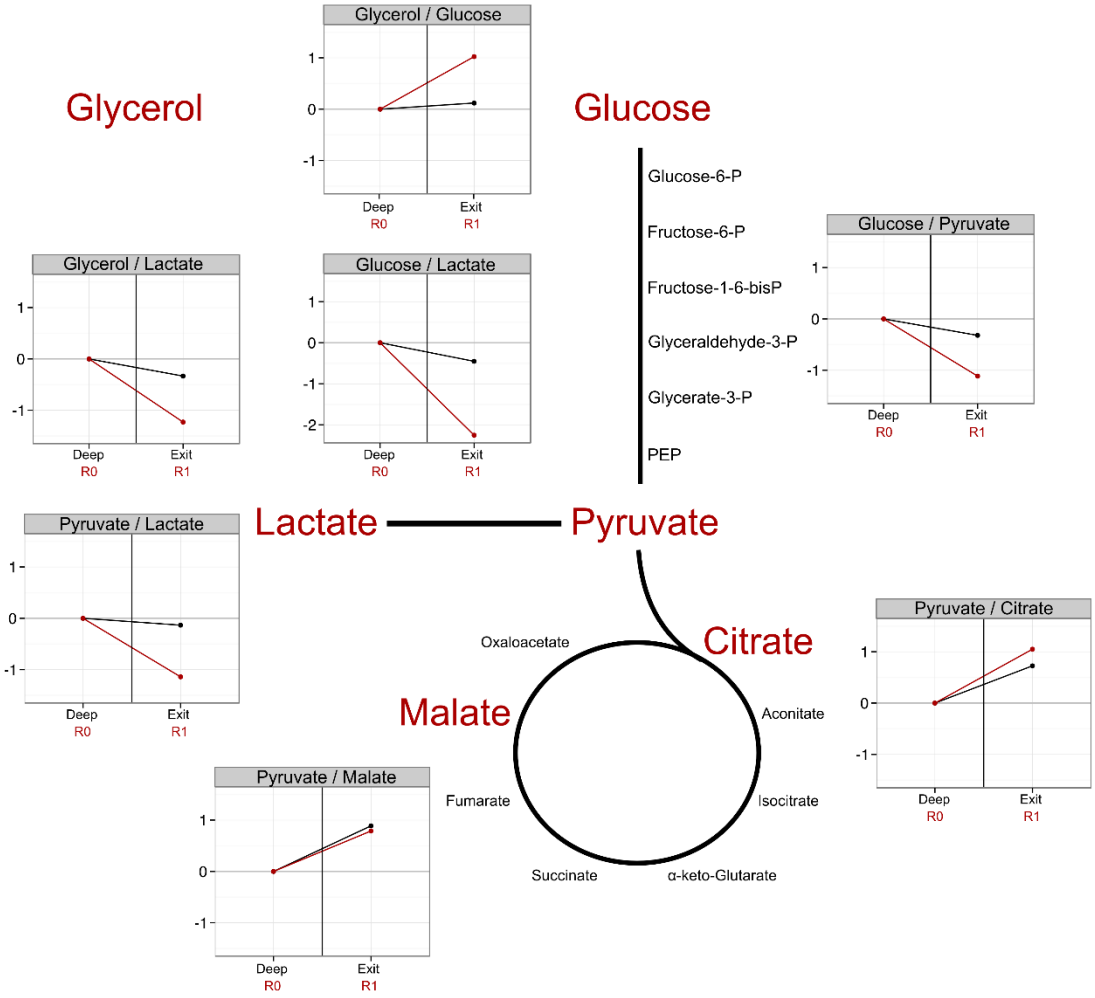


**Figure 4.11 – Ratios of key metabolites of glycolysis, fat store mobilization, and the TCA cycle in blood are indicative of pathway activities in internal organs.** An illustration of glycolysis and the TCA cycle is displayed. Metabolites used to build ratios are colored red and other pathway intermediates black. Ratios are plotted as the log2 fold change to the initial condition. Campus Run ratios are plotted in red, torpor ratios in black. Ratios between glycerol and metabolites involved in glycolysis indicate the mobilization of fat stores. Ratios between glucose and the glycolysis end products pyruvate and lactate, as well as ratios between pyruvate and the TCA cycle intermediates citrate and malate indicate the strong activation of glycolysis during exercise initiation and torpor arousal. The differences in magnitude of changes of ratios between torpor and the Campus Run are due to the anticipatory accumulation of glucose through hepatic gluconeogenesis during the deep torpor phase. This pre-emptive supplication of future fuel did not occur previous to exercise initiation in the Campus Run, rendering the magnitudes of change more extreme.

The ratio between glycerol and glucose increased in both the Campus Run and torpor in agreement with fat store mobilization at those time points. Similarly, the increase in glycolytic activity observed in both datasets was reflected in decreasing ratios of glucose to lactate, glucose to pyruvate, and glycerol to lactate, indicating the conversion of glucose to the end products of glycolysis. It is interesting that in all ratios that contain glucose, the ratio changes were identical in direction but of a smaller magnitude in torpor. This difference reflects the glucose accumulation in blood through hepatic gluconeogenesis during the deep phase of torpor, which anticipated the subsequent glucose requirement during arousal. Such an anticipatory process did not take place in the Campus Run so that the challenge to maintain homeostasis was likely of a greater magnitude. The glycolytic activation in both processes was also reflected in the increasing ratios of pyruvate to the TCA cycle intermediates citrate and malate, suggesting that pyruvate was generated faster than it was able to enter the TCA cycle. Indicated by the decreased ratio of pyruvate to lactate, the increased pyruvate production and its accumulation relative to TCA cycle intermediates was compensated by its abundant conversion to lactate. The smaller magnitude in the pyruvate to lactate ratio in torpor was due to a much stronger increase of lactate levels during the Campus Run when compared to that having occurred during torpor arousal (data not shown).

Taken together, these data show that ratios of blood metabolites measured before and after a challenge can encode the pathway activity of the organs being challenged, and that the direction of these ratio changes are translatable from mice to men. Crucially, the major differences observed in ratio magnitudes represent the differences in torpor and exercise physiology, in that the orchestrated process of torpor anticipates and buffers the energetic need through blood glucose enrichment, a process not observed prior to exercise initiation. Additionally, the challenges were not identical, and whereas the initial phase of exercise is reliant on glycolysis, shivering thermogenesis appears to make use of both glycolytic and oxidative muscle fibers (Haman et al. 2004). Differences seem to therefore be largely independent of blood cell contributions to the full blood metabolome when directly compared to serum. Please note that this holds true also for the novel diagnostic ratios described below. In conclusion, metabolite ratios as observed in these studies can in principle contain two vital pieces of information in the diagnostic context: 1) the direction of change in key ratios might

encode which pathways change in activity, and 2) the magnitude of change might be reflective of the degree of activity changes.

The concept of using specific challenges for diagnostic purposes is not novel and employed, for example, in glucose-tolerance tests to diagnose diabetic patients. The great improvement in using GC-MS technology is the ability to concurrently measure and analyze the response of a much greater number of metabolites indicative of a greater variety of metabolic pathways, with their interrelationships expressed as "diagnostic ratios" promising novel insights into a variety of pathologies.

One example of potential novel diagnostic ratios corresponding to physiological processes directly translated from the mouse model-based torpor study to the human Campus Run metabolome concerns changes in amino acid homeostasis. In the torpor study, several amino acids were observed to accumulate towards the deep torpor phase in liver, muscle, and blood, with a concurrent increase in ornithine levels in liver and a subsequent accumulation of urea, indicating both an amino acid accumulation due to proteolysis or an inhibition of protein synthesis, as well as active amino acid catabolism. Searching for a representation of this shift in amino acid metabolism during torpor led to the discovery of the ratios of the two essential BCAAs isoleucine and valine to the closely related amino acids glycine and serine (Figure 4.12 A). All four ratios increased upon amino acid accumulation and processing and subsequently decreased after arousal from torpor when protein synthesis presumably resumes (Figure 4.12 C) (Berriel Diaz et al. 2004).

Proteolysis actively contributes to muscle physiology during exercise and occurs upon depletion of muscle glycogen stores (De Feo et al. 2003; Wagenmakers 1998). Importantly, the ratios indicating amino acid accumulation and catabolism in torpor spiked during R3 in the Campus Run when greatest physical discomfort, the abundance of ketones and fatty acids in blood, and the increased abundance of TCA cycle intermediates (which amino acids are known to produce) are in congruence with muscle glycogen depletion and proteolysis (Figure 4.12 B). In support of active amino acid catabolism during this time in the Campus Run, urea levels displayed a sharp increase in R3 (Figure 4.12 C). Interestingly, a second, although less pronounced spike in three of the four ratios occurred in R6 and was followed by another sharp, although less

pronounced increase in urea levels immediately thereafter. I therefore propose these four ratios to be representative of a shift of amino acid metabolism towards a more catabolic state, their mechanistic origin having been first discovered in mice and then successfully translated into the context of human blood metabolomics to hopefully be of diagnostic value in the future.

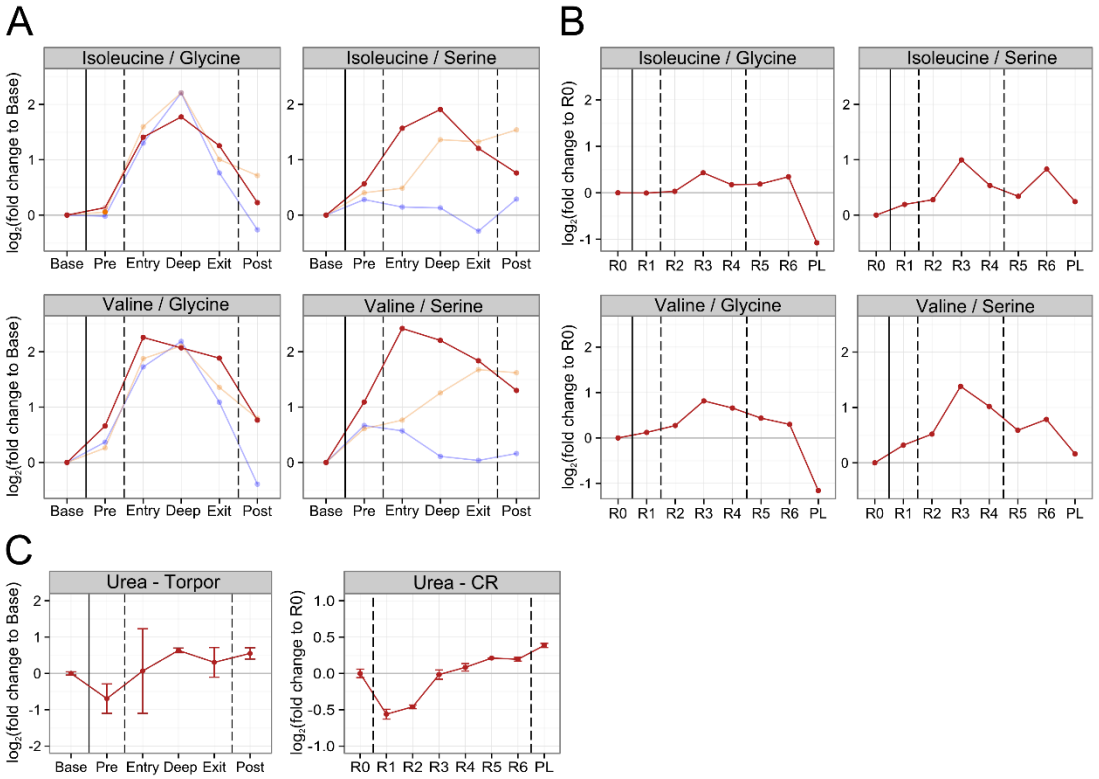


**Figure 4.12 – Diagnostic ratios indicating proteolysis in blood serum of mice are translatable to full capillary blood metabolomics in a human volunteer.** A) The ratios of isoleucine to glycine and serine, as well as valine to glycine and serine are greatest in the early torpor phases in blood serum (red) when amino acid accumulation and processing was observed in liver (light blue) and, to a lesser extent, muscle (light orange). B) The diagnostic ratios discovered in mice are consistent with proteolysis occurring in the Campus Run during a time (R3) in which they have previously been observed in studies of human exercise physiology. A second, less pronounced peak in R6 might be indicative of a second wave of protein degradation during a time in which muscle fatigue was experienced. C) Urea levels rise immediately after diagnostic ratios indicate proteolysis in both mice (between entry and deep phase, Urea-Torpor) and humans (R3, and to a lesser extent, PL, Urea-CR), indicating subsequent amino acid catabolism.

### 4.4.3 Translational Systems Biology – From Bench to Bedside

In addition to the translation of biological insight from model system-based experiments into the context of human physiology, two major issues need to be resolved before the proof-of-principle Campus Run study and its simple yet powerful sampling strategy can be moved into a clinical context:

1) Beyond the use of ratios, a useful large-scale diagnostic metabolomic assay should ideally determine absolute metabolite concentrations in such a way that comparability between different patients measured at different time points and even on different machines is guaranteed. Only by robustly and reproducibly obtaining absolute metabolite concentrations can the full potential of metabolomic diagnostics be realized, as future meta-analyses on thousands of patient samples to classify physiological patterns and discover mechanistic insights can only be as powerful as the comparability of the underlying data.

2) Reasonable estimates of the biological variation of known and unknown metabolites that are detectable in human blood are required in order to be able to realistically distinguish biologically significant from insignificant differences in metabolite abundance and their ratios.

A study addressing the latter issue is planned and will soon be under way. It will profile roughly four hundred male and female volunteers of different ages and various physical conditions, record physiological and physical characteristics, and collect information on dietary habits in order to obtain a reasonable representation of the biological variation of the general population.

An implementation of a possible solution for issues of reproducibility, robustness, and absolute quantification has in principle been established in collaboration with the Pischon lab at the ECRC/MDC in Berlin-Buch. Stable isotope normalization and quantification (SINQ) is an isotope dilution strategy to absolutely quantify and normalize patient serum and full blood samples by means of internal heavy isotope standards. The concept of isotope dilution is not novel in the context of MS but is nonetheless technically challenging (Meija & Mester 2008). It had not been employed

before measurement of the patient sera provided by the Pischon group as it was beyond practical and efficient use before its computational processing was implemented in SILVIA.

In the SINQ methodology, samples are supplemented with $^{13}C$ containing standard metabolites in known quantity in the first step of the sample preparation procedure (in this case carried out by Julia Diesbach, a technician in the Kempa Lab). They therefore undergo all processing steps identically to their patient-derived $^{12}C$ counterpart, and therefore contain all processing variation information. $^{13}C$-containing and $^{12}C$-containing metabolites (isotopologues) behave essentially and are detected identically in GC-MS, meaning that they co-elute and their mass spectrum contains both signals from the $^{12}C$ sample metabolite and the $^{13}C$ standard. The fact that the $^{13}C$ reference metabolite is treated, passes the GC, and is detected in the MS at the same time and in an identical way makes isotope dilution in theory the best internal quantification standard.

Using SILVIA, comparing $^{13}C$ signal with $^{12}C$ signal abundance allows for the calculation of the relative intensity of $^{12}C$ to $^{13}C$ metabolite fragments, and given the known concentration of $^{13}C$ standard added to the sample, SILVIA calculates the absolute concentration of the patient's target metabolite. The natural abundance of $^{13}C$ in metabolite fragments is taken into consideration (see Maui-SILVIA Results section). Because all samples contain identical standards as internal controls, one obtains a near perfect normalization, absolute quantification, and comparability between different samples. At the risk of being disproved in the future by a currently unforeseeable development, the use of $^{13}C$ standards for absolute quantification and normalization represents the best technically possible strategy to date (Meija & Mester 2008). Its implementation is therefore a significant success.

Using the SINQ strategy, an analysis of a first set of human patients' blood serum was carried out to attain a feeling for the reproducibility and biological variation of metabolite abundances. In this proof-of-principle study, twenty-five metabolites in over eighty patients were normalized and absolutely quantified using SINQ (Supplementary Table 1, Figure 4.13). As exemplified by the symmetric nature of the boxplots for all metabolites, most patients fitted well into a normal distribution of metabolite

abundances, with some metabolites having mild and others strong outliers. While this is a preliminary result, it is already of potential significance. It indicates that the biological variation appears to fit near-normal distributions for all metabolites (Figure 4.13, data not shown), and furthermore that the isotope dilution method has been established in the form of SINQ. The study in collaboration with the Pischon lab will now consider in detail the technical aspects of reproducibility and compare SINQ to other absolute quantification strategies currently in use, as well as correlate metabolite levels with other physiological parameters of the patients in an attempt to discover biomarkers or potential mechanisms of pathological states.

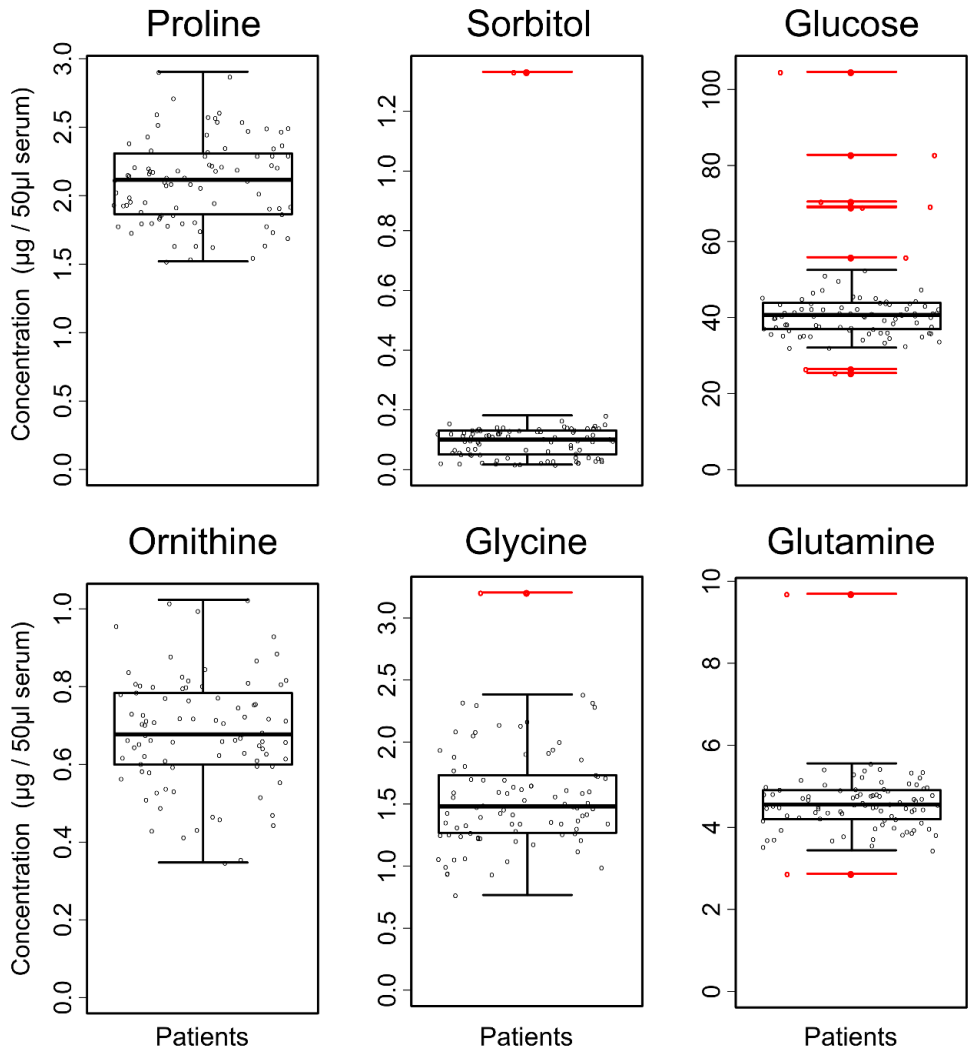


**Figure 4.13 – Distributions of SINQ-quantified metabolites in human blood serum.** Box-plots of six metabolites quantified with SINQ show near-normal distributions with no, one, or a few outliers (each spot represents a single patient, red points and lines indicate outliers) in human blood serum obtained from a patient cohort in collaboration with AG Pischon.

In summary, the Campus Run itself, the translatability of mechanistic observations of a model system-based basic research study to human physiology as assessed by full capillary blood metabolomics, and successful implementation of SINQ provide the proof-of-principle evidence required to advance towards mechanistic and diagnostic insights from blood metabolomics in human disease.

# 5. Conclusions and Perspective

This dissertation describes recent efforts in trying to realize the full potential of metabolomics for mechanistic studies in systems biology research and its translation into systems medicine in the form of full capillary blood metabolomics. Its ambitious scope encompasses many facets of the systems biology approach, including methodological and extensive computational developments, the extensive metabolomic analysis of several tissues and body fluids throughout a biological process of medical relevance, as well as the first steps of their translation into the context of human systems medicine.

With SILVIA, I have developed software that for the first time allowed the efficient processing of manually validated data of a large number of samples, facilitating methodological developments and vastly improving user-friendliness. Using SILVIA, the metabolically dynamic process of daily torpor was assessed in mice, providing novel and time-resolved mechanistic insights into liver, muscle, and WAT function. Due to its extensive coverage of metabolites and concurrent analysis of several tissues, CSF, and blood serum simultaneously and throughout a biological phenomenon, it revealed the surprising extend of differences between the blood serum and CSF, and allowed for a first rudimentary understanding of how organ metabolism is reflected in the blood metabolome during the entry into, maintenance of, and exit from a hypometabolic state.

In collaboration with Tobias Opialla I developed a method to combine a simple, fast, minimally invasive, and convenient patient blood sampling procedure with the GC-MS technological platform. It was employed in the Campus Run study to show that subjective grades of feeling of well-being were encoded in the changes of the full capillary blood metabolome over the course of an exercise regime. Similar to the torpor study, the Campus Run blood metabolomes reflected metabolic process known to occur in muscle and liver during exercise and both recapitulated and extended previous findings. Crucially, changes in diagnostic ratios concerning fuel source utilization and amino acid homeostasis observed in blood serum metabolomes of mice during torpor were translatable into the context of the human full capillary blood metabolome during

exercise. In combination with the first successful implementation of the isotope dilution quantification strategy SINQ, the methodological maturity of metabolomics might be sufficient to be instructional in human patient-based research and medical diagnostics in the near future.

In their combination, the studies presented in this dissertation exemplify a first implementation of a strategy of translational systems biology that I believe will be instrumental in elucidating metabolic mechanisms of human diseases.

This strategy is composed of three basic elements. First, continuous development of high quality software will facilitate methodological advances and increase the processing speed, user-friendliness, and validity of GC-MS, or in a more general context, omics data. Secondly, studies dynamically tracking the metabolic changes occurring in both organs and blood in model systems like the laboratory mouse will lead to an understanding of how organ physiology and pathophysiology are reflected in the blood metabolome. Finally, continuous investigation and the resulting accumulation of human blood metabolome data of the homeostatic state and specific challenge protocols will allow for both classification of patients into disease, prognostic, and treatment option categories, and, using insights gained from corresponding model system studies, the understanding of disease mechanisms.

It is my hope that with this three-tiered strategy, metabolomic profiling will soon advance to be a standard of care in hospitals around the world, aiding doctors in diagnostic decisions and providing a plethora of data from which novel mechanistic knowledge can be generated.

# 6. Publications

## 6.1 Maui-SILVIA

Publication of the SILVIA software package has been held back in favor of patenting its visualization and processing approach in combination with the Ident mixes. The "Erfindungsmeldung" has been completed and will soon be under scrutiny before the finalization of a patent application at Ascenion GmbH, Berlin.

## 6.2 Torpor

Publication of the torpor study has been held back in favor of measuring the kidney samples in addition to liver, muscle, WAT, blood serum, and CSF. The manuscript should be completed and submitted by Summer 2014.

## 6.3 Campus Run

The Campus Run study will be submitted for publication at the time of completion of this thesis.

# 7. Supplement

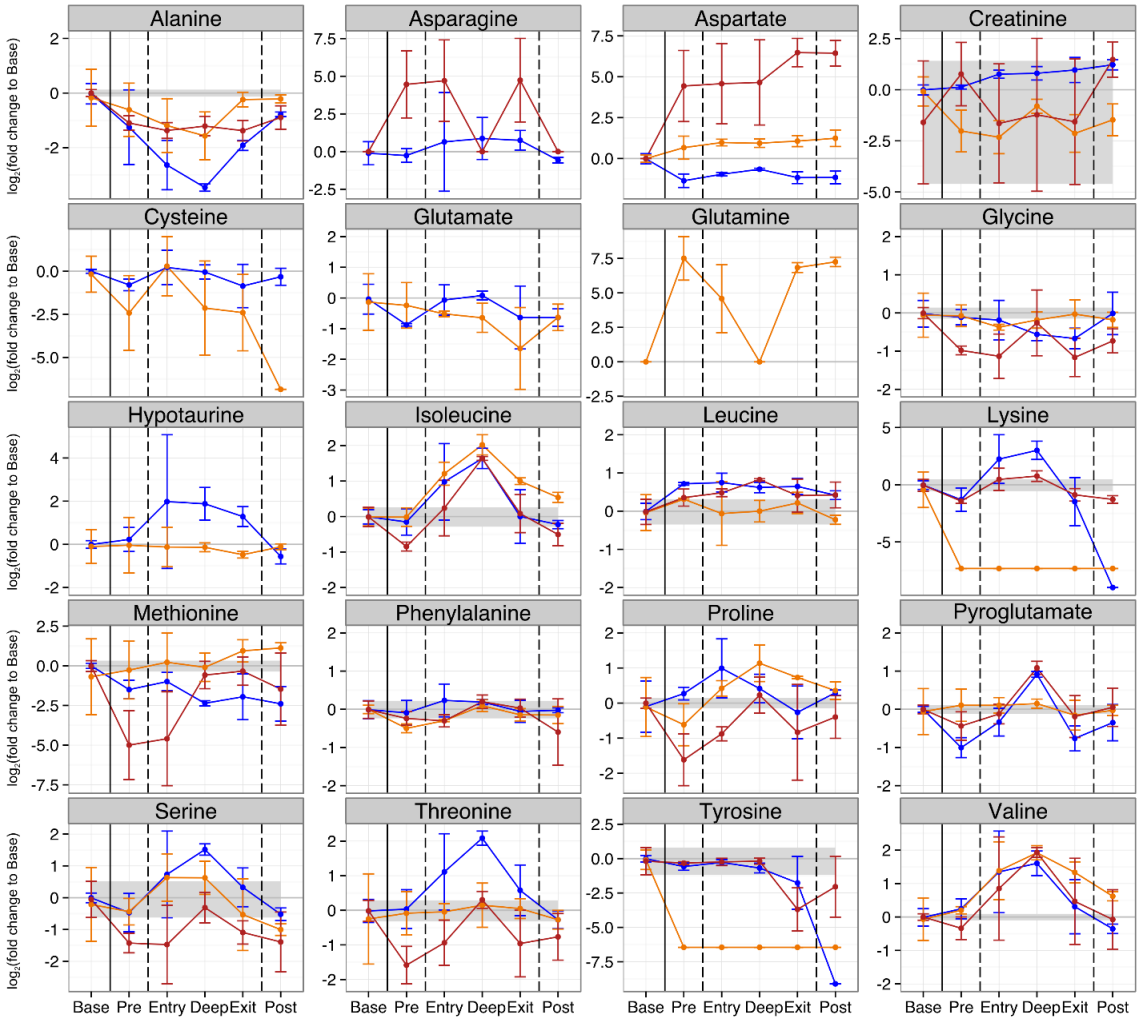


**Supplementary Figure 1 – Amino acids in blood serum, liver, and muscle during Torpor**. Plots of all detected amino acids showing their changes in abundance in blood serum (red), liver (blue), and muscle (orange). While correlations between all three tissues can be observed for some amino acids (isoleucine, valine), most behave differently, making a generalized conclusion about the site/s of proteolysis and/or secretion difficult.

**Supplementary Table 1 – $^{13}C$ standards used in the SINQ study.**

| Catalog No. | Isotope | Produced By | Supplier | Concentration in Sample (mM) |
|---|---|---|---|---|
| 604623-1G | Alanine | Sigma | Sigma | 2.664 |
| CNLM-539-H-1 | Arginine | Campro Scientific | Eurisotop | 0.091 |
| 750824-SPEC | Asparagine | Sigma | Sigma | 0.601 |
| 488607-100MG | Citrate | Sigma | Sigma | 0.206 |
| 488615-500MG | Creatinine | Sigma | Sigma | 2.103 |
| 415553-250MG | Fructose | Sigma | Sigma | 0.132 |
| CS01-183_417 | Glucose | Campro Scientific | Eurisotop | 8.597 |
| CLM-1822-0.5 | Glutamine | Campro Scientific | Eurisotop | 4.235 |
| 279439-250MG | Glycine | Sigma | Sigma | 0.526 |
| 604771-SPEC | Isoleucine | Sigma | Sigma | 0.605 |
| CLM1579 | Lactate | Campro Scientific | Eurisotop | 0.695 |
| 490059-1G | Leucine | Sigma | Sigma | 0.303 |
| CNLM-291-H-PK | Lysine | Campro Scientific | Eurisotop | 0.420 |
| 603899-SPEC | Malate | Sigma | Sigma | 0.030 |
| 736147-SPEC | Ornithine | Sigma | Sigma | 0.115 |
| 490091-250MG | Phenylalanine | Sigma | Sigma | 0.120 |
| 654183-SPEC | Proline | Sigma | Sigma | 0.207 |
| CLM-2440-1 | Pyruvate | Campro Scientific | Eurisotop | 0.071 |
| 604720-100MG | Serine | Sigma | Sigma | 0.377 |
| CS01-183_762 | Sorbitol | Campro Scientific | Eurisotop | 0.009 |
| 485349-500MG | Succinate | Sigma | Sigma | 0.013 |
| 604836-SPEC | Tryptophan | Sigma | Sigma | 0.117 |
| 486264-500MG | Uracil | Sigma | Sigma | 0.035 |
| 603430-SPEC | Urea | Sigma | Sigma | 2.621 |
| 490164-1G | Valine | Sigma | Sigma | 0.677 |

# 8. References


Aslami, H. & Juffermans, N.P., 2010. Induction of a hypometabolic state during critical illness - a new concept in the ICU? *The Netherlands journal of medicine*, 68(5), pp.190–8. Available at: http://www.ncbi.nlm.nih.gov/pubmed/20508267 [Accessed February 26, 2014].

Bahr, R., Hansson, P. & Sejersted, O.M., 1990. Triglyceride/fatty acid cycling is increased after exercise. *Metabolism*, 39(9), pp.993–999. Available at: http://www.sciencedirect.com/science/article/pii/0026049590903132 [Accessed March 25, 2014].

Bandzar, S., Gupta, S. & Platt, M.O., Crohn's disease: a review of treatment options and current research. *Cellular immunology*, 286(1-2), pp.45–52. Available at: http://www.ncbi.nlm.nih.gov/pubmed/24321565 [Accessed February 21, 2014].

Banfi, G. et al., 2012. Metabolic markers in sports medicine. *Advances in clinical chemistry*, 56, pp.1–54. Available at: http://www.ncbi.nlm.nih.gov/pubmed/22397027 [Accessed March 3, 2014].

Barnes, B.M., 1989. Freeze avoidance in a mammal: body temperatures below 0 degree C in an Arctic hibernator. *Science (New York, N.Y.)*, 244(4912), pp.1593–5. Available at: http://www.ncbi.nlm.nih.gov/pubmed/2740905 [Accessed February 26, 2014].

Bass, J. & Takahashi, J.S., 2010. Circadian integration of metabolism and energetics. *Science (New York, N.Y.)*, 330(6009), pp.1349–54. Available at: http://www.pubmedcentral.nih.gov/articlerender.fcgi?artid=3756146&tool=pmcentrez&rendertype=abstract [Accessed January 23, 2014].

Baumber, J. & Denyes, A., 1963. Acetate-1-C14 metabolism of white fat from hamsters in cold exposure and hibernation. *The American journal of physiology*, 205(5), pp.905–8. Available at: http://www.ncbi.nlm.nih.gov/pubmed/5896306 [Accessed February 28, 2014].

Bechtold, D. a et al., 2012. A role for the melatonin-related receptor GPR50 in leptin signaling, adaptive thermogenesis, and torpor. *Current biology : CB*, 22(1), pp.70–7. Available at: http://www.ncbi.nlm.nih.gov/pubmed/22197240 [Accessed June 7, 2013].

Benesch, R. & Benesch, R.E., 1967. The effect of organic phosphates from the human erythrocyte on the allosteric properties of hemoglobin. *Biochemical and biophysical research communications*, 26(2), pp.162–7. Available at: http://www.ncbi.nlm.nih.gov/pubmed/6030262 [Accessed March 17, 2014].

Benjamini, Y. & Hochberg, Y., 1995. Controlling the false discovery rate: a practical and powerful approach to multiple testing. *Journal of the Royal Statistical Society. Series B …*, 57(1), pp.289–300. Available at: http://www.jstor.org/stable/2346101 [Accessed March 25, 2014].

Berriel Diaz, M. et al., 2004. Depression of transcription and translation during daily torpor in the Djungarian hamster (Phodopus sungorus). *Journal of comparative physiology. B, Biochemical, systemic, and environmental physiology*, 174(6), pp.495–502. Available at: http://www.ncbi.nlm.nih.gov/pubmed/15232707 [Accessed February 28, 2014].

Bickler, P., 1984. CO2 balance of a heterothermic rodent: comparison of sleep, torpor, and awake states. *... Journal of Physiology-Regulatory, Integrative and ...*, 84, pp.49–55. Available at: http://ajpregu.physiology.org/content/246/1/R49.short [Accessed February 28, 2014].

Bickler, P.E., 1984. Blood acid-base status of an awake heterothermic rodent, Spermophilus tereticaudus. *Respiration physiology*, 57(3), pp.307–16. Available at: http://www.ncbi.nlm.nih.gov/pubmed/6441212 [Accessed May 29, 2013].

Blackstone, E., Morrison, M. & Roth, M., 2005. H2S induces a suspended animation–like state in mice. *Science*, 308, p.518. Available at: http://www.sciencemag.org/content/308/5721/518.short [Accessed February 26, 2014].

Blanksby, S.J. & Mitchell, T.W., 2010. Advances in mass spectrometry for lipidomics. *Annual review of analytical chemistry (Palo Alto, Calif.)*, 3, pp.433–65. Available at: http://www.ncbi.nlm.nih.gov/pubmed/20636050 [Accessed February 3, 2014].

Bouma, H.R. et al., 2012. Induction of torpor: mimicking natural metabolic suppression for biomedical applications. *Journal of cellular physiology*, 227(4), pp.1285–90. Available at: http://www.ncbi.nlm.nih.gov/pubmed/21618525 [Accessed June 7, 2013].

Brooks, G.A., 1998. Mammalian fuel utilization during sustained exercise. *Comparative biochemistry and physiology. Part B, Biochemistry & molecular biology*, 120(1), pp.89–107. Available at: http://www.ncbi.nlm.nih.gov/pubmed/9787780 [Accessed March 3, 2014].

Brosnan, J.T., 2003. Interorgan amino acid transport and its regulation. *The Journal of nutrition*, 133(6 Suppl 1), p.2068S–2072S. Available at: http://www.ncbi.nlm.nih.gov/pubmed/12771367 [Accessed March 17, 2014].

Broux, B., Stinissen, P. & Hellings, N., 2013. Which immune cells matter? The immunopathogenesis of multiple sclerosis. *Critical reviews in immunology*, 33(4), pp.283–306. Available at: http://www.ncbi.nlm.nih.gov/pubmed/23971528 [Accessed February 26, 2014].

Brown, J.C.L., Gerson, A.R. & Staples, J.F., 2007. Mitochondrial metabolism during daily torpor in the dwarf Siberian hamster: role of active regulated changes and passive thermal effects. *American journal of physiology. Regulatory, integrative and comparative physiology*, 293(5), pp.R1833–45. Available at: http://www.ncbi.nlm.nih.gov/pubmed/17804585 [Accessed February 28, 2014].

Brown, J.C.L. & Staples, J.F., 2010. Mitochondrial metabolism during fasting-induced daily torpor in mice. *Biochimica et biophysica acta*, 1797(4), pp.476–86. Available at: http://www.sciencedirect.com/science/article/pii/S0005272810000101 [Accessed January 29, 2014].

Cannon, B. & Nedergaard, J., 2011. Nonshivering thermogenesis and its adequate measurement in metabolic studies. *The Journal of experimental biology*, 214(Pt 2), pp.242–53. Available at: http://www.ncbi.nlm.nih.gov/pubmed/21177944 [Accessed February 21, 2014].

Carey, H. V, Andrews, M.T. & Martin, S.L., 2003. Mammalian hibernation: cellular and molecular responses to depressed metabolism and low temperature. *Physiological reviews*, 83(4), pp.1153–81. Available at: http://www.ncbi.nlm.nih.gov/pubmed/14506303 [Accessed February 14, 2014].

Cariou, B. et al., 2007. FXR-deficiency confers increased susceptibility to torpor. *FEBS letters*, 581(27), pp.5191–8. Available at: http://www.ncbi.nlm.nih.gov/pubmed/17950284 [Accessed May 29, 2013].

Ciana, P. et al., 2006. The orphan receptor GPR17 identified as a new dual uracil nucleotides/cysteinyl-leukotrienes receptor. *The EMBO journal*, 25(19), pp.4615–27. Available at: http://www.pubmedcentral.nih.gov/articlerender.fcgi?artid=1589991&tool=pmcentrez&rendertype=abstract [Accessed March 17, 2014].

Cochet, N. et al., 1999. Regional variation of white adipocyte lipolysis during the annual cycle of the alpine marmot. *Comparative biochemistry and physiology. Part C, Pharmacology, toxicology & endocrinology*, 123(3), pp.225–32. Available at: http://www.ncbi.nlm.nih.gov/pubmed/10530894 [Accessed February 28, 2014].

Cox, J. & Mann, M., 2008. MaxQuant enables high peptide identification rates, individualized p.p.b.-range mass accuracies and proteome-wide protein quantification. *Nature biotechnology*, 26(12), pp.1367–72. Available at: http://www.ncbi.nlm.nih.gov/pubmed/19029910 [Accessed January 21, 2014].

Dalziel, H.H. & Westfall, D.P., 1994. Receptors for adenine nucleotides and nucleosides: subclassification, distribution, and molecular characterization. *Pharmacological reviews*, 46(4), pp.449–66. Available at: http://www.ncbi.nlm.nih.gov/pubmed/7899473 [Accessed March 17, 2014].

Dark, J. et al., 2003. Noradrenaline-induced lipolysis in adipose tissue is suppressed at hibernation temperatures in ground squirrels. *Journal of neuroendocrinology*, 15(5), pp.451–8. Available at: http://www.ncbi.nlm.nih.gov/pubmed/12694370 [Accessed February 28, 2014].

Datta, G., Fuller, B.J. & Davidson, B.R., 2013. Molecular mechanisms of liver ischemia reperfusion injury: insights from transgenic knockout models. *World journal of gastroenterology : WJG*, 19(11), pp.1683–98. Available at: http://www.pubmedcentral.nih.gov/articlerender.fcgi?artid=3607745&tool=pmcentrez&rendertype=abstract [Accessed February 26, 2014].

Dawe, a R., Spurrier, W. a & Armour, J. a, 1970. Summer hibernation induced by cryogenically preserved blood "trigger". *Science (New York, N.Y.)*, 168(3930), pp.497–8. Available at: http://www.ncbi.nlm.nih.gov/pubmed/5436088.

Dawe, A. & Spurrier, W., 1969. Hibernation induced in ground squirrels by blood transfusion. *Science*, 163(3864), pp.298–299. Available at: http://www.sciencemag.org/content/163/3864/298.short [Accessed February 26, 2014].

Drew, K.L. et al., 2001. Neuroprotective adaptations in hibernation: therapeutic implications for ischemia-reperfusion, traumatic brain injury and neurodegenerative diseases. *Free radical biology & medicine*, 31(5), pp.563–73. Available at: http://www.ncbi.nlm.nih.gov/pubmed/11522441 [Accessed February 26, 2014].

Dunn, W.B. et al., 2011. Systems level studies of mammalian metabolomes: the roles of mass spectrometry and nuclear magnetic resonance spectroscopy. *Chemical Society reviews*, 40(1),

pp.387–426. Available at: http://www.ncbi.nlm.nih.gov/pubmed/20717559 [Accessed February 7, 2014].

Epperson, L.E. et al., 2011. Metabolic cycles in a circannual hibernator. *Physiological genomics*, 43(13), pp.799–807. Available at: http://www.pubmedcentral.nih.gov/articlerender.fcgi?artid=3132838&tool=pmcentrez&rendertype=abstract [Accessed May 29, 2013].

De Feo, P. et al., 2003. Metabolic response to exercise. *Journal of endocrinological investigation*, 26(9), pp.851–4. Available at: http://www.ncbi.nlm.nih.gov/pubmed/14964437 [Accessed March 25, 2014].

Fisher, K.C., 1964. On the Mechanism of Periodic Arousal in the hibernating ground squirrel. *Ann. Acad. Sci. Fenn. Ser. A*, IV(71), pp.141–156. Available at: http://books.google.de/books/about/On_the_Mechanism_of_Periodic_Arousal_in.html?id=D_C5tgAACAAJ&pgis=1 [Accessed February 26, 2014].

Flier, J.S., 1998. Clinical review 94: What's in a name? In search of leptin's physiologic role. *The Journal of clinical endocrinology and metabolism*, 83(5), pp.1407–13. Available at: http://www.ncbi.nlm.nih.gov/pubmed/9589630 [Accessed March 29, 2014].

Freeman, D. a et al., 2004. Reduced leptin concentrations are permissive for display of torpor in Siberian hamsters. *American journal of physiology. Regulatory, integrative and comparative physiology*, 287(1), pp.R97–R103. Available at: http://www.ncbi.nlm.nih.gov/pubmed/15191926.

Friedman, J.M. & Halaas, J.L., 1998. Leptin and the regulation of body weight in mammals. *Nature*, 395(6704), pp.763–70. Available at: http://www.ncbi.nlm.nih.gov/pubmed/9796811.

Gavrilova, O. et al., 1999. Torpor in mice is induced by both leptin-dependent and -independent mechanisms. *Proceedings of the National Academy of Sciences of the United States of America*, 96(25), pp.14623–8. Available at: http://www.ncbi.nlm.nih.gov/pubmed/21963898.

Geiser, F., 2004. Metabolic rate and body temperature reduction during hibernation and daily torpor. *Annual review of physiology*, 66, pp.239–74. Available at: http://www.ncbi.nlm.nih.gov/pubmed/14977403 [Accessed March 5, 2013].

Geiser, F. & Drury, R.L., 2003. Radiant heat affects thermoregulation and energy expenditure during rewarming from torpor. *Journal of comparative physiology. B, Biochemical, systemic, and environmental physiology*, 173(1), pp.55–60. Available at: http://www.ncbi.nlm.nih.gov/pubmed/12592443 [Accessed February 27, 2014].

Gluck, E.F., Stephens, N. & Swoap, S.J., 2006. Peripheral ghrelin deepens torpor bouts in mice through the arcuate nucleus neuropeptide Y signaling pathway. *American journal of physiology. Regulatory, integrative and comparative physiology*, 291(5), pp.R1303–9. Available at: http://www.ncbi.nlm.nih.gov/pubmed/16825418 [Accessed March 29, 2014].

Goodwin, M.L., 2010. Blood glucose regulation during prolonged, submaximal, continuous exercise: a guide for clinicians. *Journal of diabetes science and technology*, 4(3), pp.694–705. Available at: http://www.pubmedcentral.nih.gov/articlerender.fcgi?artid=2901048&tool=pmcentrez&rendertype=abstract [Accessed March 25, 2014].

Haman, F. et al., 2004. Effects of carbohydrate availability on sustained shivering II. Relating muscle recruitment to fuel selection. *Journal of applied physiology (Bethesda, Md. : 1985)*, 96(1), pp.41–9. Available at: http://jap.physiology.org/content/96/1/41.full [Accessed March 27, 2014].

Hamanaka, R.B. & Chandel, N.S., 2012. Targeting glucose metabolism for cancer therapy. *The Journal of experimental medicine*, 209(2), pp.211–5. Available at: http://www.pubmedcentral.nih.gov/articlerender.fcgi?artid=3280882&tool=pmcentrez&rendertype=abstract [Accessed February 24, 2014].

Haouzi, P. et al., 2008. H2S induced hypometabolism in mice is missing in sedated sheep. *Respiratory physiology & neurobiology*, 160(1), pp.109–15. Available at: http://www.ncbi.nlm.nih.gov/pubmed/17980679 [Accessed February 26, 2014].

Hargreaves, M., 2000. Skeletal muscle metabolism during exercise in humans. *Clinical and Experimental Pharmacology and …*, 27, pp.225–228. Available at: http://onlinelibrary.wiley.com/doi/10.1046/j.1440-1681.2000.03225.x/full [Accessed March 5, 2014].

Heldmaier, G. et al., 1999. Metabolic adjustments during daily torpor in the Djungarian hamster. *American Journal of Physiology Endocrinology and Metabolism*, 276, pp.896–906. Available at: http://ajpendo.physiology.org/content/276/5/E896.short [Accessed March 1, 2014].

Heller, H.C., Colliver, G.W. & Bread, J., 1977. Thermoregulation during entrance into hibernation. *Pflügers Archiv : European journal of physiology*, 369(1), pp.55–9. Available at: http://www.ncbi.nlm.nih.gov/pubmed/560008 [Accessed March 17, 2014].

Henry, P.-G. et al., 2007. Brain energy metabolism and neurotransmission at near-freezing temperatures: in vivo (1)H MRS study of a hibernating mammal. *Journal of neurochemistry*, 101(6), pp.1505–15. Available at: http://www.ncbi.nlm.nih.gov/pubmed/17437538 [Accessed February 26, 2014].

Hoffmann, N. et al., 2014. BiPACE 2D--graph-based multiple alignment for comprehensive 2D gas chromatography-mass spectrometry. *Bioinformatics (Oxford, England)*. Available at: http://www.ncbi.nlm.nih.gov/pubmed/24363380 [Accessed February 4, 2014].

Hoffmann, N. et al., 2012. Combining peak- and chromatogram-based retention time alignment algorithms for multiple chromatography-mass spectrometry datasets. *BMC bioinformatics*, 13, p.214. Available at: http://www.pubmedcentral.nih.gov/articlerender.fcgi?artid=3546004&tool=pmcentrez&rendertype=abstract [Accessed February 4, 2014].

Hoffmann, N., 2014. *Computational Methods for High-Throughput Metabolomics*. Bielefeld University, Germany.

Hudson, J. & Scott, I., 1979. Daily Torpor in the Laboratory Mouse, Mus musculus Var. Albino. *Physiological Zoology*, 52(2), pp.205–218. Available at: http://www.jstor.org/discover/10.2307/30152564?uid=29277&uid=3737864&uid=2&uid=3&uid=67&uid=29276&uid=62&uid=5910216&sid=21102029198863 [Accessed May 21, 2013].

Iliff, B.W. & Swoap, S.J., 2012. Central adenosine receptor signaling is necessary for daily torpor in mice. *American journal of physiology. Regulatory, integrative and comparative physiology*,

303(5), pp.R477–84. Available at: http://www.ncbi.nlm.nih.gov/pubmed/22785425 [Accessed June 7, 2013].

Jeppesen, J. & Kiens, B., 2012. Regulation and limitations to fatty acid oxidation during exercise. *The Journal of physiology*, 590(Pt 5), pp.1059–68. Available at: http://www.pubmedcentral.nih.gov/articlerender.fcgi?artid=3381814&tool=pmcentrez&rendertype=abstract [Accessed January 28, 2014].

Ju, H. et al., 2011. Sustained torpidity following multi-dose administration of 3-iodothyronamine in mice. *Journal of cellular physiology*, 226(4), pp.853–8. Available at: http://www.ncbi.nlm.nih.gov/pubmed/21268024 [Accessed June 7, 2013].

Katajamaa, M., Miettinen, J. & Oresic, M., 2006. MZmine: toolbox for processing and visualization of mass spectrometry based molecular profile data. *Bioinformatics (Oxford, England)*, 22(5), pp.634–6. Available at: http://www.ncbi.nlm.nih.gov/pubmed/16403790 [Accessed January 26, 2014].

Kempa, S. et al., 2009. An automated GCxGC-TOF-MS protocol for batch-wise extraction and alignment of mass isotopomer matrixes from differential 13C-labelling experiments: a case study for photoautotrophic-mixotrophic grown Chlamydomonas reinhardtii cells. *Journal of basic microbiology*, 49(1), pp.82–91. Available at: http://www.ncbi.nlm.nih.gov/pubmed/19206143 [Accessed March 20, 2014].

Klement, R.J., 2013. Calorie or carbohydrate restriction? The ketogenic diet as another option for supportive cancer treatment. *The oncologist*, 18(9), p.1056. Available at: http://www.ncbi.nlm.nih.gov/pubmed/24062422 [Accessed February 26, 2014].

Knight, J.E. et al., 2000. mRNA stability and polysome loss in hibernating Arctic ground squirrels (Spermophilus parryii). *Molecular and cellular biology*, 20(17), pp.6374–9. Available at: http://www.pubmedcentral.nih.gov/articlerender.fcgi?artid=86112&tool=pmcentrez&rendertype=abstract [Accessed February 28, 2014].

Koizumi, A. et al., 1996. A tumor preventive effect of dietary restriction is antagonized by a high housing temperature through deprivation of torpor. *Mechanisms of ageing and development*, 92(1), pp.67–82. Available at: http://www.ncbi.nlm.nih.gov/pubmed/9032756 [Accessed February 26, 2014].

Koizumi, A. et al., 1993. Energy restriction that inhibits cellular proliferation by torpor can decrease susceptibility to spontaneous and asbestos-induced lung tumors in A/J mice. *Laboratory investigation; a journal of technical methods and pathology*, 68(6), pp.728–39. Available at: http://www.ncbi.nlm.nih.gov/pubmed/8515658 [Accessed February 26, 2014].

Koizumi, A. et al., 1992. Mitotic activity in mice is suppressed by energy restriction-induced torpor. *The Journal of nutrition*, 122(7), pp.1446–53. Available at: http://www.ncbi.nlm.nih.gov/pubmed/1619471 [Accessed February 26, 2014].

Könner, a C., Klöckener, T. & Brüning, J.C., 2009. Control of energy homeostasis by insulin and leptin: targeting the arcuate nucleus and beyond. *Physiology & behavior*, 97(5), pp.632–8. Available at: http://www.ncbi.nlm.nih.gov/pubmed/19351541 [Accessed March 8, 2013].

Kopka, J. et al., 2005. GMD@CSB.DB: the Golm Metabolome Database. *Bioinformatics (Oxford, England)*, 21(8), pp.1635–8. Available at: http://www.ncbi.nlm.nih.gov/pubmed/15613389 [Accessed January 28, 2014].

Kosmides, A.K. et al., 2013. Metabolomic fingerprinting: challenges and opportunities. *Critical reviews in biomedical engineering*, 41(3), pp.205–21. Available at: http://www.ncbi.nlm.nih.gov/pubmed/24579644 [Accessed March 17, 2014].

Kovats, E., 1958. Gas-chromatographische Charakterisierung organischer Verbindungen. Teil 1: Retentionsindices aliphatischer Halogenide, Alkohole, Aldehyde und Ketone. *Helvetica Chimica Acta*, 41(7), pp.1915–1932. Available at: http://doi.wiley.com/10.1002/hlca.19580410703 [Accessed March 20, 2014].

Krug, S. et al., 2012. The dynamic range of the human metabolome revealed by challenges. *FASEB journal : official publication of the Federation of American Societies for Experimental Biology*, 26(6), pp.2607–19. Available at: http://www.ncbi.nlm.nih.gov/pubmed/22426117 [Accessed January 22, 2014].

Kruskal, W. & Wallis, W., 1952. Use of ranks in one-criterion variance analysis. *Journal of the American statistical …*, 47(260), pp.583–621. Available at: http://www.tandfonline.com/doi/abs/10.1080/01621459.1952.10483441 [Accessed March 25, 2014].

Kutschke, M. et al., 2013. Depression of mitochondrial respiration during daily torpor of the Djungarian hamster, Phodopus sungorus, is specific for liver and correlates with body temperature. *Comparative Biochemistry and Physiology Part A: Molecular & Integrative Physiology*, 164(4), pp.584–589. Available at: http://www.sciencedirect.com/science/article/pii/S109564331300007X [Accessed January 29, 2014].

Lass, A. et al., 2011. Lipolysis - a highly regulated multi-enzyme complex mediates the catabolism of cellular fat stores. *Progress in lipid research*, 50(1), pp.14–27. Available at: http://www.pubmedcentral.nih.gov/articlerender.fcgi?artid=3031774&tool=pmcentrez&rendertype=abstract [Accessed March 19, 2014].

Lee, K. et al., 2010. Molecular mechanism underlying muscle mass retention in hibernating bats: role of periodic arousal. *Journal of cellular physiology*, 222(2), pp.313–9. Available at: http://www.ncbi.nlm.nih.gov/pubmed/19847807 [Accessed February 28, 2014].

Lehtinen, M.K. et al., 2013. The choroid plexus and cerebrospinal fluid: emerging roles in development, disease, and therapy. *The Journal of neuroscience : the official journal of the Society for Neuroscience*, 33(45), pp.17553–9. Available at: http://www.ncbi.nlm.nih.gov/pubmed/24198345 [Accessed February 23, 2014].

Leite, T.C. et al., 2011. Lactate downregulates the glycolytic enzymes hexokinase and phosphofructokinase in diverse tissues from mice. *FEBS letters*, 585(1), pp.92–8. Available at: http://www.ncbi.nlm.nih.gov/pubmed/21074528 [Accessed March 23, 2014].

Li, J. et al., 2008. Effect of inhaled hydrogen sulfide on metabolic responses in anesthetized, paralyzed, and mechanically ventilated piglets. *Pediatric critical care medicine : a journal of the Society of*

*Critical Care Medicine and the World Federation of Pediatric Intensive and Critical Care Societies*, 9(1), pp.110–2. Available at: http://www.ncbi.nlm.nih.gov/pubmed/18477923 [Accessed February 26, 2014].

Likić, V.A. et al., 2010. Systems biology: the next frontier for bioinformatics. *Advances in bioinformatics*, pp.1–10. Available at: http://www.pubmedcentral.nih.gov/articlerender.fcgi?artid=3038413&tool=pmcentrez&rendertype=abstract [Accessed March 20, 2014].

Lisec, J. et al., 2006. Gas chromatography mass spectrometry-based metabolite profiling in plants. *Nature protocols*, 1(1), pp.387–96. Available at: http://dx.doi.org/10.1038/nprot.2006.59 [Accessed January 26, 2014].

Liu, L. et al., 2012. Deregulated MYC expression induces dependence upon AMPK-related kinase 5. *Nature*, 483(7391), pp.608–12. Available at: http://www.ncbi.nlm.nih.gov/pubmed/22460906 [Accessed February 26, 2014].

Lommen, A. & Kools, H.J., 2012. MetAlign 3.0: performance enhancement by efficient use of advances in computer hardware. *Metabolomics : Official journal of the Metabolomic Society*, 8(4), pp.719–726. Available at: http://www.pubmedcentral.nih.gov/articlerender.fcgi?artid=3397215&tool=pmcentrez&rendertype=abstract [Accessed February 4, 2014].

Maalouf, M., Rho, J.M. & Mattson, M.P., 2009. The neuroprotective properties of calorie restriction, the ketogenic diet, and ketone bodies. *Brain research reviews*, 59(2), pp.293–315. Available at: http://www.pubmedcentral.nih.gov/articlerender.fcgi?artid=2649682&tool=pmcentrez&rendertype=abstract [Accessed February 22, 2014].

Matsumura, K., Nakayama, T. & Kaminaga, T., 1987. Effects of carbon dioxide on preoptic thermosensitive neurons in vitro. *Pflügers Archiv : European journal of physiology*, 408(2), pp.120–3. Available at: http://www.ncbi.nlm.nih.gov/pubmed/3104876 [Accessed March 17, 2014].

Meija, J. & Mester, Z., 2008. Paradigms in isotope dilution mass spectrometry for elemental speciation analysis. *Analytica chimica acta*, 607(2), pp.115–25. Available at: http://www.ncbi.nlm.nih.gov/pubmed/18190799 [Accessed March 23, 2014].

Milne, S.B. et al., 2013. Sum of the parts: mass spectrometry-based metabolomics. *Biochemistry*, 52(22), pp.3829–40. Available at: http://www.ncbi.nlm.nih.gov/pubmed/23442130 [Accessed February 21, 2014].

Mitrakou, A., 2011. Kidney: its impact on glucose homeostasis and hormonal regulation. *Diabetes research and clinical practice*, 93 Suppl 1, pp.S66–72. Available at: http://www.ncbi.nlm.nih.gov/pubmed/21864754 [Accessed March 19, 2014].

Morhardt, J.E., 1970. Heart rates, breathing rates and the effects of atropine and acetylcholine on white-footed mice (Peromyscus sp.) during daily torpor. *Comparative biochemistry and physiology*, 33(2), pp.441–57. Available at: http://www.ncbi.nlm.nih.gov/pubmed/5428031.

Morris, S.M., 2002. Regulation of enzymes of the urea cycle and arginine metabolism. *Annual review of nutrition*, 22, pp.87–105. Available at: http://www.ncbi.nlm.nih.gov/pubmed/12055339 [Accessed March 4, 2014].

Morrison, S.F. & Nakamura, K., 2011. Central neural pathways for thermoregulation. *Frontiers in bioscience : a journal and virtual library*, 16, pp.74–104. Available at: http://www.pubmedcentral.nih.gov/articlerender.fcgi?artid=3051412&tool=pmcentrez&rendertype=abstract.

Mortimore, G.E., Pösö, A.R. & Lardeux, B.R., 1989. Mechanism and regulation of protein degradation in liver. *Diabetes/metabolism reviews*, 5(1), pp.49–70. Available at: http://www.ncbi.nlm.nih.gov/pubmed/2649336 [Accessed March 18, 2014].

Nelson, C.J. et al., 2009. Analysis of the hibernation cycle using LC-MS-based metabolomics in ground squirrel liver. *Physiological Genomics*, (37), pp.43–51.

Nelson, C.J., Otis, J.P. & Carey, H. V, 2010. Global analysis of circulating metabolites in hibernating ground squirrels. *Comparative biochemistry and physiology. Part D, Genomics & proteomics*, 5(4), pp.265–273. Available at: http://www.ncbi.nlm.nih.gov/pubmed/20728417.

Nestler, J.R. et al., 1997. Glycolytic enzyme binding during entrance to daily torpor in deer mice (Peromyscus maniculatus). *Physiological zoology*, 70(1), pp.61–7. Available at: http://www.ncbi.nlm.nih.gov/pubmed/9231377 [Accessed February 27, 2014].

Nestler, J.R., 1990a. Intracellular pH during daily torpor in Peromyscus maniculatus. *Journal of comparative physiology. B, Biochemical, systemic, and environmental physiology*, 159(6), pp.661–6. Available at: http://www.ncbi.nlm.nih.gov/pubmed/2335594 [Accessed May 29, 2013].

Nestler, J.R., 1991. Metabolic substrate change during daily torpor in deer mice. *Canadian Journal of Zoology*, 69, pp.322–327.

Nestler, J.R., 1990b. Relationship between Respiratory Quotient and Metabolic Rate during Entry to and Arousal from Daily Torpor in Deer Mice (Peromyscus maniculatus). *Physiological Zoology*, 63(3), pp.504–515. Available at: http://www.jstor.org/discover/10.2307/30156225?uid=29277&uid=3737864&uid=2129&uid=2&uid=70&uid=3&uid=67&uid=29276&uid=62&uid=5910216&sid=21102054802753 [Accessed May 29, 2013].

Nestler, J.R., 1990c. Relationships Quotient Respiratory Metabolic Rate during Entry to and Arousal from Daily Torpor in Deer Mice ( Peromyscus maniculatus ). , 63(3), pp.504–515.

Nestler, J.R., 1992. Tissue-specific metabolism during normothermy and daily torpor in deer mice (Peromyscus maniculatus). *The Journal of experimental zoology*, 261(4), pp.406–13. Available at: http://www.ncbi.nlm.nih.gov/pubmed/1569409.

Newman, J.C. & Verdin, E., 2014. Ketone bodies as signaling metabolites. *Trends in endocrinology and metabolism: TEM*, 25(1), pp.42–52. Available at: http://www.ncbi.nlm.nih.gov/pubmed/24140022 [Accessed January 27, 2014].

Nugent, S. et al., 2014. Brain glucose and acetoacetate metabolism: a comparison of young and older adults. *Neurobiology of aging*, 35(6), pp.1386–95. Available at: http://www.ncbi.nlm.nih.gov/pubmed/24388785 [Accessed March 29, 2014].

Oelkrug, R., Heldmaier, G. & Meyer, C.W., 2011. Torpor patterns, arousal rates, and temporal organization of torpor entry in wildtype and UCP1-ablated mice. *Journal of comparative physiology. B, Biochemical, systemic, and environmental physiology*, 181(1), pp.137–45. Available at: http://www.ncbi.nlm.nih.gov/pubmed/20680295 [Accessed March 17, 2014].

Olson, J. et al., 2013. Circannual Rhythm in Body Temperature, Torpor, and Sensitivity to A1 Adenosine Receptor Agonist in Arctic Ground Squirrels. *Journal of Biological Rhythms*, 28(3), pp.201–207. Available at: http://jbr.sagepub.com/content/28/3/201.abstract.

Ouarour, A., Cutrera, R.A. & Pévet, P., 1995. Effects of 5-HT denervation of the suprachiasmatic nuclei or lesions of the median raphe nucleus on daily torpor in the Djungarian hamster, Phodopus sungorus. *Biological signals*, 4(1), pp.51–8. Available at: http://www.ncbi.nlm.nih.gov/pubmed/7550584 [Accessed May 21, 2013].

Pablos, J.L. & Cañete, J.D., 2013. Immunopathology of rheumatoid arthritis. *Current topics in medicinal chemistry*, 13(6), pp.705–11. Available at: http://www.ncbi.nlm.nih.gov/pubmed/23574519 [Accessed February 26, 2014].

Panas, H.N. et al., 2010. Normal thermoregulatory responses to 3-iodothyronamine, trace amines and amphetamine-like psychostimulants in trace amine associated receptor 1 knockout mice. *Journal of neuroscience research*, 88(9), pp.1962–9. Available at: http://www.pubmedcentral.nih.gov/articlerender.fcgi?artid=3587846&tool=pmcentrez&rendertype=abstract [Accessed February 26, 2014].

Parisi, R. et al., 2013. Global epidemiology of psoriasis: a systematic review of incidence and prevalence. *The Journal of investigative dermatology*, 133(2), pp.377–85. Available at: http://www.ncbi.nlm.nih.gov/pubmed/23014338 [Accessed January 30, 2014].

Pelz, K.M. et al., 2008. Monosodium glutamate-induced arcuate nucleus damage affects both natural torpor and 2DG-induced torpor-like hypothermia in Siberian hamsters. *American journal of physiology. Regulatory, integrative and comparative physiology*, 294(1), pp.R255–65. Available at: http://www.ncbi.nlm.nih.gov/pubmed/17959707 [Accessed May 9, 2013].

Quiroga, A.D. & Lehner, R., 2012. Liver triacylglycerol lipases. *Biochimica et biophysica acta*, 1821(5), pp.762–9. Available at: http://www.ncbi.nlm.nih.gov/pubmed/21963564 [Accessed March 23, 2014].

Radziuk, J.M., 2013. The suprachiasmatic nucleus, circadian clocks, and the liver. *Diabetes*, 62(4), pp.1017–9. Available at: http://www.ncbi.nlm.nih.gov/pubmed/23520276 [Accessed May 21, 2013].

Rapoport, B.I., 2010. Metabolic factors limiting performance in marathon runners. *PLoS computational biology*, 6(10), p.e1000960. Available at: http://www.pubmedcentral.nih.gov/articlerender.fcgi?artid=2958805&tool=pmcentrez&rendertype=abstract [Accessed March 25, 2014].

Romijn, J.A. et al., 1993. Regulation of endogenous fat and carbohydrate metabolism in relation to exercise intensity and duration. *The American journal of physiology*, 265(3 Pt 1), pp.E380–91. Available at: http://www.ncbi.nlm.nih.gov/pubmed/8214047 [Accessed March 17, 2014].

Rose, A.J. & Richter, E.A., 2005. Skeletal muscle glucose uptake during exercise: how is it regulated? *Physiology (Bethesda, Md.)*, 20, pp.260–70. Available at: http://www.ncbi.nlm.nih.gov/pubmed/16024514 [Accessed February 17, 2014].

Rossi, D.J., Brady, J.D. & Mohr, C., 2007. Astrocyte metabolism and signaling during brain ischemia. *Nature neuroscience*, 10(11), pp.1377–86. Available at: http://www.ncbi.nlm.nih.gov/pubmed/17965658 [Accessed February 20, 2014].

Ruby, N. et al., 1996. Ablation of suprachiasmatic nucleus alters timing of hibernation in ground squirrels. *Proceedings of the …*, 93(September), pp.9864–9868. Available at: http://www.pnas.org/content/93/18/9864.short [Accessed May 21, 2013].

Saito, H., 2005. Much atopy about the skin: genome-wide molecular analysis of atopic eczema. *International archives of allergy and immunology*, 137(4), pp.319–25. Available at: http://www.ncbi.nlm.nih.gov/pubmed/15970641 [Accessed February 26, 2014].

Sanderson, T.H. et al., 2013. Molecular mechanisms of ischemia-reperfusion injury in brain: pivotal role of the mitochondrial membrane potential in reactive oxygen species generation. *Molecular neurobiology*, 47(1), pp.9–23. Available at: http://www.pubmedcentral.nih.gov/articlerender.fcgi?artid=3725766&tool=pmcentrez&rendertype=abstract [Accessed February 23, 2014].

Satinoff, E., 1967. Disruption of hibernation caused by hypothalamic lesions. *Science*, 155(3765), pp.1031–1033. Available at: http://www.sciencemag.org/content/155/3765/1031.short [Accessed May 21, 2013].

Scanlan, T.S. et al., 2004. 3-Iodothyronamine is an endogenous and rapid-acting derivative of thyroid hormone. *Nature medicine*, 10(6), pp.638–42. Available at: http://www.ncbi.nlm.nih.gov/pubmed/15146179 [Accessed February 26, 2014].

Schaefer, K.E. & Wünnenberg, W., 1976. Threshold temperatures for shivering in acute and chronic hypercapnia. *Journal of applied physiology*, 41(1), pp.67–70. Available at: http://www.ncbi.nlm.nih.gov/pubmed/972134 [Accessed March 17, 2014].

Schofield, Z.V. et al., 2013. Neutrophils-a key component of ischemia-reperfusion injury. *Shock (Augusta, Ga.)*, 40(6), pp.463–70. Available at: http://www.ncbi.nlm.nih.gov/pubmed/24088997 [Accessed February 24, 2014].

Schwanhäusser, B. et al., 2011. Global quantification of mammalian gene expression control. *Nature*, 473(7347), pp.337–42. Available at: http://www.ncbi.nlm.nih.gov/pubmed/21593866 [Accessed February 19, 2014].

Serkova, N.J. et al., 2007. Quantitative analysis of liver metabolites in three stages of the circannual hibernation cycle in 13-lined ground squirrels by NMR. *Physiological genomics*, (31), pp.15–24.

Simon, F. et al., 2008. Hemodynamic and metabolic effects of hydrogen sulfide during porcine ischemia/reperfusion injury. *Shock (Augusta, Ga.)*, 30(4), pp.359–64. Available at: http://www.ncbi.nlm.nih.gov/pubmed/18323742 [Accessed January 29, 2014].

Simone, B.A. et al., 2013. Selectively starving cancer cells through dietary manipulation: methods and clinical implications. *Future oncology (London, England)*, 9(7), pp.959–76. Available at: http://www.ncbi.nlm.nih.gov/pubmed/23837760 [Accessed February 26, 2014].

Skoog, D.A., Universi, S. & Crouch, S.R., 2007. *Principles of Instrumental Analysis* 6th ed., Harris, David.

Smith, C.A. et al., 2006. XCMS: processing mass spectrometry data for metabolite profiling using nonlinear peak alignment, matching, and identification. *Analytical chemistry*, 78(3), pp.779–87. Available at: http://www.ncbi.nlm.nih.gov/pubmed/16448051 [Accessed February 4, 2014].

Smolinska, A. et al., 2012. Simultaneous analysis of plasma and CSF by NMR and hierarchical models fusion. *Analytical and bioanalytical chemistry*, 403(4), pp.947–59. Available at: http://www.pubmedcentral.nih.gov/articlerender.fcgi?artid=3336062&tool=pmcentrez&rendertype=abstract [Accessed February 17, 2014].

Somero, G., 1981. pH-Temperature interactions on proteins - principles of optimal pH and buffer system design. *Marine biology letters*, 2(3), pp.163–178. Available at: http://scholar.google.de/scholar?q=Somero+PH-temperature+interactions+on+proteins:+principles+of+optimal+pH+and+buffer+system+design&btnG=&hl=en&as_sdt=0,5#0 [Accessed February 28, 2014].

Song, Y. et al., 2014. Point-of-care technologies for molecular diagnostics using a drop of blood. *Trends in biotechnology*, 32(3), pp.132–139. Available at: http://www.ncbi.nlm.nih.gov/pubmed/24525172 [Accessed February 19, 2014].

Sonnewald, U. et al., 1994. NMR spectroscopic study of cell cultures of astrocytes and neurons exposed to hypoxia: compartmentation of astrocyte metabolism. *Neurochemistry international*, 24(5), pp.473–83. Available at: http://www.ncbi.nlm.nih.gov/pubmed/7647701 [Accessed March 17, 2014].

Spencer, W.A., Grodums, E.I. & Dempster, G., 1966. The glyceride fatty acid composition and lipid content of brown and white adipose tissue of the hibernator Citellus lateralis. *Journal of cellular physiology*, 67(3), pp.431–41. Available at: http://www.ncbi.nlm.nih.gov/pubmed/5963067 [Accessed February 28, 2014].

Staples, J.F. & Brown, J.C.L., 2008. Mitochondrial metabolism in hibernation and daily torpor : a review. *Journal Comp Physiol B*, 178, pp.811–827.

Stevinson, C.D. & Biddle, S.J., 1998. Cognitive orientations in marathon running and "hitting the wall." *British Journal of Sports Medicine*, 32(3), pp.229–234. Available at: http://bjsm.bmj.com/content/32/3/229.abstract [Accessed March 25, 2014].

Sturm, M. et al., 2008. OpenMS - an open-source software framework for mass spectrometry. *BMC bioinformatics*, 9, p.163. Available at: http://www.pubmedcentral.nih.gov/articlerender.fcgi?artid=2311306&tool=pmcentrez&rendertype=abstract [Accessed February 20, 2014].

Swoap, S.J. et al., 2006. The full expression of fasting-induced torpor requires beta 3-adrenergic receptor signaling. *The Journal of neuroscience : the official journal of the Society for*

*Neuroscience*, 26(1), pp.241–5. Available at: http://www.ncbi.nlm.nih.gov/pubmed/16399693 [Accessed February 26, 2014].

Swoap, S.J., 2008. The pharmacology and molecular mechanisms underlying temperature regulation and torpor. *Biochemical pharmacology*, 76(7), pp.817–24. Available at: http://www.pubmedcentral.nih.gov/articlerender.fcgi?artid=2582020&tool=pmcentrez&rendertype=abstract [Accessed May 9, 2013].

Swoap, S.J. & Gutilla, M.J., 2009. Cardiovascular changes during daily torpor in the laboratory mouse. *American journal of physiology. Regulatory, integrative and comparative physiology*, 297(3), pp.R769–74. Available at: http://www.ncbi.nlm.nih.gov/pubmed/19587115 [Accessed April 1, 2013].

Swoap, S.J., Rathvon, M. & Gutilla, M., 2007. AMP does not induce torpor. *American journal of physiology. Regulatory, integrative and comparative physiology*, 293(1), pp.R468–73. Available at: http://www.ncbi.nlm.nih.gov/pubmed/17409259 [Accessed June 7, 2013].

Swoap, S.J. & Weinshenker, D., 2008. Norepinephrine controls both torpor initiation and emergence via distinct mechanisms in the mouse. *PloS one*, 3(12), p.e4038. Available at: http://www.pubmedcentral.nih.gov/articlerender.fcgi?artid=2602851&tool=pmcentrez&rendertype=abstract [Accessed February 26, 2014].

Takemoto, Y., 2011. Intracisternally injected L-proline activates hypothalamic supraoptic, but not paraventricular, vasopressin-expressing neurons in conscious rats. *Journal of amino acids*, 2011, pp.1–8. Available at: http://www.pubmedcentral.nih.gov/articlerender.fcgi?artid=3268034&tool=pmcentrez&rendertype=abstract [Accessed March 29, 2014].

Tøien, Ø. et al., 2011. Hibernation in black bears: independence of metabolic suppression from body temperature. *Science (New York, N.Y.)*, 331(6019), pp.906–9. Available at: http://www.ncbi.nlm.nih.gov/pubmed/21330544 [Accessed January 29, 2014].

Velickovska, V. et al., 2005. Proteolysis is depressed during torpor in hibernators at the level of the 20S core protease. *Journal of comparative physiology. B, Biochemical, systemic, and environmental physiology*, 175(5), pp.329–35. Available at: http://www.ncbi.nlm.nih.gov/pubmed/15912363 [Accessed February 28, 2014].

Velickovska, V. & van Breukelen, F., 2007. Ubiquitylation of proteins in livers of hibernating golden-mantled ground squirrels, Spermophilus lateralis. *Cryobiology*, 55(3), pp.230–5. Available at: http://www.pubmedcentral.nih.gov/articlerender.fcgi?artid=2700031&tool=pmcentrez&rendertype=abstract [Accessed February 28, 2014].

Viscarra, J.A. & Ortiz, R.M., 2013. Cellular mechanisms regulating fuel metabolism in mammals: role of adipose tissue and lipids during prolonged food deprivation. *Metabolism: clinical and experimental*, 62(7), pp.889–97. Available at: http://www.ncbi.nlm.nih.gov/pubmed/23357530 [Accessed March 20, 2014].

Wagenmakers, A.J., 1998. Muscle amino acid metabolism at rest and during exercise: role in human physiology and metabolism. *Exercise and sport sciences reviews*, 26, pp.287–314. Available at: http://europepmc.org/abstract/MED/9696993 [Accessed March 25, 2014].

Walker, L.E. et al., 1983. A continuum of sleep and shallow torpor in fasting doves. *Science (New York, N.Y.)*, 221(4606), pp.194–5. Available at: http://www.ncbi.nlm.nih.gov/pubmed/17769218 [Accessed February 28, 2014].

Wang, L.C. et al., 1988. The "hibernation induction trigger": specificity and validity of bioassay using the 13-lined ground squirrel. *Cryobiology*, 25(4), pp.355–62. Available at: http://www.ncbi.nlm.nih.gov/pubmed/3409709.

Wang, P. et al., 1997. Seasonal changes in enzymes of lipogenesis and triacylglycerol synthesis in the golden-mantled ground squirrel (Spermophilus lateralis). *Comparative biochemistry and physiology. Part B, Biochemistry & molecular biology*, 118(2), pp.261–7. Available at: http://www.ncbi.nlm.nih.gov/pubmed/9440219 [Accessed February 28, 2014].

Ward, J.H., 1963. Hierarchical Grouping to Optimize an Objective Function. *Journal of the American Statistical Association*, 58(301), pp.236–244. Available at: http://www.bibsonomy.org/bibtex/22d1e7fc2532d9b74204f09c3c797fd6f/ds9?lang=de [Accessed March 23, 2014].

Webb, G.P., Jagot, S. a & Jakobson, M.E., 1982. Fasting-induced torpor in Mus musculus and its implications in the use of murine models for human obesity studies. *Comparative biochemistry and physiology. A, Comparative physiology*, 72(1), pp.211–9. Available at: http://www.ncbi.nlm.nih.gov/pubmed/6124358.

Woolf, E.C. & Scheck, A.C., 2014. The Ketogenic Diet for the Treatment of Malignant Glioma. *Journal of lipid research*. Available at: http://www.ncbi.nlm.nih.gov/pubmed/24503133 [Accessed March 29, 2014].

Wright, C.L. & Boulant, J.A., 1985. Carbon dioxide and pH effects on temperature-sensitive and -insensitive hypothalamic neurons. *Journal of Applied Physiology*, 102(4), pp.1357–66. Available at: http://www.ncbi.nlm.nih.gov/pubmed/17138840 [Accessed March 17, 2014].

Wu, A.L. & Windmueller, H.G., 1979. Relative contributions by liver and intestine to individual plasma apolipoproteins in the rat. *The Journal of biological chemistry*, 254(15), pp.7316–22. Available at: http://www.ncbi.nlm.nih.gov/pubmed/457683 [Accessed March 23, 2014].

Xia, J. et al., 2009. MetaboAnalyst: a web server for metabolomic data analysis and interpretation. *Nucleic acids research*, 37, pp.W652–60. Available at: http://nar.oxfordjournals.org/content/37/suppl_2/W652.full [Accessed March 29, 2014].

Yuen, K.C.J., McDaniel, P.A. & Riddle, M.C., 2012. Twenty-four-hour profiles of plasma glucose, insulin, C-peptide and free fatty acid in subjects with varying degrees of glucose tolerance following short-term, medium-dose prednisone (20 mg/day) treatment: evidence for differing effects on insulin secreti. *Clinical endocrinology*, 77(2), pp.224–32. Available at: http://www.pubmedcentral.nih.gov/articlerender.fcgi?artid=3700529&tool=pmcentrez&rendertype=abstract [Accessed March 25, 2014].

Zappaterra, M.W. & Lehtinen, M.K., 2012. The cerebrospinal fluid: regulator of neurogenesis, behavior, and beyond. *Cellular and molecular life sciences : CMLS*, 69(17), pp.2863–78. Available at:

http://www.pubmedcentral.nih.gov/articlerender.fcgi?artid=3856656&tool=pmcentrez&rendertype=abstract [Accessed January 23, 2014].

Zhang, A. et al., 2012. Modern analytical techniques in metabolomics analysis. *The Analyst*, 137(2), pp.293–300. Available at: http://www.ncbi.nlm.nih.gov/pubmed/22102985 [Accessed February 21, 2014].

Zhang, J. et al., 2006. Constant darkness is a circadian metabolic signal in mammals. *Nature*, 439(7074), pp.340–3. Available at: http://www.ncbi.nlm.nih.gov/pubmed/16421573 [Accessed May 23, 2013].

Zhang, Y., Kuang, Y., LaManna, J.C., et al., 2013. Contribution of brain glucose and ketone bodies to oxidative metabolism. *Advances in experimental medicine and biology*, 765, pp.365–70. Available at: http://www.ncbi.nlm.nih.gov/pubmed/22879057 [Accessed March 17, 2014].

Zhang, Y., Kuang, Y., Xu, K., et al., 2013. Ketosis proportionately spares glucose utilization in brain. *Journal of cerebral blood flow and metabolism : official journal of the International Society of Cerebral Blood Flow and Metabolism*, 33(8), pp.1307–11. Available at: http://www.ncbi.nlm.nih.gov/pubmed/23736643 [Accessed February 27, 2014].

Zhang, Y. et al., 1994. Positional cloning of the mouse obese gene and its human homologue. *Nature*, 372, pp.425–432. Available at: http://www.tmd.ac.jp/med/phy2/Rindokupapers/2008_11OB.pdf [Accessed February 26, 2014].

Zhang, Y. et al., 2013. Protein analysis by shotgun/bottom-up proteomics. *Chemical reviews*, 113(4), pp.2343–94. Available at: http://www.ncbi.nlm.nih.gov/pubmed/23438204 [Accessed March 17, 2014].

Zhou, Y. & Danbolt, N.C., 2014. Glutamate as a neurotransmitter in the healthy brain. *Journal of neural transmission (Vienna, Austria : 1996)*. Available at: http://www.ncbi.nlm.nih.gov/pubmed/24578174 [Accessed March 29, 2014].

Zinker, B.A., Britz, K. & Brooks, G.A., 1990. Effects of a 36-hour fast on human endurance and substrate utilization. *J Appl Physiol*, 69(5), pp.1849–1855. Available at: http://jap.physiology.org/content/69/5/1849.abstract Zinker1990, [Accessed March 25, 2014].

# 9. References – R


1. H. Wickham. ggplot2: elegant graphics for data analysis. Springer New York, 2009.

2. Hadley Wickham (2007). Reshaping Data with the reshape Package. Journal of Statistical Software, 21(12), 1-20. URL: http://www.jstatsoft.org/v21/i12/.

3. Hadley Wickham (2012). scales: Scale functions for graphics.. R package version 0.2.3. URL: http://CRAN.R-project.org/package=scales

4. Hadley Wickham (2011). The Split-Apply-Combine Strategy for Data Analysis. Journal of Statistical Software, 40(1), 1-29. URL: http://www.jstatsoft.org /v40/i01/.

5. Søren Højsgaard, Ulrich Halekoh with contributions from Jim Robison-Cox, Kevin Wright and Alessandro A. Leidi (2013). doBy: doBy - Groupwise summary statistics, LSmeans, general linear contrasts, various utilities. R package version 4.5-10. URL: http://CRAN.R-project.org/package=doBy

6. Revelle, W. (2013) psych: Procedures for Personality and Psychological Research, Northwestern University, Evanston, Illinois, USA, URL: http://CRAN.R-project.org/package=psych Version = 1.4.2.

7. Peter Carl and Brian G. Peterson (2013). PerformanceAnalytics: Econometric tools for performance and risk analysis. R package version 1.1.0. URL: http://CRAN.R-project.org/package=PerformanceAnalytics

8. Raiche, G. (2010). nFactors: an R package for parallel analysis and non graphical solutions to the Cattell scree test.R package version 2.3.3.

9. Bernaards, Coen A. and Jennrich, Robert I. (2005) Gradient Projection Algorithms and Software for Arbitrary Rotation Criteria in Factor Analysis, Educational and Psychological Measurement: 65, 676-696. URL: http://www.stat.ucla.edu/ research/gpa

10. Felipe de Mendiburu (2014). agricolae: Statistical Procedures for Agricultural Research. R package version 1.1-7. URL: http://CRAN.R-project.org/package=agricolae

11. Maechler, M., Rousseeuw, P., Struyf, A., Hubert, M., Hornik, K. (2013). cluster: Cluster Analysis Basics and Extensions. R package version 1.14.4.

12. Kevin Wright (2013). corrgram: Plot a correlogram. R package version 1.5. URL: http://CRAN.R-project.org/package=corrgram

13. Daniel Adler, Duncan Murdoch and others (2014). rgl: 3D visualization device system (OpenGL). R package version 0.93.996. URL: http://CRAN.R-project.org/package=rgl